

**Comprehensive analysis of nanodiamond evidence relating
to the Younger Dryas Impact Hypothesis.**

Journal:	<i>Journal of Quaternary Science</i>
Manuscript ID	JQS-15-0072.R1
Wiley - Manuscript type:	Review Article
Date Submitted by the Author:	17-Mar-2016
Complete List of Authors:	Daulton, Tyrone; Washington University in St. Louis in St. Louis, Department of Physics and Laboratory for Space Sciences Amari, Sachiko; Washington University in St. Louis, Department of Physics and Laboratory for Space Sciences Scott, Andrew; Royal Holloway University of London, Department of Earth Sciences Hardiman, Mark; University of Portsmouth, Department of Geography Pinter, Nicholas; Southern Illinois University, Department of Geology Anderson, R.; Northern Arizona University, Center for Sustainable Environments
Keywords:	nanodiamonds, cubic diamond, hexagonal diamond, lonsdaleite, Younger Dryas Impact Hypothesis

SCHOLARONE™
Manuscripts

Comprehensive analysis of nanodiamond evidence relating to the Younger Dryas Impact Hypothesis

Tyrone L. Daulton^{1,2*}, Sachiko Amari¹, Andrew C. Scott³, Mark Hardiman⁴, Nicholas Pinter⁵, R. Scott Anderson⁶

¹Washington University in St. Louis, Department of Physics and Laboratory for Space Sciences, St. Louis, Missouri 63130, U.S.A.

²Washington University in St. Louis, Institute for Materials Science and Engineering, St. Louis, Missouri 63130, U.S.A.

³Department of Earth Sciences, Royal Holloway University of London, Egham, Surrey, TW20 0EX, U.K.

⁴Department of Geography, University of Portsmouth, Portsmouth, PO1 3HE, U.K.

⁵Department of Earth and Planetary Sciences, University of California Davis, Davis California 95616, U.S.A.

⁶School of Earth Sciences and Environmental Sustainability, Northern Arizona University, Flagstaff, Arizona 86011, U.S.A.

*correspondence: T. L. Daulton, e-mail: tdaulton@physics.wustl.edu

submitted to *Journal of Quaternary Science*

June 25, 2015

Modified March 3, 2016

ABSTRACT: During the end of the last glacial period in the Northern Hemisphere near 12.9k cal a BP, deglacial warming of the Bølling-Ållerød interstadial ceased abruptly and the climate returned to glacial conditions for a $\approx 1,300$ year interval known as the Younger Dryas stadial. The Younger Dryas Impact Hypothesis proposes that the onset of the Younger Dryas climate reversal, Pleistocene megafaunal extinctions, and disappearance of the Clovis paleoindian lithic technology were coeval and caused by continent-wide catastrophic effects of impact/bolide events in North America. While there are no known impact structures dated to the Younger Dryas onset, physical evidence of the impact/bolide events is argued to be present in sediments spanning several continents at stratigraphic levels inferred to date to the Bølling-Ållerød / Younger Dryas boundary (YDB). Reports of nanometer to submicron-sized diamonds in YDB sediments, in particular the rare 2H hexagonal polytype of diamond, lonsdaleite, have been presented as strong evidence for shock processing of crustal materials. We review the available data on diamonds in sediments and provide new data. We find no evidence for lonsdaleite in YDB sediments and find no evidence of a spike in nanodiamond concentration at the YDB layer to support the impact hypothesis.

KEYWORDS: Nanodiamonds; cubic diamond; hexagonal diamond; lonsdaleite; Younger Dryas Impact Hypothesis

Introduction

The Younger Dryas (YD) Impact Hypothesis attempts to explain the rapid and dramatic changes that occurred at the end of the Pleistocene as arising from catastrophic extraterrestrial mechanisms. The earliest versions of the YD Impact Hypothesis speculated that North America was impacted by intense cosmic rays from a supernova (Brakenridge, 1981, 2011; Firestone and Topping, 2001, 2002; Firestone *et al.*, 2006), mineral debris that condensed in the supernova outflow (Firestone and Topping, 2001, 2002; Firestone *et al.*, 2006), and a comet (Melton and Schriever, 1933; Sass, 1944) whose orbit was perturbed into the inner solar system by the supernova shockwave (Firestone *et al.*, 2006). Multiple comet fragments have also been hypothesized to have struck the oceans across the globe (Kristan-Tollmann and Tollmann, 1992, 1994; Tollmann, 2001). A planet-sized fragment of a supernova has even been speculated to have entered the solar system, modified planetary orbits, and caused terrestrial impacts (Allan and Belair, 1994, 1997). A body ejected from a supernova has also been suggested to have struck North America (Firestone, 2009). Other early versions speculated that, during the Late Pleistocene, the Earth was irradiated by a burst of cosmic rays from the galactic core (LaViolette, 1987, 2005) and/or impacted by large solar flares in addition to coronal mass ejections from the sun (LaViolette, 2005, 2011), where the solar eruptions were induced by a supernova shockwave (Firestone *et al.*, 2006). The YD Impact Hypothesis has since evolved into several highly-controversial versions, most proposing that the abrupt YD climate reversal, Pleistocene megafaunal extinctions, and disappearance of the Clovis paleoindian lithic technology were coeval and caused by continent-wide catastrophic effects of one or more impact/bolide events in North America 12.9k cal a BP (e.g., Firestone *et al.*, 2007).

The coeval timing of the above events, a requirement for a singular causal mechanism, has not been firmly established (see van Hoesel *et al.*, 2014) and is a point of controversy. The onset of the YD stadial either spanned, or is dated to within, a couple hundred years of 12.9k cal a BP, depending on the applied chronometer (see, Meltzer and Holliday, 2010; Fiedel, 2011; van Hoesel *et al.*, 2014; Meltzer *et al.*, 2014). However, the chronologies of the Pleistocene megafaunal extinctions (timing and rate of population decline) are not well constrained and are debated. During the Pleistocene, at least 33 (or > 70%) of North American

1
2
3 megafaunal genera disappeared (Barnosky *et al.*, 2004) and, of these, the extinction of
4 16 genera (e.g., mammoths, mastodons, giant short-faced bears, saber-tooth tigers) are
5 constrained between 12,000 and 10,000 ¹⁴C a BP (~13,800 - 11,400 cal a BP)
6 (Grayson, 2007; Faith and Surovell, 2009; Woodman and Athfield, 2009).
7
8 Additionally, a recent study that compared ancient DNA and radiocarbon data over
9 the last 56k a concluded that the megafauna extinction events are correlated with the
10 multiple Dansgaard-Oeschger interstadial warming events (Copper *et al.*, 2015),
11 suggesting the YD stadial is not unique. Furthermore, Pleistocene megafaunal
12 extinctions were not limited to North America and also occurred at different times in
13 South America, the Caribbean, Africa, Eurasia, and Australia. For discussions on the
14 climatic changes that define the YD stadial see e.g., Berger (1990) and Carlson
15 (2013), and on the dynamics of the paleoindian populations during this period see
16 Collard *et al.* (2010).
17

18
19
20
21
22
23
24
25
26
27
28
29
30
31
32
33
34
35
36
37
38
39
40
41
42
43
44
45
46
47
48
49
50
51
52
53
54
55
56
57
58
59
60
There are no recognized impact structures in North America that date to the onset
of the YD stadial. Several geomorphic features have been suggested as possible YD
craters: oriented shallow depressions in Alaskan, Canadian, and Siberian permafrost
(Allan and Belair, 1994, 1997), the Carolina Bays (Melton and Schriever, 1933; Allan
and Belair, 1994, 1997; Firestone and Topping, 2001; Firestone *et al.*, 2007, 2010a;
Firestone, 2009; Kinzie *et al.*, 2014, Kennett *et al.*, 2015a), small playa basins of the
High Plains (Firestone *et al.*, 2006), and deep depressions in four of the Great Lakes
(Firestone *et al.*, 2007, 2010a; Firestone, 2009); however, there is no evidence to
support their impact origin (see Holliday *et al.*, 2014). The 4 km-diameter, circular
Corossol structure in the Gulf of St. Lawrence has also been suggested as a possible
YD-age crater based on the discovery of a single 4 cm long breccia clast suggesting
impact metamorphism (Higgins *et al.*, 2011). However, the breccia clast could have
been deposited by glacial activity from one of many distal impact structures in
Quebec (Reimold *et al.*, 2014). More importantly, the age of the Corossol structure is
poorly constrained between the Mid-Ordovician to just prior to the Quaternary
glaciations (Lajeunesse *et al.*, 2013).

To account for a non-crater-forming YD impact event, the inferred YD impactor
has been variously interpreted as a porous, loosely-bound, low-density impactor
(Firestone *et al.*, 2006); as highly fragmented multiple impactors (Kristan-Tollmann
and Tollmann, 1992, 1994; Firestone *et al.*, 2007; Firestone, 2009; Kennett *et al.*,
2009a,b; Bunch *et al.*, 2012; Wittke *et al.*, 2013; Napier *et al.*, 2013; Petaev *et al.*,

1
2
3 2013a,b); as oblique-trajectory impactors into the Laurentide ice sheet (Firestone *et al.*, 2007); or as a bolide airburst similar to the Tunguska event, but orders of
4 magnitude larger (Firestone, 2009; Israde-Alcántara *et al.*, 2012a). However,
5 bolide/impact scenarios that produce catastrophic environmental effects on an
6 intercontinental scale and disperse shock-transformation products globally – while not
7 forming a crater – have been argued to be improbable and inconsistent with geologic
8 evidence and physical models (Deutsch *et al.*, 1994; Melosh, 2009; French and
9 Koeberl, 2010; Boslough 2012; Boslough *et al.*, 2012, 2013; Boslough, 2013a;
10 Holliday *et al.*, 2014). It has further been suggested that the YD impact crater
11 remains undiscovered (Kristan-Tollmann and Tollmann, 1994; Firestone *et al.*, 2010a;
12 Kinzie *et al.*, 2014), despite suggestions that such a large and geologically young
13 crater should be easily recognized.
14
15
16
17
18
19
20
21
22

23 While there are no known impact structures in North America that date to the YD
24 onset, YD impact proponents nonetheless argue that physical evidence of the
25 impact/bolide event is present in sediments, at multiple sites in North America, South
26 America, Europe, and the Middle East that are claimed to be chronologically
27 synchronous with the Bølling-Ållerød / YD boundary (YDB) layer (see, Kennett *et al.*,
28 2015a,b). Elevated concentrations of a range of minerals interpreted as products
29 of impact/bolide processes and geochemical indicators of the impactor/bolide are
30 reported in these inferred YDB layers. Multifarious criticisms have been raised
31 regarding the identification, analysis, and interpretation of these materials as impact
32 markers (Deutsch *et al.*, 1994; Southon and Taylor, 2002; Pinter and Ishman, 2008;
33 Marlon *et al.*, 2009; Surovell *et al.*, 2009; Gill *et al.*, 2009; Paquay *et al.*, 2009, 2010;
34 Haynes *et al.*, 2010a,b; Scott *et al.*, 2010; Daulton *et al.*, 2010; Daulton, 2012; Pinter
35 *et al.*, 2011; Pigati *et al.*, 2012; Hardiman *et al.*, 2012; Boslough, 2013a,b; van
36 Hoesel, 2014; van Hoesel *et al.*, 2014; 2015; Holliday *et al.*, 2014; Thy *et al.*, 2015;
37 Scott *et al.*, 2015) as well as regarding the dating of their host sediment horizons (e.g.,
38 see Blaauw *et al.*, 2012; van Hoesel *et al.*, 2013, 2014; van Hoesel, 2014; Ives and
39 Froese, 2013; Meltzer *et al.*, 2014; Holliday *et al.*, 2014, Boslough *et al.*, 2015;
40 Holliday *et al.*, 2015). Accurate dating of stratigraphy at high resolution (required for
41 proper evaluation of the YD Impact Hypothesis) is difficult because sites frequently
42 have complex depositional/erosional histories and, except for lakebeds or ice sheets,
43 rarely preserve a continuous record of sedimentation. Consequently, measurements
44 that can provide sufficient chronological control are often poorly constrained or
45
46
47
48
49
50
51
52
53
54
55
56
57
58
59
60

1
2
3 nonexistent. Meltzer *et al.* (2014) performed a critical analysis of the chronologies at
4 29 sites (including the Greenland ice sheet) in which the YDB layer has been studied
5 in detail. The nature of the site, luminescence and radiocarbon ages, and age-depth
6 models were examined. Meltzer *et al.* (2014) concluded that sediments at only three
7 sites (Daisy Cave, San Miguel Island, California; Sheriden Cave, Ohio; and Big Eddy,
8 Missouri) could be dated with any confidence to the YD onset.

9
10 Materials that have been reported in YDB layer sediments and interpreted as
11 markers of supernova/impact/bolide processes include: tektites including one
12 embedded in a YD-dated tree trunk (Kristan-Tollmann and Tollmann, 1994);
13 paleoindian chert artifacts with high-velocity particle tracks, with embedded
14 chondritic micrometeorites, and with isotopic anomalies in K, U, and Pu (Firestone
15 and Topping, 2001; Firestone *et al.*, 2006, 2010a; Firestone, 2009); millimeter-scale
16 magnetic particles embedded in mammoth tusks and other Pleistocene megafaunal
17 remains (Firestone *et al.*, 2006); iron micrometeorites and mammoth tusks with rusty
18 pits (Baker *et al.*, 2008); radioactive sediment; radioactive mammoth bones and teeth
19 (Firestone *et al.*, 2006, 2007, 2010a,b); magnetic grains and elevated Ir concentrations
20 inside an extinct horse skull (West *et al.*, 2007; Firestone *et al.*, 2010a); magnetic
21 grains (Darrah *et al.*, 2007) and fullerenes with isotopically anomalous helium
22 (Darrah *et al.*, 2007; Firestone *et al.*, 2007); high abundance of unoxidized Fe-Ni, Cu-
23 Ni, Fe-Sn-Ni, and Pt minerals (Darrah *et al.*, 2007), anomalously high concentrations
24 of elements including U, Th, Ir, Pt, Ni, Cr, and Cu (see Firestone *et al.*, 2007; Bunch
25 *et al.*, 2010; Petaev *et al.*, 2013a,b; Andronikov *et al.*, 2014); chondritic iron oxide
26 framboids (Fayek *et al.*, 2012); pyrite framboids (Israde-Alcántara *et al.*, 2012a);
27 shocked quartz with planar deformation features (Mahaney *et al.*, 2010); siliceous
28 “scoria-like objects”; and lechatelierite (amorphous SiO₂) (Bunch *et al.*, 2012; Wittke
29 *et al.*, 2013a,b,c). While all the proposed impact markers discussed up to this point
30 are reported in one or several YDB sediments, the following markers are reported in
31 many to most YDB sediments studied: magnetic minerals (“grains”,
32 “microspherules”); carbonaceous combustion products (charcoal/soot, “glass-like
33 carbon,” “carbon elongates,” and “carbon spherules”) (e.g., see Firestone *et al.*, 2007;
34 Kennett *et al.*, 2008); nanometer to submicron-sized diamonds (loosely termed
35 “nanodiamonds”); as well as controversial phases “n-diamond” and “i-carbon” (e.g.,
36 see Kennett *et al.*, 2009a,b; Kinzie *et al.*, 2014). Further, excess ¹⁴C (defined by the
37 difference between radiocarbon dates and actual dates) is reported in terrestrial YDB
38
39
40
41
42
43
44
45
46
47
48
49
50
51
52
53
54
55
56
57
58
59
60

1
2
3 sediments, including tree remains, carbon spherules, glass-like carbon, and charcoal
4 contained within those sediments, as well in Icelandic YDB marine sediments (see
5 Kristan-Tollmann and Tollmann, 1994; Firestone and Topper 2001; Firestone *et al.*,
6 2006; Firestone, 2009; LaViolette, 2011). A number of these reported markers are no
7 longer considered credible, some are currently considered credible by only a few YD
8 impact proponents, and others continue to be widely debated (for reviews see Pinter *et*
9 *al.*, 2011; Boslough *et al.*, 2012; van Hoesel, 2014; van Hoesel *et al.*, 2014; Holliday
10 *et al.*, 2014; Taylor and Bar-Yosef, 2014).

11
12 Reports of nanodiamonds, in particular the rare 2H hexagonal polytype of
13 diamond, lonsdaleite, in YDB sediments; carbonaceous forms in these sediments
14 (carbon elongates, carbon spherules, and glass-like carbon); and Greenland ice, all
15 reportedly dating to the YDB, continue to be presented as strong evidence for
16 multiple impact/bolide events. We review the available data on diamonds as well as
17 associated carbonaceous minerals in sediments and provide additional data for
18 evaluating the YD Impact Hypothesis.

29 30 **Experimental Methods**

31
32 Millimeter-scale carbonaceous spherules and/or their fragments were isolated
33 from Arlington Canyon, Santa Rosa Island California sediments AC-003 (Kennett *et*
34 *al.*, 2008; 2009b) and SRI 09-28A from Locality III (Scott *et al.*, 2010; 2016) that
35 were dated to the YDB (12,800-13,100 cal a BP and 12,718-13,079 cal a BP,
36 respectively). Full details describing the collection/acquisition of those sediments are
37 provided in, Scott *et al.* (2016). Three different specimen sets were separately
38 crushed between sapphire discs: 1) five spherules/fragments from SRI 09-28A; 2)
39 eight spherules/fragments from AC-003; and 3) 13 acid-washed spherules/fragments
40 from AC-003. Each specimen set should contain at least one spherule containing
41 nanodiamonds given that Kinzie *et al.* (2014) state, “For carbon spherules, 111 of 153
42 samples investigated (73%) contained no detectable NDs [nanodiamonds]” and “ND
43 concentrations in carbon spherules is >35% at three sites.”

44
45 The finely crushed material from each set was deposited directly on amorphous
46 carbon-coated Cu transmission electron microscopy (TEM) grids (dry mount).
47 Additional TEM grids were prepared by depositing several μL aliquots of ethanol- or
48 nanopure water-suspended particles on the support film of the TEM grids (wet
49 mount).

1
2
3 In addition, a sequence of sediment from Lommel Belgium that bracketed and
4 included the presumed YDB-aged black mat that is reported to contain nanodiamonds
5 (Tian *et al.*, 2011) was provided by Ph. Claeys. Black mat sediment (7.064g) was
6 processed by acid dissolution. The sediment was first treated with 10M HF - 1M HCl
7 followed by 6M HCl, and this alternating treatment was repeated eight additional
8 times to remove silicates. This was followed by an alternating treatment of 6M HCl -
9 2M HF followed by 6M HCl - 0.6M H₃BO₃ and this was repeated four additional
10 times to dissolve remaining silicates. The residue was divided into colloidal and non-
11 colloidal fractions by colloidal separation using NaOH (pH = 10) following the
12 procedure commonly used to concentrate nanodiamonds from primitive meteorites
13 (see Lewis *et al.*, 1987). Due to the surface charge on the diamonds, they are
14 expected to stay in suspension in basic solution (Lewis *et al.*, 1989). The colloidal
15 fraction was then oxidized with Cr₂O₇²⁻ for 20.5 hours at ~80°C, and the remaining
16 residue was treated with HClO₄ for 2.0 hours at 204°C to further remove
17 carbonaceous matter other than the diamond. Colloidal separation of the residue was
18 again carried out in an attempt to further concentrate diamonds. Several µL aliquots
19 of the final colloidal suspension were deposited on TEM grids.
20
21

22 Specimen nanostructure was characterized using a JEOL JEM-2100F field
23 emission scanning transmission electron microscope. This instrument was equipped
24 with a high-resolution pole piece and a Schottky field emission gun: 0.5 nA at 1 nm
25 full width at half maximum probe diameter. This instrument was operated at 200kV
26 and, at that energy, has a rated point resolution of 0.23 nm and a lattice resolution of
27 0.1 nm. The instrument was equipped with a Bruker Quantax 200-STEM energy
28 dispersive X-ray spectroscopy (EDXS) system that consisted of an XFlash 60 mm²
29 active-area silicon drifted detector (SDD) as well as drift correction and HyperMap
30 software packages for spectral mapping. The instrument was also equipped with a
31 Gatan Model 863 Tridiem electron energy-imaging filter (GIF) with spectrum
32 imaging package (model 777 STEMPack) capable of electron energy loss
33 spectroscopy (EELS), EELS spectral imaging, and electron energy-filtered imaging.
34 The GIF utilized an Ultrascan 1000 FT 2048 x 2048 pixel, 16-bit, fiber optically
35 coupled, peltier-cooled, charge-coupled device (CCD) camera as the main detector.
36 For scanning (S)-TEM imaging, the instrument is equipped with Gatan Model 805
37 dark-field (DF) and bright-field (BF) STEM detectors as well as a Gatan Model 806
38 high angle annular (HAA)-DF STEM detector capable of Z-contrast imaging. For
39
40
41
42
43
44
45
46
47
48
49
50
51
52
53
54
55
56
57
58
59
60

conventional TEM imaging, the instrument has a retractable Gatan Orius SC1000B 2672 x 4008 pixels, 14 bit, fiber optically coupled, peltier-cooled CCD camera mounted on-axis directly above the GIF.

Elemental maps were acquired by STEM-EELS and STEM-EDXS spectral imaging in which EELS and EDXS spectra, respectively, were collected at each pixel position within a STEM region of interest. For STEM-EELS, a spectrometer 5 mm diameter entrance aperture, a collection angle of $2\beta = 22.66 \pm 0.06$ mrad, and an energy dispersion of 0.2 eV/channel were used to measure an energy loss region of 640 to 1050 eV. The EELS spectra were corrected for dark current and channel-to-channel gain variation of the CCD detector array and collected in the diffraction mode of the microscope (i.e., image coupling to the EELS spectrometer). Ratios of integrated EELS core-loss signal between elements were converted to their corresponding atomic ratios using partial cross-sections that were calculated from theoretical Hartree-Slater models. Unlike maps of EELS core-loss signal, maps of relative elemental compositions are, in principle, not influenced by variations in specimen thickness and electron diffraction. Ratios of integrated EDXS signal between elements were converted to their corresponding atomic ratios using standardless k-factors.

Experimental Results

Grain fragments of crushed carbonaceous spherules deposited on the TEM grids were systematically examined using a variety of techniques, including: selected area electron diffraction (SAED); bright-field, dark-field, and high-resolution imaging; and EDXS spot analysis. In total for all specimens, approximately 2000 grains were individually examined. The carbonaceous spherules primarily consisted of amorphous material (~95%) dominated by C and O, but also exhibiting a range of common elements that varied and included: Al, Ca, Fe, K, Mg, Na, P, S, Si, and/or Ti. A small fraction of these amorphous grains (~ several percent thereof) contained nanocrystals embedded within their matrix. In no case were any of these nanocrystals found to be carbonaceous, and no nanocrystals of diamond were observed. The remainder of the material (~5%) on the TEM grids from the crushed spherules consisted of submicron- (hundreds of nanometer-) sized monocrystalline non-carbonaceous minerals (e.g., aluminosilicates, pyrite), disordered graphite, and

1
2
3 polycrystalline aggregates of graphene/graphane/graphite (with some trace elements
4 present). In comparison, spherules examined in Daulton *et al.* (2010) contained
5 higher abundances of graphene/graphane/graphite aggregates than those examined
6 here. No diamonds were observed.
7
8

9
10 The acid-dissolution residues of YDB Lommel sediments contained submicron
11 crystals that were rich in O, Al, Si, Zr, and/or Ti. No diamonds were observed. The
12 Lommel residue was subsequently subjected to harsher acid dissolution treatment to
13 remove more of the non-diamond minerals. These further-processed residues still
14 contained abundant non-carbonaceous submicron crystals that survived acid
15 dissolution. Again no diamonds were observed, although an exhaustive search was
16 not performed. It was our intention to perform mass balance measurements of the
17 nanodiamond abundance in Lommel sediment horizons across the YDB. In the mass
18 balance approach, abundance is estimated from the initial mass of the sediment and
19 the mass of the resultant acid dissolution residue (assuming pure diamond isolates).
20 For non-pure isolates, mass modal abundances of minerals present in the residues are
21 required to estimate the initial diamond abundance. Due to the large amounts of
22 surviving non-diamond minerals in the Lommel black mat acid residue, and as will be
23 discussed later, quantitative mass balance measurements are incapable of yielding
24 any reliable abundance estimations for diamond. Therefore, it was not possible to
25 determine if there was a peak in the diamond concentration at the Lommel YDB.
26
27

28
29 van Hoesel (2014) were similarly unable to find nanodiamonds in their acid
30 dissolution residues of “black mat” YDB sediment from Lommel or from Murray
31 Springs, Arizona. As is the case for any mineral phase that was not observed, lack of
32 observation of diamond does not demonstrate the total absence of said mineral in the
33 samples examined; it can, at best, only constrain its possible abundance. For the
34 specimens we examined, it was not possible to accurately constrain the possible
35 abundance of nanodiamonds.
36
37

38 39 40 41 42 43 44 45 46 47 48 49 50 **The Nanodiamond Evidence**

51
52 One of the main lines of evidence presented to support the YD Impact Hypothesis
53 has been the reports of cubic and hexagonal nanodiamonds within bulk terrestrial and
54 lacustrine sediments; carbonaceous forms in these sediments (carbon elongates,
55 carbon spherules, and glass-like carbon); and Greenland ice, all reportedly dating to
56
57
58
59
60

1
2
3 the YDB (Firestone *et al.*, 2007, 2010a; Kennett *et al.*, 2009a,b; Kurbatov *et al.*, 2010;
4 Israde-Alcántara *et al.*, 2012a,b; Kinzie *et al.*, 2014). In a culmination of several
5 connected studies, Kinzie *et al.* (2014) report a nanodiamond-containing YDB
6 sediment horizon (with nanodiamonds completely absent above and below this
7 horizon) that span several continents at 9 out of 22 YDB sites studied. If correct, this
8 would suggest that a unique event occurred at the time this layer was deposited. In
9 regard to the nature of this event, much emphasis has been placed on the reported
10 discovery of lonsdaleite in YDB sediments (Kennett *et al.*, 2009b; Redmond and
11 Tankersley, 2011; Israde-Alcántara *et al.*, 2012a; Kinzie *et al.*, 2014).
12
13
14
15
16
17
18

19 *Lonsdaleite*

20
21 Lonsdaleite is the 2H hexagonal polytype of diamond (space group 194, $P6_3/mmc$:
22 $a = 2.508 \text{ \AA}$, $c = 4.183 \text{ \AA}$; Yoshiasa *et al.*, 2003) that differs structurally from the 3C
23 cubic polytype of diamond (space group 227, Fd_3m : $a = 3.567 \text{ \AA}$) in the stacking
24 sequence of tetrahedral close packed planes. In cubic diamond, the stacking sequence
25 is $(A^b)(B^c)(C^a)\dots$, whereas in lonsdaleite it is $(A^b)(B^a)\dots$ (Fig. 1). Lonsdaleite was
26 first discovered in laboratory experiments to synthesize diamond. Bundy and Kasper
27 (1967) after discovering lonsdaleite in transformation products of their high-static-
28 pressure compression experiments, became aware of a Netherlands patent (1965)
29 reporting the formation of hexagonal diamond by shock compression. They
30 subsequently identified lonsdaleite in the Canyon Diablo iron meteorite and attributed
31 it to shock formation (Bundy and Kasper, 1967). Additional reports of lonsdaleite
32 soon followed in meteorites (Hanneman *et al.*, 1967; Frondel and Marvin, 1967;
33 Clarke Jr. *et al.*, 1981; Daulton *et al.*, 1996); interplanetary dust (Rietmeijer and
34 Mackinnon, 1987); material from Ries, Popigai, Sudbury, and Obolon impact
35 structures (Hough *et al.*, 1995; Koeberl *et al.*, 1997; Goryainov *et al.*, 2014;
36 Shumilova *et al.*, 2014; Masaitis *et al.*, 1999; Gurov *et al.*, 2009); and peat from the
37 Tunguska bolide epicenter (Kvasnitsa *et al.*, 1979; Kvasnytsya *et al.*, 2013). This has
38 led to the perception that natural lonsdaleite was exclusively associated with shock
39 metamorphism. Although in the case of interplanetary dust, Rietmeijer and
40 Mackinnon (1987) argued against shock formation of the lonsdaleite they observed.
41
42
43
44
45
46
47
48
49
50
51
52
53
54

55 By contrast, the broader literature contains reports of natural lonsdaleite with no
56 directly connected association with shock processes. The Russian literature reports
57
58
59
60

1
2
3 lonsdaleite within titanium placers of the Ukrainian Shield (Sokhor *et al.*, 1973);
4 eclogites in Sal'niye Tundra, Kola Peninsula and the Urals (Golovnya *et al.*, 1977);
5 metamorphosed and metasomatically modified rocks of the Kumdykol diamond
6 deposit in North Kazakhstan (Shumilova *et al.*, 2011); and metamorphic rocks of the
7 Kokchetav Massif in North Kazakhstan (Dubinchuk *et al.*, 2010). Additionally,
8 lonsdaleite is reported in polycrystalline diamonds from the Udachnaya kimberlite
9 pipe, Yakutiya (Gorshkov *et al.*, 1999; Titkov *et al.*, 2001) and in similar
10 polycrystalline diamond from placers in Yakutiya (Kaminsky *et al.*, 1985; Petrovsky
11 *et al.*, 2013). The situation is complicated further in that some published data
12 identifying natural lonsdaleite, whether at impact structures or not, is not rigorously
13 convincing, with identifications sometimes based on several diffuse X-ray lines or a
14 few transmission electron microscopy (TEM) electron diffraction patterns. In some
15 studies (Koeberl *et al.*, 1997; Masaitis *et al.*, 1999; Titkov *et al.*, 2001), no data are
16 presented to support the lonsdaleite identification.
17
18
19
20
21
22
23
24
25

26 Microanalysis of lonsdaleite is difficult because it is always reported intergrown
27 with cubic diamond and sometimes graphite on the nanometer to submicron scale.
28 These phases often have high defect densities (e.g. dislocations, stacking faults, twin
29 planes, and disordered grain boundaries). Consequently, the interpretation of
30 structural measurements performed at a spatial scale greater than the grain size of
31 these polycrystalline diamonds (such as with X-ray diffraction and TEM SAED) is
32 not straightforward (see Daulton *et al.*, 2003). Németh *et al.* (2014) go so far as to
33 speculate that lonsdaleite does not exist and is an illusion created by lattice faults in
34 polycrystalline cubic diamond having nanometer grain size. Earlier, Cayron *et al.*
35 (2008) had shown that many reports of hexagonal-diamond Si had misinterpreted
36 micro/nanotwins in cubic-diamond Si; note that these Si phases are isostructural to
37 carbon's lonsdaleite and cubic diamond, respectively. A stacking fault of tetrahedral
38 close-packed planes in cubic diamond, $\dots(A^b)[(B^a)(A^b)(B^c)](C^a)\dots$ where a (C^b) plane
39 is missing and the preceding (B^c) plane is altered to (B^a) , necessarily forms a unit cell
40 and a half wide lamellae of lonsdaleite. While such lamellae should not be considered
41 a 2H hexagonal phase, there is sufficient evidence that well ordered $\dots(A^b)(B^a)\dots$
42 stacking of tetrahedral planes (Fig. 1, 2) occurs at scales up to, at least, tens of
43 nanometers for C (e.g., see Chen *et al.*, 1996; Daulton *et al.*, 1996; Lifshitz *et al.*,
44 2001; Kulnitskiy *et al.*, 2013), Si (Dahmen *et al.*, 1989; Cerva, 1991; Algra *et al.*,
45
46
47
48
49
50
51
52
53
54
55
56
57
58
59
60

1
2
3 2011; Hauge *et al.*, 2015), Ge (Xiao and Pirouz, 1992; Vincent *et al.*, 2014), and SiC
4 (Daulton *et al.*, 2003). Therefore, lonsdaleite, as well as other 2H hexagonal-diamond
5 isostructural phases, do exist on at least this spatial scale. Nevertheless, some
6 previous diffraction studies of heavily disordered cubic diamond minerals may have
7 overestimated or misidentified the presence of lonsdaleite.
8
9

10
11 While the literature on lonsdaleite can be murky, it is clear that shock
12 metamorphism has not been established as the exclusive mechanism by which
13 lonsdaleite is formed in terrestrial deposits. Recall that lonsdaleite has been reported
14 to form under high-static pressure (Bundy and Kasper, 1967). With the exception of
15 lonsdaleite, none of the studies of YDB sediments report identification of any of the
16 generally accepted and recognized shock minerals found at known impact structures
17 (c.f., French and Koeberl, 2010; van Hoesel, 2014; van Hoesel *et al.*, 2014).
18 Therefore, in the absence of other shocked minerals, the presence of lonsdaleite in
19 sediments can only provide tenuous evidence for an association with shock
20 processing. While it can be debated under what circumstances lonsdaleite can be
21 used as an impact marker, it is premature to consider this question further in assessing
22 the YD impact hypothesis as the reports of lonsdaleite in YDB sediments are not well
23 supported.
24
25

26
27
28
29
30
31
32
33 Daulton *et al.* (2010) demonstrated that Kennett *et al.* (2009b) misidentified
34 polycrystalline aggregates of graphene and graphane present in various carbonaceous
35 forms within the sediments as lonsdaleite. Independent studies have confirmed this
36 conclusion (Madden *et al.*, 2012; van Hoesel *et al.*, 2012; van Hoesel, 2014; Bement
37 *et al.*, 2014) and have failed to observe lonsdaleite in YDB sediments (Tian *et al.*,
38 2011). Graphene is a two-dimensional, single-atom-thick planar molecule with sp^2
39 bonded carbon (1.42 ± 0.1 Å bond length) in a hexagonal arrangement of 2.46 ± 0.02
40 Å edge length (Geim and Novoselov, 2007; Elias *et al.*, 2009). Graphene was first
41 observed as randomly oriented and uncorrelated sheets (i.e., a polycrystalline
42 aggregate) within the cores of many circumstellar graphite spherules isolated from
43 chondritic meteorites (Bernatowicz *et al.*, 1996). When graphene sheets are
44 periodically stacked normal to their plane (e.g., *AB*, *AA*, or *ABC* stacking), they form
45 various graphite polytype structures or turbostratic graphite if the stacking is
46 disordered. Graphane is a hydrogenated form of graphene, with H bonded on the
47 surface resulting in a out-of-plane puckering of C bonds and an effective contraction
48 of the hexagonal edge length to between $\approx 2.34 - 2.46$ Å (Elias *et al.*, 2009).
49
50
51
52
53
54
55
56
57
58
59
60

1
2
3 Kuratov *et al.* (2010) and Israde-Alcántara *et al.* (2012a), in which Kennett is a
4 coauthor, also misidentified lonsdaleite. For example, the high-resolution (HR)-TEM
5 lattice image of a nanocrystal from residues of Greenland ice shown in Figure 6 of
6 Kuratov *et al.* (2010) and identified as lonsdaleite is inconsistent with the crystal
7 structure of lonsdaleite. No crystallographic zone axis of lonsdaleite exists that can
8 display two differently oriented sets of 2.06 Å spaced {002} planes because there is
9 only one such set of planes in the structure (Fig. 3). The HR-TEM lattice image of a
10 nanocrystal from Lake Cuitzeo identified as twinned lonsdaleite and shown in Figure
11 11B of Israde-Alcántara *et al.* (2012a) is inconsistent with the crystal structure of
12 lonsdaleite. Using as spatial calibration the annotated 1.93 Å {101} spacing and scale
13 marker of their figure, we measure a spacing of 1.75 ± 0.05 Å for the nearly vertical
14 atomic planes (whose plane normal is perpendicular to the direction of the arrows in
15 the figure) with cross plane angle of $67.4 \pm 0.4^\circ$. Lonsdaleite lacks 1.75 Å spaced
16 planes (see Table 1). If the plane spacings were both 1.93 Å (i.e., closest lonsdaleite
17 spacing to our measured 1.75 Å spacing, see Table 1), the cross plane angle is
18 restricted to 52.41° for $\langle 011 \rangle$, 55.81° for $\langle 110 \rangle$, or 80.15° for $\langle 121 \rangle$, and all are
19 inconsistent with the HR-TEM image. Furthermore, the most common twin
20 configuration in diamond is twinning across the tetrahedral basal plane (e.g., $\{111\}_{3C}$
21 and $\{002\}_{2H}$) with twin angle of 70.53° ($\Sigma=3$) (see, Daulton *et al.*, 2003), and this
22 twin configuration will not alter the 2H lonsdaleite structure (i.e., stacking sequence).
23 Although stacking faults in lonsdaleite are frequently reported, twinning in lonsdaleite
24 is yet to be reported, with the exception of Israde-Alcántara *et al.* (2012a).
25
26
27
28
29
30
31
32
33
34
35
36
37
38
39

40 The recent study by Kinzie *et al.* (2014) reports no new or convincing evidence
41 for lonsdaleite. Contrary to earlier publications (Kennett *et al.*, 2009b; Kuratov *et al.*,
42 2010; Israde-Alcántara *et al.*, 2012a), the term “lonsdaleite-like” is now used to
43 describe these grains in Kinzie *et al.* (2014); note that all of these publications share at
44 least one coauthor. Curiously, Kinzie *et al.* (2014) also state that “lonsdaleite has
45 never been observed in any deposits of any age in Europe or North America, where
46 YDB lonsdaleite-like crystals are currently found.” The reason the term lonsdaleite-
47 like is now used is simple; these grains are not consistent with lonsdaleite. Kinzie *et al.*
48 (2014) argue that the grain shown in their Fig. 15, which is the same grain as
49 shown in Figures 2a-c and S2 of Kennett *et al.* (2009b), is a lonsdaleite-like grain.
50 The original identification of this grain by Kennett *et al.* (2009b) as lonsdaleite was
51
52
53
54
55
56
57
58
59
60

1
2
3 questioned by Daulton *et al.* (2010). Kinzie *et al.* (2014) wrote in response, “He
4 [Daulton *et al.* (2010)] questioned figure 2A-2C of Kennett *et al.* (2009b). Although
5 the analyses were insufficient to conclusively identify the nanocrystal shown as
6 lonsdaleite, we find no evidence to eliminate it as a possibility.” Despite their
7 inability to conclusively identify the grain, Kennett *et al.* (2009b) categorically
8 identified it as lonsdaleite, and Kinzie *et al.* (2014) identified it as lonsdaleite-like.
9

10 The grain in question displayed an azimuthally asymmetric polycrystalline
11 diffraction pattern with partial rings (forming doubled rings, see Fig. 4), and this is
12 indicative of heterogeneity either in the form of texturing or a multiphase mixture.
13 Texturing (defined as a distribution of crystallographic orientations of polycrystalline
14 grains, in which all possible orientations do not occur with equal probability) can
15 produce asymmetric ring intensity. However, texturing can be ruled out because this
16 diffraction pattern completely lacks intensity from many lonsdaleite reflections (see
17 Fig. 4) including (101) and (102) (see Table 1; Bundy and Kasper, 1967; Frondel and
18 Marvin, 1967) even for a wide range of specimen orientations achieved by tilting the
19 TEM goniometer. The diffraction pattern is thus inconsistent with the lonsdaleite
20 structure; however it is consistent with a two-phase aggregate of polycrystalline
21 graphene/graphane, a mineral assemblage (Fig. 5) observed ubiquitously in the
22 sediments (Daulton *et al.*, 2010; van Hoesel *et al.*, 2012; Bement *et al.*, 2014).
23
24
25
26
27
28
29
30
31
32
33
34

35 The identification by Kinzie *et al.* (2014) of other reported lonsdaleite-like grains
36 is based on the same analysis used by Israde-Alcántara *et al.* (2012a) to identify
37 lonsdaleite. Both use single, off-zone-axis HR-TEM lattice images and their fast
38 Fourier transformations (FFTs) that can easily yield misleading results (e.g., see
39 Kohno *et al.*, 2003; Cayron *et al.*, 2008; den Hertog *et al.*, 2012) and cannot provide a
40 conclusive mineral identification. In particular, Kohno *et al.* (2003) demonstrated
41 that HR-TEM images of twinned nanocrystals of cubic-diamond Si can be confused
42 with hexagonal-diamond Si. The structural information contained in an individual
43 HR-TEM image and its associated diffraction pattern is incomplete because they are
44 two-dimensional projections of three-dimensional structures with potentially complex
45 twin and stacking-fault configurations (see, Daulton *et al.*, 2003; den Hertog *et al.*,
46 2012). The analysis of a single HR-TEM image cannot conclusively determine the
47 structure of a nanocrystal; instead, methods such as comparison of simulated phase-
48 contrast lattice images to a through-focus series of HR-TEM images must be applied
49 for a range of nanocrystal orientations (see also Billinge and Levin, 2007).
50
51
52
53
54
55
56
57
58
59
60

1
2
3 Kinzie *et al.* (2014) comment on an EELS analysis of a lonsdaleite-like grain,
4 “Figure 17B is an HR-TEM image of a rounded 10-nm lonsdaleite-like crystal. The
5 ED[X]S results were presented in Kurbatov *et al.* (2010), confirming that the crystal
6 is carbon, and an EELS spectrum indicated high sp^3 bonding.” However, the only
7 EDXS and EELS results presented in Kurbatov *et al.* (2010) are found in their Figure
8 8 for a grain they claim is “n-diamond,” not lonsdaleite. Further, the EELS C-K edge
9 spectra and the associated low-loss plasmon peak at 22 eV reported by Kurbatov *et al.*
10 (2010) are consistent with amorphous C (e.g., see Kincaid *et al.*, 1978; Fallon and
11 Brown, 1993) from the ~ 70 nm thick TEM support film upon which the nanocrystals
12 were mounted. The EELS spectra shown by Kinzie *et al.* (2014) for “n-diamond” is
13 also consistent with amorphous C; as in the case of Kurbatov *et al.* (2010) and others,
14 the spectra is likely dominated by contributions from the amorphous C TEM support
15 film. Nevertheless, no C-K edge EELS spectrum of the lonsdaleite-like grain was
16 published that can be evaluated here. Adding to the confusion, Kinzie *et al.* (2014)
17 state in their Figure 17b caption, “B, HR-TEM image of a 10-nm lonsdaleite-like
18 monocystal from Lake Cuitzeo (YDB: 493 ppb at 280 cmbs).” However, Kurbatov
19 *et al.* (2010) did not examine Lake Cuitzeo specimens.
20
21
22
23
24
25
26
27
28
29
30
31
32

33 *Cubic Diamond*

34
35 Nanometer-sized grains of the 3C cubic polytype of diamond in YDB sediments
36 has also been interpreted as supporting the YD Impact Hypothesis. This
37 interpretation is based on reports of cubic diamonds of nanometer to tens-of-micron
38 size in Cretaceous/Tertiary boundary sediments (Carlisle and Braman, 1991; Hough *et al.*,
39 1997); of submicron to millimeter size at Ries, Popigai, Sudbury, Gardnos, and
40 Obolon impact structures (Hough *et al.*, 1995; Koeberl *et al.*, 1997; Masaitis *et al.*,
41 1999; Gilmour *et al.*, 2003; Gurov *et al.*, 2009); and of submillimeter size in peat at
42 the Tunguska bolide epicenter (Kvasnitsa *et al.*, 1979; Kvasnytsya *et al.*, 2013).
43 Furthermore, ureilite and iron meteorites contain submicron- to millimeter-sized cubic
44 diamond believed formed by shock (see Ksanda and Henderson, 1939; Nakamuta and
45 Aoki, 2000) and primitive carbonaceous chondrites contain presolar cubic
46 nanodiamonds (0.5-10 nm diameter, mean 2.6 nm) believed formed primarily by gas
47 condensation (Lewis *et al.*, 1987; Daulton *et al.*, 1996). Submillimeter to centimeter
48 polycrystalline aggregates of cubic diamond found in alluvial placers, known as
49
50
51
52
53
54
55
56
57
58
59
60

1
2
3 carbonados (from Mesoproterozoic deposits in Brazil and Central Africa) and
4 yakutites/carbonados (from Yakutiya, Russia), have been attributed to formation by
5 shock metamorphism (see Smith and Dawson, 1985; Kaminsky, 1994). However,
6 Cartigny (2010) argued that a mantle origin for carbonados cannot be excluded.
7 Formation mechanisms other than shock such as crystallization from a carbon-
8 supersaturated fluid have been suggested (Ketcham and Koeberl, 2013), and the
9 origins of carbonados remain poorly understood (Haggerty, 1999; 2014; Heaney,
10 2005; McCall, 2009; Cartigny, 2010). Yakutites have been described as differing
11 from carbonados in several aspects (but see McCall, 2009), one being that they
12 contain lonsdaleite (Kaminsky, 1994; Heaney *et al.*, 2005), which is traditionally
13 associated with shock processing. However, yakutites have been reported in
14 kimberlite pipes (Gorshkov *et al.*, 1999; Titkov *et al.*, 2001), which are volcanic in
15 origin.
16

17
18 On the other hand, cubic diamonds of non-impact and non-shock origin occur
19 widely in the crust. Centimeter-size down to tens-of-micron, or smaller, cubic
20 diamonds (including polycrystalline aggregates variously known as framesite, boart,
21 ballas, stewartite, diamondite, and sometimes carbonado/yakutite) occur as xenocrysts
22 in volcanic rocks (e.g., kimberlites, lamproites, and ultramafic lamprohyres) of pipe
23 structures formed during mantle eruptions through the crust (see Haggerty, 1999;
24 Gorshkov *et al.*, 1999; Kurat and Dobosi, 2000; Titkov *et al.*, 2001; Nowicki *et al.*,
25 2007; Dobosi *et al.*, 2008; Shirey *et al.*, 2013). Micron- to tens-of-micron-sized cubic
26 diamonds (microdiamonds) have been found worldwide as inclusions within or in
27 association with metamorphosed crustal rocks of regional metamorphic terrains:
28 Kokchetav Massif, Kazakhstan (Rozen *et al.*, 1972; Sobolev and Shatsky, 1990);
29 Maksyutov Complex, Russia (Bostick *et al.*, 2003); Western Gneiss region, Norway
30 (Dobrzhinetskaya *et al.*, 1995); Bohemian Massif, Germany (Stöckhert *et al.*, 2001);
31 Lago di Cignana Western Alps, Italy (Frezzotti *et al.*, 2014); Rhodope Massif, Greece
32 (Schmidt *et al.*, 2010); Dabie Shan, Su-Lu, and Qinling regions, China (Xu *et al.*,
33 1992, 2005; Yang *et al.*, 2003); and Akluilák minette dike system, Canada (Cartigny
34 *et al.*, 2004). Polycrystalline cubic microdiamonds have also been found in the
35 ultrahigh-pressure metamorphic terrain of Erzgebirge, Germany (Dobrzhinetskaya *et al.*
36 *et al.*, 2013). The formation of metamorphic microdiamonds has been attributed to deep
37 continental subduction of primary crustal rocks followed by rapid tectonic uplift of
38 recrystallized material to the crust (see Ogasawara, 2005; Dobrzhinetskaya *et al.*,
39
40
41
42
43
44
45
46
47
48
49
50
51
52
53
54
55
56
57
58
59
60

1
2
3 2007; Dobrzhinetskaya, 2012). However, fluid-metasomatic formation of
4 microdiamond in the crust has also been suggested (see Pechnikov and Kaminsky,
5 2008). Hawaiian mantle-derived, garnet pyroxenite xenoliths have been found to
6 contain cubic nanodiamonds within melt inclusions (Wirth and Rocholl, 2003) and
7 CO₂-H₂O-H₂S fluid inclusions (Frezzotti and Peccerillo, 2007). Cubic nanodiamonds
8 also may be prevalent in metamorphic terrains; MicroRaman spectra of inclusions in
9 garnets from the Maksyutov Massif (Bostick *et al.*, 2003) and the Rhodope Massif
10 (Perraki *et al.*, 2006) suggest the presence of nanodiamonds or nanodiamond
11 aggregates, although this has not been confirmed by other microanalytical techniques.
12 All of these diamonds can be eroded from their source rocks, transported, and
13 deposited into placer deposits, sediments (see de Wit, 2004), and sedimentary
14 conglomerates (see Fleischer, 1998).
15
16
17
18
19
20
21
22

23 Cubic nanodiamonds have also been reported in sediments and in carbonaceous
24 forms within sediments without clear association with impact structures and which do
25 not date to the YDB. Nanometer to submicron-sized diamond were reported in
26 carbon spherules, similar to those reported at the YDB, but from modern forest soils
27 in Germany and Belgium (Yang *et al.*, 2008). Similar sized nanodiamonds were also
28 reported in glass-like carbon from the Usselo horizon in Geldrop-Aalsterhut, The
29 Netherlands; however that horizon postdates the YD onset by two centuries (van
30 Hoesel *et al.*, 2012, 2013).
31
32
33
34
35

36 Diamond is chemically inert, highly resistant to weathering (e.g., decomposition
37 and transformation), and will persist in the surface environment. Erosion of diamond-
38 bearing source rocks and transport by wind or water could widely redistribute
39 nanometer- to submicron-sized diamonds into distant alluvial deposits and sediments
40 that bear little resemblance to the diamond source rocks. Similarly could be the case
41 for micron-sized host grains containing nanodiamond inclusions, and those inclusions
42 would be extracted from their host minerals during laboratory acid dissolution of the
43 sediments. It is intriguing that nanodiamonds are present in the Pleistocene to
44 Holocene sediments, and work is clearly needed to understand their origin. Similar to
45 lonsdaleite, the literature on nanometer- to submicron-sized cubic diamonds in
46 terrestrial deposits is complicated by the varying strength of the published data. Also,
47 questions of laboratory contamination have been raised for some metamorphic rocks
48 (see Chopin and Sobolev, 1995). Nevertheless, it is clear that the presence of these
49 cubic diamonds in sediments cannot be used as an impact marker because shock
50
51
52
53
54
55
56
57
58
59
60

1
2
3 metamorphism does not appear to be the predominant formation mechanism of
4 diamonds of that size found in the crust.
5
6

7 8 *Nanocrystals of “n-diamond” and “i-carbon”* 9

10 In addition to the two known polytypes of diamond, impact proponents also report
11 nanometer-sized crystals of “n-diamond” and “i-carbon” in YDB sediments and
12 Greenland ice (Kinzie *et al.*, 2014). While neither are polytypes of diamond, impact
13 proponents often describe them as nanodiamonds. They also interpret these
14 nanocrystals as evidence for a YD impact event. “N-diamond” is a hypothesized
15 carbonaceous phase that displays diffraction lines strikingly similar to that of 3C
16 diamond, with the notable exception that the Bragg reflections kinematically
17 forbidden in 3C diamond are present. This has led to the speculation that “n-
18 diamond” is a modified form of 3C diamond polytype (Hirai and Kondo, 1991).
19 Aggregates of nanocrystals that display “n-diamond” reflections sometimes exhibit
20 additional reflections that are attributed to another hypothesized nanocrystalline
21 carbon phase termed “C₈” or “i-carbon” (see, Matyushenko *et al.*, 1979; Hirai and
22 Kondo, 1991). The atomic structure of “n-diamond” has yet to be determined and its
23 identification as a modified form of 3C diamond remains controversial (e.g., see Wen
24 *et al.*, 2007). Similarly, “i-carbon” is controversial, and its atomic structure has not yet
25 been determined.
26
27

28 In YDB sediments, “n-diamonds” are usually reported at much higher
29 concentrations than cubic diamonds, and in many cases where “n-diamonds” are
30 reported cubic diamonds are not observed. Table D2 of the supplementary materials
31 of Kinzie *et al.* (2014) report “n-diamonds” present in 22 of 24 sites that date to the
32 YDB, “i-carbon” in 20 of these sites, cubic diamonds were reported in only 8 of these
33 sites, and hexagonal diamond in only 5. Israde-Alcántara *et al.* (2012a) report “n-
34 diamonds” at Lake Cuitzeo, but write, “. . . we could not unequivocally identify the
35 cubic allotrope. This may be due to masking by i-carbon and/or n-diamonds, which
36 share some d-spacings with cubic NDs.” Kinzie *et al.* (2014) write in regard to Lake
37 Cuitzeo, “Using HRTEM and FFT, we identified . . . n-diamonds, i-carbon, and
38 cubics [cubic diamond] have a ratio of 3:1:1.”
39
40
41
42
43
44
45
46
47
48
49
50
51
52
53
54

55 The presence of “n-diamonds” in sediments cannot be used as an impact marker
56 because they are also reported in sediments that do not date to the YDB and,
57
58
59
60

1
2
3 importantly, their formation by impact processes has not be demonstrated.
4 Nanocrystals with diffraction patterns consistent with “n-diamond” were reported in
5 surface forest soils in Germany and Belgium (Yang *et al.*, 2008). At Bull Creek,
6 Oklahoma, cubic nanodiamonds were not found, but nanocrystals of “n-diamond”
7 were reported in multiple horizons (Madden *et al.*, 2012) and in sediments dated
8 <3000 ¹⁴C a BP (Bement *et al.*, 2014). Firestone *et al.* (2007) reported nanodiamonds
9 in glass-like carbon from the rims of Carolina Bays using nuclear magnetic resonance
10 (NMR); while that identification was questioned (Kerr *et al.*, 2008), Kinzie *et al.*
11 (2014) reported confirmation by TEM. Kinzie *et al.* (2014) wrote, “We used a
12 focused ion beam to mill a piece of glass-like carbon extracted from the YDB layer at
13 the M33 site, the rim of a Carolina Bay in Myrtle Beach, South Carolina (for site
14 details, see Firestone *et al.*, 2007). The TEM analyses showed that diamonds were
15 present only from the surface down to a depth of ≈0.75 μm and were not observed in
16 the interior (fig. 14A).” The caption for Figure 14 of Kinzie *et al.* (2014) identifies
17 these nanocrystals as “n-diamond”. Firestone *et al.* (2010) earlier reported, “All of
18 the Bay rims examined [15 in total] were found to have, throughout their entire 1.5-
19 m sandy rims, a typical assemblage of YDB markers (magnetic grains, magnetic
20 microspherules, iridium, charcoal, soot, glass-like carbon, *nanodiamonds* [emphasis
21 added], carbon spherules, and fullerenes with helium-3).” However, Firestone *et al.*
22 (2010a) did not disclose the methods and data by which the nanodiamonds were
23 identified.
24
25
26
27
28
29
30
31
32
33
34
35
36
37

38 The Carolina Bays are thousands of shallow elliptical depressions with elevated
39 rims scattered along the Atlantic Coastal Plain (see Brooks *et al.*, 2010), which
40 formed asynchronously over a significant period of time with multiple periods of rim
41 accretion with intervening periods of erosion (Grant *et al.*, 1998; Rodriguez *et al.*,
42 2012). Meltzer *et al.* (2014) write, “Firestone *et al.* (2) subsequently admitted that the
43 ages of the Carolina Bays vary but then suggested that because sediment from 15
44 Carolina Bays contained supposed impact markers and because such impact markers
45 occur only in the supposed YDB layer and were ‘identical to those found elsewhere in
46 the YDB layers that date to 12.9 ka,’ the supposed YDB layer in the Carolina Bays
47 must be the same age (ref. 2, p. 16019).” Rodriguez *et al.* (2012) studied Lake
48 Mattamuskeet, one of four Carolina Bays on the Albemarle-Pamlico Peninsula of
49 North Carolina that Firestone *et al.* (2007, 2010a) reported contain impact markers
50 (including nanodiamonds) and concluded that rim accretion significantly postdated
51
52
53
54
55
56
57
58
59
60

1
2
3 the YD stadial. In fact, Firestone (2009) measured radiocarbon ages between 685-
4 8455 ^{14}C a BP for glass-like carbon from several Carolina Bays including Myrtle that
5 is reported to contain nanodiamonds (Firestone *et al.*, 2007; Kinzie *et al.*, 2014).
6 Firestone (2009) suggests that the glass-like carbon from the Carolina Bays must be
7 enriched in ^{14}C relative to their *assumed* YD age and offered the implausible scenario
8 that the YD impactor was ejected from a near-Earth supernova to account for the
9 enrichment. A more probable explanation is that the assumed YD age of those
10 Carolina Bays is incorrect.
11
12
13
14
15
16
17

18 *Nanodiamond Host Minerals*

19
20 Nanometer-sized diamond, “n-diamond”, and/or “i-carbon” have been reported
21 within glass-like carbons (Firestone *et al.*, 2007, 2010a; Firestone, 2009; Israde-
22 Alcántara *et al.*, 2012a supplemental materials; Kinzie *et al.*, 2014), carbon elongates
23 (Kennett *et al.*, 2009b), and carbon spherules (Firestone, 2009, Firestone *et al.*, 2010a;
24 Kennett *et al.*, 2009a; Israde-Alcántara *et al.*, 2012a supplemental materials; Kinzie *et*
25 *al.*, 2014) from YDB sediments as well as acid dissolution residues of these
26 sediments. Glass-like carbon was described by Firestone *et al.* (2007) as “Pieces up
27 to several cm in diameter . . . associated with the YDB and [Carolina] Bays, and their
28 glassy texture suggests melting during formation, with some fragments grading into
29 charcoal.” Firestone *et al.* (2007) also describe “Carbon spherules (0.15–2.5 mm) are
30 black, highly vesicular, subspherical-to-spherical objects (Fig. 3). SEM analyses
31 show them to have cracked and patterned surfaces, a thin rind, and honeycombed
32 (spongy) interiors. SEM/energy dispersive spectrometer and microprobe analyses
33 show that the spherules are dominantly carbon (75%).” Kennett *et al.* (2009b)
34 describes, “Carbon elongates differ from the carbon spherules in having an irregular
35 array of walls and voids, whereas carbon spherule interiors display a well-organized
36 honeycomb (reticulated) pattern. Both types are composed entirely of glass-like
37 amorphous carbon indicative of high-temperature formation. The general shape of
38 elongates ranges from angular (hexagonal in cross-section) to subrounded.” Kinzie *et*
39 *al.* (2014), with Kennett as a coauthor, report carbon spherule abundances at
40 Arlington Canyon that are equal to the sum of carbon spherule and carbon elongate
41 concentrations reported by Kennett *et al.* (2008, 2009b). No explanation was
42
43
44
45
46
47
48
49
50
51
52
53
54
55
56
57
58
59
60

1
2
3 provided by Kinzie *et al.* (2014) on why they reclassified the so-called carbon
4 elongates as carbon spherules (see also Hardiman *et al.*, 2012).
5

6 While carbon spherules may have multiple origins, most carbon spherules studied
7 in YDB sediments have external and internal morphologies indistinguishable from
8 sclerotia (Fig. 6) of saprobic (e.g., *Sclerotium Athelia rolfsii*), phytopathogenic (e.g.,
9 *Rhizoctonia solani*, *Botryotinia cinerea*), and ectomycorrhizal (e.g., *Cenococcum*
10 *geophilum*) fungi (Scott *et al.*, 2010), to name a few. Sclerotia are resting bodies (i.e.,
11 persistent propagules) of fungi, composed of closely packed (pseudoparenchymatous)
12 hyphae, which have a range of morphologies and form during periods of environmental
13 stress (see Smith *et al.*, 2015). Typically, they usually consist of an outer rind of
14 tightly packed hyphal tips that develop an impervious thick-walled and pigmented
15 (melanized) layer surrounding a medulla of hyphae with extended vacuoles that store
16 reserves of glycogen, proteins, lipids, and polyphosphates. Viable sclerotia can remain
17 dormant for many years during adverse conditions and germinate in favorable
18 conditions to produce mycelia. Sclerotia are ubiquitous in forest litter and soils, and
19 even after death can persist for at least many thousands of years (see Trappe, 1969;
20 Hormes *et al.*, 2004; Benedict, 2011; McLaren *et al.*, 2014). Further, fossil sclerotia
21 (or similar structures) of *Palaeosclerotium pusillum* have been reported preserved in
22 the matrix of coal dated to the Middle Pennsylvanian (≈ 310 Ma) (Rothwell, 1972;
23 Dennis, 1976; Taylor *et al.*, 2015). Consequently, sclerotia are common at
24 archaeological sites (e.g., see McWeeney, 1989; Shay and Kapinga, 1997; Deal,
25 2005), and the common association of sclerotia with wood-charcoal in sediments has
26 lead to the suggestion that charring of sclerotia by wildfires may contribute to their
27 long-term preservation (Benedict, 2011). Carbon spherules were extracted from YDB
28 sediments by flotation (Firestone *et al.*, 2007; Kennett *et al.*, 2008, 2009b; Israde-
29 Alcántara *et al.*, 2012a; Kinzie *et al.*, 2014), and this method will readily collect dead
30 sclerotia, which float in water (see Trappe, 1969; Shay and Kapinga, 1997, Benedict,
31 2011). Scott *et al.* (2010) suggested that carbon elongates in YDB and other
32 sediments include non-spherical sclerotia and/or arthropod fecal material.
33
34
35
36
37
38
39
40
41
42
43
44
45
46
47
48
49
50

51 Israde-Alcántara *et al.* (2012a) responded to Scott *et al.* (2010), asserting that “. . .
52 charred and uncharred sclerotia have textured, filamentous, low-reflectivity interiors,
53 whereas at Cuitzeo [their study site], SEM imaging demonstrates that CSp have
54 smooth, glassy, highly reflective interiors with no evidence of filamentous structure
55 observed in fungal sclerotia (or cellular structure found in charcoal) (SI Appendix,
56
57
58
59
60

1
2
3 Fig. 5)” (see also Israde-Alcántara *et al.*, 2012b). However, fungal sclerotia can be
4 hollow (see, Ferdinandsen and Winge, 1925; Trappe, 1931) and have smooth interior
5 surfaces (Fig. 7) (private communication M. Watanabe). In the image of a carbon
6 spherule from Arlington Canyon shown in the supplemental materials of Kennett *et*
7 *al.* (2009b) septal pores which allow movement of cytoplasm and organelles in fungi
8 hyphae (see, Reichle and Alexander, 1965; van Peer *et al.*, 2009) are clearly evident
9 (Fig. 8) and conclusively identify it as a fungal sclerotia at some undetermined stage
10 of diagenesis (private communication M. Watanabe). Septa pores are also clearly
11 evident in the image of a carbon spherule from a Carolina Bay that is attributed to
12 Allen West (see, Largent, 2008). We also observed septal pores in carbon spherules
13 from the YDB layer at Arlington Canyon provided to us by G. J. West and J. J.
14 Johnson (e.g., see Fig. S5D of the supplemental materials of Scott *et al.*, 2010).
15 Indeed, we found sclerotia at many levels at locality AC003 and other localities at
16 Arlington. Further, our measured elemental composition of an Arlington Canyon
17 carbon spherule is similar to that of fossil sclerotia. The amorphous matrix of the
18 spherules had an elemental composition, as determined by EDXS, of 82.49 at.% C,
19 13.40 at.% O, and 0.35 at.% Si, consistent with that reported for YDB carbon
20 spherules (Firestone *et al.*, 2010a; Israde-Alcántara *et al.*, 2012a). In comparison,
21 fossilized sclerotia from sediments of Lake Biwa, Japan contained 83 at.% C, 15 at.%
22 O, and 2 at.% Si (Itoh *et al.*, 2013). Sclerotia undergo diagenetic changes in
23 composition and structure while in sediments. Itoh *et al.* (2012) demonstrated that the
24 high $O/C \approx 0.5$ in initially viable *C. geophilum* sclerotia within soils decreased to 0.3 to
25 0.1 with increased diagenesis.

26
27
28
29
30
31
32
33
34
35
36
37
38
39
40
41
42
43
44
45
46
47
48
49
50
51
52
53
54
55
56
57
58
59
60
61
62
63
64
65
66
67
68
69
70
71
72
73
74
75
76
77
78
79
80
81
82
83
84
85
86
87
88
89
90
91
92
93
94
95
96
97
98
99
100
101
102
103
104
105
106
107
108
109
110
111
112
113
114
115
116
117
118
119
120
121
122
123
124
125
126
127
128
129
130
131
132
133
134
135
136
137
138
139
140
141
142
143
144
145
146
147
148
149
150
151
152
153
154
155
156
157
158
159
160
161
162
163
164
165
166
167
168
169
170
171
172
173
174
175
176
177
178
179
180
181
182
183
184
185
186
187
188
189
190
191
192
193
194
195
196
197
198
199
200
201
202
203
204
205
206
207
208
209
210
211
212
213
214
215
216
217
218
219
220
221
222
223
224
225
226
227
228
229
230
231
232
233
234
235
236
237
238
239
240
241
242
243
244
245
246
247
248
249
250
251
252
253
254
255
256
257
258
259
260
261
262
263
264
265
266
267
268
269
270
271
272
273
274
275
276
277
278
279
280
281
282
283
284
285
286
287
288
289
290
291
292
293
294
295
296
297
298
299
300
301
302
303
304
305
306
307
308
309
310
311
312
313
314
315
316
317
318
319
320
321
322
323
324
325
326
327
328
329
330
331
332
333
334
335
336
337
338
339
340
341
342
343
344
345
346
347
348
349
350
351
352
353
354
355
356
357
358
359
360
361
362
363
364
365
366
367
368
369
370
371
372
373
374
375
376
377
378
379
380
381
382
383
384
385
386
387
388
389
390
391
392
393
394
395
396
397
398
399
400
401
402
403
404
405
406
407
408
409
410
411
412
413
414
415
416
417
418
419
420
421
422
423
424
425
426
427
428
429
430
431
432
433
434
435
436
437
438
439
440
441
442
443
444
445
446
447
448
449
450
451
452
453
454
455
456
457
458
459
460
461
462
463
464
465
466
467
468
469
470
471
472
473
474
475
476
477
478
479
480
481
482
483
484
485
486
487
488
489
490
491
492
493
494
495
496
497
498
499
500
501
502
503
504
505
506
507
508
509
510
511
512
513
514
515
516
517
518
519
520
521
522
523
524
525
526
527
528
529
530
531
532
533
534
535
536
537
538
539
540
541
542
543
544
545
546
547
548
549
550
551
552
553
554
555
556
557
558
559
560
561
562
563
564
565
566
567
568
569
570
571
572
573
574
575
576
577
578
579
580
581
582
583
584
585
586
587
588
589
590
591
592
593
594
595
596
597
598
599
600
601
602
603
604
605
606
607
608
609
610
611
612
613
614
615
616
617
618
619
620
621
622
623
624
625
626
627
628
629
630
631
632
633
634
635
636
637
638
639
640
641
642
643
644
645
646
647
648
649
650
651
652
653
654
655
656
657
658
659
660
661
662
663
664
665
666
667
668
669
670
671
672
673
674
675
676
677
678
679
680
681
682
683
684
685
686
687
688
689
690
691
692
693
694
695
696
697
698
699
700
701
702
703
704
705
706
707
708
709
710
711
712
713
714
715
716
717
718
719
720
721
722
723
724
725
726
727
728
729
730
731
732
733
734
735
736
737
738
739
740
741
742
743
744
745
746
747
748
749
750
751
752
753
754
755
756
757
758
759
760
761
762
763
764
765
766
767
768
769
770
771
772
773
774
775
776
777
778
779
780
781
782
783
784
785
786
787
788
789
790
791
792
793
794
795
796
797
798
799
800
801
802
803
804
805
806
807
808
809
810
811
812
813
814
815
816
817
818
819
820
821
822
823
824
825
826
827
828
829
830
831
832
833
834
835
836
837
838
839
840
841
842
843
844
845
846
847
848
849
850
851
852
853
854
855
856
857
858
859
860
861
862
863
864
865
866
867
868
869
870
871
872
873
874
875
876
877
878
879
880
881
882
883
884
885
886
887
888
889
890
891
892
893
894
895
896
897
898
899
900
901
902
903
904
905
906
907
908
909
910
911
912
913
914
915
916
917
918
919
920
921
922
923
924
925
926
927
928
929
930
931
932
933
934
935
936
937
938
939
940
941
942
943
944
945
946
947
948
949
950
951
952
953
954
955
956
957
958
959
960
961
962
963
964
965
966
967
968
969
970
971
972
973
974
975
976
977
978
979
980
981
982
983
984
985
986
987
988
989
990
991
992
993
994
995
996
997
998
999
1000

Israde-Alcántara *et al.* (2012a) also responded that “CSp also contain numerous noncarbon particles, including aluminosilicates, indicating that these cannot be primary biological entities, such as sclerotia.” Their reasoning is inconsistent with their own observation that “CSp are dominantly carbon (>87%) with minor particulates, such as Si, Al, and Fe, concentrated in the rind,” suggesting that the aluminosilicates are embedded in or present on the surface of the carbon spherules. Furthermore, Israde-Alcántara *et al.* (2012a) neglect studies such as Watanabe *et al.* (2001, 2004a) that found the exteriors and interiors of sclerotia contained inorganic components such as Al_2O_3 , SiO_2 , and Fe_2O_2 . Inorganic nanocrystals (e.g., boehmite) were also reported in *C. geophilum* sclerotia and were thought to have formed by Al dissolution-precipitation reactions (Watanabe *et al.*, 2004b).

1
2
3 Kinzie *et al.* (2014) claimed that, “There is no credible mechanism by which fungi
4 can create NDs in sclerotia,” and “There is no plausible process by which sclerotia
5 could extract NDs from surrounding sediment.” Within crushed spherule fragments
6 that we studied (from Arlington Canyon, AC-003), TEM revealed the presence of
7 amorphous-carbonaceous grains with numerous rounded nanocrystals embedded with
8 their matrix (Fig. 9) that were strikingly similar to nanodiamond containing fragments
9 reported by Kennett *et al.* (2009b), Bement *et al.* (2014), and Kinzie *et al.* (2014).
10 Electron diffraction from the embedded nanocrystals is nearly identical to that
11 reported for “n-diamond” in YD boundary sediments (Fig. 10). Kinzie *et al.* (2014)
12 report that “n-diamond” is far less resistant to oxidation by perchloric acid during acid
13 dissolution than cubic diamond, and state, “This was an advantage when analyzing
14 cubic NDs but a major disadvantage for the other allotropes, which were no longer
15 present [in the acid residues].”

16
17
18
19
20
21
22
23
24
25 To further characterize the nanocrystals embedded in the Arlington Canyon
26 carbon spherule fragments, EDXS and EELS spectral image maps were collected, and
27 representative elemental maps are shown in Fig. 11. These maps revealed that the
28 nanocrystals were Cu (see also Daulton *et al.*, 2010). Native Cu (space group 225,
29 *Fm-3m*: $a = 3.6149 \text{ \AA}$) has the same diffraction lines as “n-diamond” that differ by \approx
30 1% in plane spacing (Table 2). The Cu nanoparticles may be stabilized from
31 oxidation by the amorphous carbon that surrounds them, by adsorbed surface groups,
32 or by a protective oxide surface layer. The primary oxidation product of copper,
33 Cu_2O , is also present in the spherules (Daulton *et al.*, 2010). Cuprite, Cu_2O (Space
34 Group 224, *Pn-3m*: $a = 4.2696 \text{ \AA}$), has essentially the same diffraction lines as the
35 controversial “i-carbon”, with planar spacings differing by $\approx 1\%$ (Table 2). The
36 crushed spherules also contained nanocrystals that were not embedded in any matrix
37 (Fig. 12). Elemental mapping demonstrated these nanocrystals were copper sulfides
38 (e.g., covellite, chalcocite, digenite, geerite, anilite, djurleite and/or roxbyite). All the
39 amorphous carbon fragments with embedded nanocrystals that we examined
40 contained Cu nanocrystals. We found no nanocrystals (embedded within amorphous
41 C or not) that were consistent with diamond, “n-diamond”, or “i-carbon”. While our
42 observations cannot prove that diamond, “n-diamond,” and “i-carbon” are not present
43 in the carbon spherules (and sediments), they clearly demonstrate that native Cu
44 nanocrystals occur at far higher concentrations than “n-diamond” – should that
45 modified form of 3C diamond exist and be present in the YDB. Since Cu
46
47
48
49
50
51
52
53
54
55
56
57
58
59
60

1
2
3 nanocrystals were not reported in previous studies of YDB nanodiamonds, they were
4 undoubtedly misidentified as “n-diamond” in the previous studies. Similarly, Cu₂O
5 nanocrystals were not reported and were likely misidentified as “i-carbon” in those
6 studies.
7
8

9
10 Interestingly, common wetlands plants (undoubtedly present in “black mat”
11 forming environments) have been shown to form nanocrystals of Cu near roots with
12 the possible assistance by endomycorrhizal fungi (Manceau *et al.*, 2008), and such
13 fungi include species known to form sclerotia (Münzenberger *et al.*, 2009). The
14 filamentous fungi *Hypocrea lixii* (Salvadori *et al.*, 2013) and *Trichoderma*
15 *koningiopsis* (Salvadori *et al.*, 2014) have been shown to synthesize spherical
16 nanocrystals of Cu from mine waste waters. *Hypocrea lixii* is the telomorph (i.e.,
17 sexual reproductive stage) of *Trichoderma harzianum*, a widely distributed fast
18 growing soil fungal species (Chaverri and Samuels, 2002). Mycoparasitic species of
19 *Hypocrea/Trichoderma* can grow on sclerotia surfaces and penetrate the rind (Elad
20 *et al.*, 1984; Benhamou and Chet, 1996). Sclerotia in forest soils have been shown to
21 contain *H. lixii* (Asmaya *et al.*, 2015). Further, the sclerotia colonizing fungus
22 *Fusarium oxysporum* (Xu *et al.*, 2008) has been shown to form nanoparticles of
23 copper sulfide (chalcocite) (Hosseini *et al.*, 2012). Biomineralization mechanisms
24 (see Pantidos and Horsfall, 2014) could account for the nanocrystalline Cu and Cu
25 compounds observed in the carbon spherules.
26
27

28
29 Furthermore, nanocrystals (e.g., aluminosilicates and other minerals including
30 diamond, if present) associated with the carbon spherules could be located on surfaces
31 or within the often-reported fissures and cracks that exist now (e.g., Fig. 10), or
32 existed previously but were closed by organic carbon accumulation and/or by low-
33 intensity burning/annealing in sporadic wildfires. Furthermore, nanometer-sized
34 minerals including diamond can readily enter biological systems, and this has opened
35 the possibility of their use for drug delivery and raised concerns over their toxicity in
36 the environment (e.g., Zhang *et al.*, 2012; Perevedentseva *et al.*, 2013). For example,
37 nanodiamonds labeled with tritium were shown to adsorb on the surface of roots and
38 penetrate into wheat shoots (Myasnikov *et al.*, 2014).
39
40
41
42
43
44
45
46
47
48
49
50
51
52
53
54

55 *Nanodiamond Abundances*

56
57 Whether or not a unique event – but not necessarily an impact – occurred at the
58
59
60

1
2
3 onset of the YD stadial depends on if nanodiamonds occur in YDB sediments at
4 concentrations significantly elevated with respect to underlying and overlaying
5 sediments. Kinzie *et al.* (2014) reported nanodiamond concentrations of several
6 hundred *parts per billion* (ppb) at the YDB layer and 0 ppb for multiple horizons at
7 depths of tens to hundreds of centimeters above and below the YDB layer for 9 sites
8 worldwide. However, it is technologically impossible with present instrumentation
9 and techniques to accurately estimate concentrations of nanometer-sized minerals in
10 sediments at and below ~tens to hundreds of *parts per million* (ppm) concentrations.

11
12
13
14
15
16 The problems associated with representative sampling and dating of fluvial
17 sediment samples are discussed in Scott *et al.* (2016); therefore we focus on the
18 methodology used by Kinzie *et al.* (2014) to measure nanodiamond concentrations.
19 Similar methodologies were employed by several coauthors of Kinzie *et al.* (2014)
20 (e.g., Kennett *et al.*, 2009a,b; Kurbatov *et al.*, 2010; Israde-Alcántara *et al.*, 2012a), as
21 well as by (Bement *et al.*, 2014). Remarkably, Kinzie *et al.* (2014) tested their
22 nanodiamond isolation and measurement methodology using a control sediment
23 specimen loaded with a relatively large (0.01%) concentration of synthetic
24 nanodiamonds, in contrast to the three to four orders-of-magnitude lower abundances
25 (11-494 ppb) they reported for the YDB bulk sediments they processed by acid
26 dissolution. Acid dissolution is the technique by which nanodiamonds were first
27 isolated from carbonaceous chondrites (Lewis *et al.*, 1987), and the isolates were
28 initially thought to be relatively pure. However, it was later recognized they contain
29 significant amounts of amorphous to poorly crystalline carbons that were difficult to
30 quantify by TEM and X-ray diffraction. Acid-dissolution residues *always* contain
31 non-diamond impurities, representing: minerals that survive acid dissolution,
32 transformation products/residues/condensates of acid dissolution, and laboratory
33 contaminants (e.g., Gilmour *et al.*, 1992, 2003; Daulton *et al.*, 1996; Stroud *et al.*,
34 2011; Israde-Alcántara *et al.*, 2012a; Heck *et al.*, 2014; Kinzie *et al.*, 2014). The
35 amount of impurities is usually large, ~50% to near 100%, and can be dominated by
36 amorphous to poorly crystalline carbons. Israde-Alcántara *et al.* (2012a) and Kinzie
37 *et al.* (2014) subjectively estimated the purity of their acid residues at “about ±50%”
38 and “< 50%”, respectively.

39
40
41
42
43
44
45
46
47
48
49
50
51
52
53
54
55
56
57
58
59
60
Due to the significant levels of non-diamond phases in the acid dissolution
isolates, the abundance estimations of nanodiamonds in sediments based on mass
balance are subject to large error. For nanodiamond concentrations below ~several

1
2
3 ppm, where the recovered nanodiamond masses are very small (<micrograms per
4 gram of processed material) and subject to greater relative contamination, the mass
5 balance approach has extremely large errors. In fact, contamination levels are greater
6 and nanodiamonds are more readily lost when large amounts of matrix (> several tens
7 of grams) are processed, and this is particularly problematic with small nanodiamond
8 concentrations (i.e., less than a ppm). Kinzie *et al.* (2014) processed between 20 to
9 150 g of dry-sieved material per sediment horizon and state, “The acid extraction
10 process commonly yielded very little residue that was nearly invisible to the naked
11 eye inside the centrifuge tubes and often was detectable only by light microscope.”
12 They further state in their supplemental materials that, “We placed all the residue on a
13 single [TEM] grid, whenever possible. If not, we measured the total amounts used or
14 not used to get a percentage per grid.”
15
16
17
18
19
20
21
22

23 The combined errors in measurement of the minuscule mass of the recovered
24 residue, and the fraction thereof placed on the TEM grid, is compounded with the
25 error in measuring relative modal (mass) abundance of the different minerals present
26 in the non-pure residue. Accurate measurements of modal abundances are required
27 for determination of the mass of the recovered nanodiamonds from the mass of acid
28 residues or from the mass of crushed carbon spherules. Kinzie *et al.* (2014), Bement
29 *et al.* (2014), and Kurbatov *et al.* (2010) estimated modal abundances by measuring
30 projected areal densities (i.e., projected TEM support film coverage) of nanometer to
31 submicron-sized grains deposited on TEM grids. Projected areal densities are not
32 measurements of the relative mass of nanodiamonds with respect to the mass of non-
33 diamond minerals, and their use will yield large errors in the determination of the
34 nanodiamond abundance in sediments, carbon spherules, and ice cores. For example,
35 to estimate the relative mass of the ubiquitous amorphous to poorly graphitized
36 carbon within which the nanocrystals were observed requires measurement of the
37 thickness and mass density of those carbon forms, in addition to a projected areal
38 density. The thickness – and therefore mass – of the amorphous to poorly graphitized
39 carbon can vary greatly on the TEM grids.
40
41
42
43
44
45
46
47
48
49
50

51 Furthermore, the greatest limitation of the approach of Kinzie *et al.* (2014) and
52 others is that detailed measurements must be performed on each individual grain in
53 order to correctly identify it as diamond (see, Daulton *et al.*, 2010). Kinzie *et al.*
54 (2014) state, “NDs represent <50% of the residue, and the remaining non-ND residue
55 can mask the NDs, thus making them difficult to identify. In addition, there are
56
57
58
59
60

1
2
3 inherent difficulties and uncertainties in correctly identifying tiny crystals <2 nm in
4 diameter.” Kinzie *et al.* (2014) further state, “By themselves, SA[E]D patterns are
5 insufficient to identify NDs, and so further investigations, such as those using
6 HRTEM, FFT, ED[X]S, and EELS, were performed on these nanoparticles to confirm
7 that they are NDs and not some other mineral.” In their conclusions, Kinzie *et al.*
8 (2014) wrote, “The identification of the isolated NDs involves two main methods,
9 electron microscopy imaging and electron spectroscopy, using up to nine imaging,
10 analytical, or quantification procedures: scanning electron microscopy, STEM, TEM,
11 HRTEM, ED[X]S, SA[E]D, FFT, EELS, and EFTEM. The entire procedure is labor-
12 intensive and technically demanding.” However, Kinzie *et al.* (2014) perplexingly
13 describe in their supplemental materials, “. . . for the purpose of estimating
14 abundances, *we assumed that all rounded particles were NDs* [emphasis added]. We
15 also observed abundant amorphous carbon nanoparticles, but almost none were
16 rounded, and therefore, we discounted them. This estimation procedure *focused*
17 *solely on the presence or absence of rounded particles* [emphasis added].” Given the
18 importance of this point, it is troubling that it was stated not in the main paper but
19 only in the supplemental materials. We reiterate that Kinzie *et al.* (2014) measured
20 projected areal densities of “rounded particles,” not necessarily nanodiamonds, and
21 they certainly did not measure modal mass abundances. This is a critical flaw, given
22 that the acid-dissolution residues and crushed spherules are not pure diamond.
23
24
25
26
27
28
29
30
31
32
33
34
35

36 Israde-Alcántara *et al.* (2012a) report that, “[Lake] Cuitzeo [Mexico] CSp [carbon
37 spherules] contain numerous noncarbon particles including aluminosilicates.” We
38 observed a range of non-carbonaceous crystalline minerals in carbon spherules from
39 Arlington Canyon; their mass abundance was of the order of several percent of the
40 spherule mass. We also found the carbon spherules contained amorphous-carbon
41 with rounded nanocrystals embedded with their matrix (Fig. 6) that were strikingly
42 similar to nanodiamond containing spherule fragments reported by Kennett *et al.*
43 (2009b), Bement *et al.* (2014), and Kinzie *et al.* (2014). However, we found the
44 embedded nanocrystals were native Cu in all spherule fragments examined. In no
45 case did we observe diamond, “n-diamond,” and “i-carbon,” and while our
46 observations cannot prove their absence in the carbon spherules, they clearly
47 demonstrate that native Cu nanocrystals occur at far higher concentrations than “n-
48 diamond.” As in the case for the carbon spherules, glass-like carbon from YDB
49 sediments have been shown to contain nanocrystals of Ca-rich, Ti-rich, Ti-rich, and
50
51
52
53
54
55
56
57
58
59
60

1
2
3 Fe-rich phases which can have rounded morphologies (van Hoesel, 2014).
4 Nanocrystals of native Cu, Cu compounds, and other minerals that are present in
5 crushed carbon spherules are undoubtedly included in the counting statistics of Kinzie
6 *et al.* (2014) and others that counted “rounded particles.”
7
8

9
10 The method of estimating TEM grid surface coverage of rounded particles by
11 Kinzie *et al.* (2014) is further puzzling given that angular, octahedral, and euhedral
12 nanodiamonds have been reported in YDB-aged sediments. Kennett *et al.* (2009b)
13 claim, “. . . clusters of stable cubic diamonds ($\approx 1,000$ in total) were found with carbon
14 elongates . . . These diamonds appear more angular than the associated n-diamonds,”
15 and “TEM study revealed conspicuous subrounded, spherical, and octahedral
16 crystalline particles . . . Analysis of the particles by electron diffraction show
17 reflections consistent with . . . metastable ‘new-diamond’ polymorph or n-diamond.”
18 Similar descriptions of the YDB nanodiamonds appear in Kennett *et al.* (2009a).
19 Furthermore, an example of a cubic diamond from black mat sediments of presumed
20 YDB-age at Lommel Belgium, and shown in Fig. 2 of Tian *et al.* (2011), is flake-like
21 with an irregular non-rounded shape. van Hoesel *et al.* (2012) reported submicron
22 cubic diamonds with irregular non-rounded shape (their Fig. 6) in the Usselo horizon
23 at Geldrop-Aalsterhut, The Netherlands. Israde-Alcántara *et al.* (2012a) described the
24 nanodiamonds they reportedly identified as, “. . . nanocrystalline carbon particles
25 ranging in shape from spherical to elongate to euhedral . . . embedded in amorphous
26 carbon, as Tian *et al.* (14) described. We identified three of four previously reported
27 ND variants, of which, n-diamond was the most abundant.”
28
29

30 Kinzie *et al.* (2014) prepared TEM specimens by placing dried acid residues or
31 crushed spherules into suspension using NH_4OH , depositing aliquots of suspended
32 grains on the TEM grids, and allowing the aliquots to evaporate. Another limitation
33 of the TEM approach for determining modal abundances is that depositing liquid-
34 suspended grains on a TEM grid results in highly heterogeneous grain dispersions.
35 This is problematic because variation in surface chemistry of different minerals or
36 mineral grains of different sizes can result in different tendencies to cluster and/or
37 adhere to the TEM support film. Consequently, measured modal distributions based
38 only on analysis of the TEM-accessible regions, with nearly monolayer dispersions of
39 spatially well-separated grains, can be greatly skewed from the true modal
40 distribution. Often electron-transparent multilayer deposits form, consisting of
41 overlapping grains that make it difficult to identify individual grains or determine
42
43
44
45
46
47
48
49
50
51
52
53
54
55
56
57
58
59
60

1
2
3 modal abundances. Furthermore, thick grain aggregates are electron-beam opaque
4 and cannot be analyzed by TEM. These regions can have different mineral modal
5 abundances than the TEM-accessible regions.
6
7

8 Kinzie *et al.* (2014) state in their supplemental materials that they analyzed
9 between 16 and 92 (average of 28) random 350 x 350 nm² TEM field of views.
10 Unfortunately, the sampling was not identical for each TEM grid, and it is unclear
11 which sediment horizons received increased scrutiny (e.g., the horizons that were
12 expected to contain nanodiamonds). A larger problem is that their mean sampling
13 corresponds to $\approx 0.000017\%$ of the viewable area of a TEM grid. Given the highly
14 inhomogeneous grain dispersions on their TEM grids, this represents a statistically
15 inadequate grain sampling that could account for the 0 ppb nanodiamond abundances
16 they measured in sediments that bracketed the reported YDB layer. Of course, TEM
17 can provide no measure of any grains dispersed on the TEM inaccessible grid bars.
18
19

20 The numerous experiment difficulties in using TEM to measure nanodiamond
21 abundances in sediments render this approach infeasible. The only analytical method
22 accepted to reasonably assess \sim several to tens of ppm abundances of nanodiamonds
23 within a matrix is a technique applied to meteoritic nanodiamonds that measures the
24 amount of supernova-derived Xe-HL gases (see review by Daulton, 2006) released
25 during stepped combustion of acid-dissolution residues. By measuring a tracer
26 unique to the nanodiamonds, only the nanodiamonds are measured; this contrasts with
27 the mass-balance approach that measures the combined mass all the different
28 materials (including adsorbed moisture) present in the acid residue. Diamonds are
29 thought to be the only carriers of the Xe-HL gases in the non-pure nanodiamond
30 isolates, based on the smooth elemental abundance pattern of extracted noble gases
31 relative to cosmic abundances, suggesting all HL noble gases are a single gas
32 component trapped in a single mineral species (Huss and Lewis, 1994). This
33 assumption is also based on the high release temperatures (1100-1600°C) of the HL
34 gas component (Huss and Lewis, 1994). Furthermore, the release of HL gases is
35 accompanied by release of CO₂ (Lewis, 1994), indicating that the HL component
36 resides only in the most refractory carbonaceous minerals (see also Daulton, 2006).
37 This method has the advantage that it can be used to monitor any decrease in the HL
38 gas component (i.e., loss of the carrier phase) after each step of the acid-dissolution
39 process, or following any post-processing. However, the method has the
40 disadvantage that it does not directly measure nanodiamonds that lack Xe-HL gases.
41
42
43
44
45
46
47
48
49
50
51
52
53
54
55
56
57
58
59
60

1
2
3 A number of noble gas measurements have been performed on terrestrial
4 diamonds (for a review, see Basu *et al.*, 2013). For example, Verchovsky *et al.*
5 (1991) measured one diamond from the Popigai crater and reported unusually high
6 concentrations of radiogenic ^{40}Ar . Subsequent measurements of Popigai diamonds
7 yielded a similar range of $^{40}\text{Ar}/^{36}\text{Ar}$ ratios as in kimberlitic diamonds, however with
8 significantly higher ^{40}Ar concentrations (Shelkov *et al.*, 1998). Metamorphic
9 microdiamonds from the Kokchetav Massif have primary ^{40}Ar concentrations that fall
10 between the ranges exhibited by kimberlitic and Popigai impact diamonds
11 (Verchovsky *et al.*, 1993). Secondary processes, such as implantation of U and Th
12 decay products, appear to have severely modified the primary isotopic compositions
13 of the noble gases that were trapped during formation of the microdiamonds.
14 Kokchetav microdiamonds contain ^4He concentrations that are among the highest
15 observed in any terrestrial diamonds (Verchovsky *et al.*, 1993). Carbonado diamonds
16 from Africa and Brazil also contain large amounts implanted radiogenic ^4He in
17 addition to nucleogenic Xe and Kr (Ozima *et al.*, 1991). Unfortunately, there have
18 been no measurements of trapped noble gases performed on nanodiamonds from the
19 YDB boundary or the underlying/overlying sediment layers. Therefore it is unclear
20 if they carry any unique trapped gas component useful as a tracer for abundance
21 measurements.
22
23
24
25
26
27
28
29
30
31
32
33
34
35

36 *Carbon Isotopic Compositions of Nanodiamonds*

37
38 Nanodiamonds are a minor component (see Lewis *et al.*, 1987; Rietmeijer and
39 Mackinnon, 1987, Dai *et al.*, 2002) of the $\sim 4 \times 10^7$ kg/yr interplanetary dust flux that
40 is accreted by Earth (Love and Brownlee, 1993), with accretion rates in the last
41 glacial period comparable to the present (Yada *et al.*, 2004). In arguing against the
42 fall of interplanetary dust as an explanation for nanodiamonds in YDB sediments,
43 Israde-Alcántara *et al.* (2012a) incorrectly state that “Tian *et al.* (14) concluded that
44 YDB NDs are not cosmic because they display $\delta^{13}\text{C}$ abundances (-28.1 to -26.3%)
45 that are terrestrial.” van Hoesel *et al.* (2012) make a similar incorrect statement. Tian
46 *et al.* (2011) actually stated, “carbon isotope measurements and C/N values were
47 determined from the black material of the Lommel YDB layer. The nanodiamond
48 particles in the present material could not be analyzed separately because of their
49 small size.” Tian *et al.* (2011) performed these measurements to look for evidence of
50
51
52
53
54
55
56
57
58
59
60

1
2
3 an impact event through the presence of C in the sediments that originated from the
4 impactor and concluded that, “results obtained on the Lommel material do not
5 distinguish between terrestrial and extraterrestrial origins for the carbon.” Israde-
6 Alcántara *et al.* (2012a) also incorrectly concluded that “Isotopic analyses of the
7 carbon-rich YDB interval at Cuitzeo yielded values ranging from -23 to -19% for
8 $\delta^{13}\text{C}$ consistent with the formation of Cuitzeo NDs from terrestrial, not cosmic,
9 carbon.” Similar to Tian *et al.* (2011), Israde-Alcántara *et al.* (2012a) measured
10 sediment, not nanodiamond isolates. Neither of the bulk sediment $\delta^{13}\text{C}$ measurements
11 can provide direct information about the nanodiamonds, which make up only a tiny
12 fraction of the C in the sediments. Kinzie *et al.* (2014) also invoke this erroneous
13 evidence by citing both papers and stating, “($\delta^{13}\text{C}$, $\delta^{15}\text{N}$, and C/N) in YDB NDs are
14 consistent with a terrestrial origin.” They also incorrectly interpret the $\delta^{13}\text{C}$
15 measurements of sediments by Tian *et al.* (2011) as ruling out a mantle origin of the
16 nanodiamonds.
17

18
19 Measurement of the $\delta^{13}\text{C}$ compositions of nanodiamonds isolated from sediments
20 or matrix by acid dissolution is experimentally challenging. The non-diamond
21 carbonaceous phases, which can comprise over half the residue, are potentially of
22 different origin as the nanodiamonds and hence can have different C isotopic
23 compositions. While $\delta^{13}\text{C}$ values measured from C released at high temperature
24 during stepped combustion of the acid residue will limit C contributions from the
25 most labile (low-temperature released) components, it is not possible to correct for
26 contributions from the non-diamond carbonaceous minerals that combust along with
27 the nanodiamonds. Consequently, bulk C isotopic measurements of acid residues are
28 highly suspect with respect to the true nanodiamond C isotopic composition.
29 Therefore, bulk C isotopic measurements of acid dissolution isolates of terrestrial
30 sediment nanodiamonds (Carlisle, 1992; Gilmour *et al.*, 1992), impact diamonds
31 (Hough *et al.*, 1995; Gilmour *et al.*, 2003), and meteoritic nanodiamonds (c.f., Swart
32 *et al.*, 1983, Russell *et al.*, 1996) cannot provide information about their origins.
33 Indeed, this point has driven recent attempts by two groups to pursue C isotopic
34 measurements of individual meteoritic nanodiamonds using atom probe tomography
35 (Heck *et al.*, 2014).
36
37
38
39
40
41
42
43
44
45
46
47
48
49
50
51
52
53
54
55

56
57 *Synchronous Chronologies and Stratigraphic YDB Markers*
58
59
60

1
2
3 An important challenge for the YD Impact Hypothesis is that, in order to attribute
4 the source of nanodiamonds in Late Pleistocene sediments to an impactor/bolide
5 event, it is necessary that all sediments reported to contain nanodiamonds date
6 synchronous to the YD onset. However, nanodiamonds (and “n-diamond”) have been
7 reported in sediments and in carbonaceous forms within sediments that do not date
8 to the YDB (Firestone *et al.*, 2007, 2010a; Yang *et al.*, 2008; van Hoesel *et al.*, 2012,
9 2013; Bement *et al.*, 2014; Kinzie *et al.*, 2014). Most importantly, and despite
10 widespread claims of synchronicity by YD impact proponents (see, Kennett *et al.*,
11 2015a,b), age control is poor or nonexistent at nearly all sites where nanodiamonds
12 are reported “at” the YDB layer (e.g., see Blaauw *et al.*, 2012; Ives and Froese, 2013;
13 Wittke *et al.*, 2013c; van Hoesel *et al.*, 2013, 2014; Meltzer *et al.*, 2014; Holliday
14 *et al.*, 2014). There are only two sites where nanodiamonds are reported at a layer that
15 can be confidently dated to the YD onset: Daisy Cave and Sheriden Cave (Meltzer
16 *et al.*, 2014). However, Meltzer *et al.* (2014) cautions that at Sheriden Cave, “. . . the
17 supposed YDB layer has the required age, but its age is inconsistent with the ages of
18 the layers that encompass it.”

19
20
21
22
23
24
25
26
27
28
29
30
31
32
33
34
35
36
37
38
39
40
41
42
43
44
45
46
47
48
49
50
51
52
53
54
55
56
57
58
59
60
The YDB sediment layer is often described as being at the base of a dark-colored
stratum termed by YD impact proponents as “the black mat” that is used as the
primary stratigraphic marker for the YDB (Firestone *et al.*, 2007, 2010a; Firestone
2009, Mahaney *et al.*, 2010; Israde-Alcántara *et al.*, 2012a; Wittke *et al.*, 2013a).
Nanodiamonds and other proposed impact markers are reported directly beneath the
black mat (Firestone *et al.*, 2007, 2010a). A distinct, dark colored stratum is present
at the Murray Springs, Arizona archeological site, with sediments containing Clovis
artifacts and megafaunal fossils below the horizon and sediments devoid of these
materials above. Haynes (2008) identified 55 localities in the western United States
and 2 in the eastern United States with “. . . a black organic-rich layer or ‘black mat’
in the form of mollic paleosols, aquolls, diatomites, or algal mats with radiocarbon
ages suggesting they are stratigraphic manifestations of the Younger Dryas cooling
episode.” These and other similar deposits have been described as organic-rich, silty
sediments (e.g., Brakenridge, 1981; Quade *et al.*, 1998; Baker *et al.*, 2008), however
their total organic carbon content varies (most cases < 5 wt. %) and is not correlated
with sediment texture and color (see Pinter *et al.*, 2011; Harris-Parks, 2014, 2016). In
fact, such deposits vary in color and white-colored diatomites have been described as
“black mats” (Haynes, 2008). These deposits form in wet environments ranging from

1
2
3 wet meadows to shallow ponds (Quade *et al.*, 1998; Haynes, 2008; Harris-Parks,
4 2016). “Black mat” formation, at least in southern Nevada, peaked during the YD
5 from 11,200-10,000 ¹⁴C a BP (Quade *et al.*, 1998). However, formation was time-
6 transgressive across, rather than synchronous with, the YDB (Holliday and Meltzer,
7 2010; Harris-Parks, 2014, 2016). Such dark colored deposits are not unique to the
8 western United States or to the YDB, but in fact are well recognized as paleo-wetland
9 deposits found in similar settings around the world and at numerous time horizons
10 through at least the late Quaternary (e.g., Quade *et al.*, 1998; Rech *et al.*, 2003;
11 Mandel, 2008; Pinter *et al.*, 2011; Pigati *et al.*, 2012).

12
13
14
15
16
17
18 Black mats and the unreliable reports of spikes in the nanodiamond concentration,
19 as discussed previously, cannot link chronologies at different sites. The reported
20 concentration spikes of the other currently debated mineralogical and geochemical
21 markers at the YDB have all been vigorously challenged. These markers include
22 combustion products (charcoal/soot, glass-like carbon, carbon elongates, and carbon
23 spherules), magnetic minerals (grains, spherules), and Ir (see, Firestone *et al.*, 2007,
24 2010a; Firestone, 2009; Kennett *et al.*, 2008, 2009b). In addition, Bunch *et al.* (2012)
25 reported a correlation between elevated abundances of siliceous scoria-like objects
26 and Fe/Si-rich microspherules at the YDB layer at three out of 18 sites studied (Abu
27 Hureyra, Syria; Melrose, Pennsylvania; and Blackville, South Carolina). Of these
28 materials, nanodiamonds have been reported within glass-like carbons (Firestone *et al.*
29 *et al.*, 2007, 2010a; Firestone, 2009; Israde-Alcántara *et al.*, 2012a supplemental
30 materials; Kinzie *et al.*, 2014), carbon elongates (Kennett *et al.*, 2009b), and carbon
31 spherules (Firestone, 2009, Firestone *et al.*, 2010a; Kennett *et al.*, 2009a; Israde-
32 Alcántara *et al.*, 2012a supplemental materials; Kinzie *et al.*, 2014).

33
34
35
36
37
38
39
40
41
42
43 One aspect of most versions of the YD Impact Hypothesis is the assertion that
44 intense, impact-ignited wildfire raged across North America and Europe (Kristan-
45 Tollmann and Tollmann, 1992; Firestone *et al.*, 2006). Charcoal/soot, glass-like
46 carbon, carbon elongates, and carbon spherules reported in YDB sediments are
47 interpreted as high-temperature combustion products and evidence of synchronous
48 intercontinental wildfires (Firestone *et al.*, 2007, 2010a; Firestone, 2009; Kennett *et al.*
49 *et al.*, 2008, 2009a,b; Wittke *et al.*, 2013a). For instance, Firestone *et al.* (2007)
50 propose, “. . . glass-like carbon, carbon spherules, and nanodiamonds were produced
51 in the YDB by high temperatures resulting from the impact and associated biomass
52 burning.” Kennett *et al.* (2008) studied the Northern Channel Islands in California
53
54
55
56
57
58
59
60

1
2
3 and wrote, “Intense wildfire evidence is also indicated by the presence of carbon
4 spherules . . . spherules occur widely in the YDB layer in North America and have
5 also been found in surficial sediments associated with intense coniferous forest crown
6 fires (Firestone *et al.*, 2007).” In apparent contradiction, Israde-Alcántara *et al.*
7 (2012a) state that the, “. . . indication that the YDB proxies [e.g., carbon spherules,
8 nanodiamonds, magnetic spherules] are not wildfire-related is that marker peaks (2.80
9 to 2.75 m) were deposited earlier than the wildfire charcoal peak (2.70 to 2.65),”
10 suggesting wildfires were not synchronous with (and immediately caused by) the
11 impact event at their study site, Lake Cuitzeo. As for the nanodiamonds in the YDB
12 spherules, Firestone *et al.* (2006) first speculated that they “. . . rode in with an
13 asteroid or comet, or on the supernova debris cloud,” but later speculated they were
14 formed during the impact event Firestone *et al.* (2007). Kinzie *et al.* (2014) conclude,
15 “. . . the best explanation is that ND-rich carbon spherules derive from conifers that
16 were incinerated by the impact event”, and cite Israde-Alcántara *et al.*, 2012a who
17 cite Kimbel *et al.* (2008), which report the formation of “n-diamonds” in charred coal,
18 coconut shells, and wood; they state, “. . . [our] procedure is identical to the
19 commercial process for producing activated charcoal . . . The process of forming n-
20 diamonds requires conditions unlike any that are normal to the Earth's surface . . .
21 [and] match the extreme conditions that exist during an ET impact or airburst.”
22 Kinzie *et al.* (2014) stress that the nanodiamonds and their host carbon spherules must
23 have been formed within the impact fireball itself, and provide several arguments
24 against their formation by wildfire, stating, “. . . there is no evidence for and no
25 known process for production of NDs in natural wildfires.” Millimeter-diameter,
26 nanodiamond-containing carbon spherules that formed in an impact fireball should be
27 localized to the immediate area of the impact site(s). However, despite the assertion
28 by impact proponents that the primary YD impact site is in North America,
29 nanodiamond-containing carbon spherules are reported widely distributed over
30 several continents. For example, Kinzie *et al.* (2014) report the abundance of
31 nanodiamonds in carbon spherules from YDB sediments in Ommen, the Netherlands
32 are higher than at 12 out of 14 North American sites studied, and abundances in
33 Lingen, Germany are higher than at 10 of those North American sites.

34
35
36 A study of 35 lake sediment cores across North America could neither confirm a
37 continent-wide charcoal peak associated with the YDB nor find any indication of
38 continent-wide wildfire (Marlon *et al.*, 2009). Similar conclusions were drawn from
39
40
41
42
43
44
45
46
47
48
49
50
51
52
53
54
55
56
57
58
59
60

1
2
3 subsequent studies (Gill *et al.*, 2009; Daniau *et al.*, 2010; Pinter *et al.*, 2011). In fact,
4 most YD-aged “black mats” in North America contain negligible amounts of charcoal
5 (Haynes *et al.*, 2010a; Harris-Parks, 2014, 2016). As for as the other proposed
6 impact-derived combustion products, Scott *et al.* (2010) report that glass-like carbon,
7 carbon elongates, and carbon spherules are ubiquitous in sediments and occur
8 throughout Late Pleistocene to Holocene sedimentary sequences. Further, sclerotia
9 are morphologically identical to the reported YDB carbon spherules (Scott *et al.*,
10 2010), and are commonly reported in sediments (e.g., see McWeeney, 1989; Shay and
11 Kapinga, 1997; Deal, 2005).

12
13
14
15
16
17
18 The reported spikes in concentration at the YDB of magnetic spherules, siliceous
19 scoria-like objects, and Ir are also strongly contested. These markers are not reported
20 to be directly associated with nanodiamonds and, in fact, nanodiamonds are not
21 reported at the three YDB sites where lechatelierite-containing magnetic spherules
22 and scoria-like objects are reported. Therefore, these markers will not be discussed
23 further, but reviews of the contested studies are found in Pinter *et al.* (2001), van
24 Hoesel (2014), van Hoesel *et al.* (2014), and Holliday *et al.* (2014). The point is that
25 there are no clear and undisputed concentration spikes for any mineral or geochemical
26 signature that can be used identify the YDB and link chronologies at different sites.

27
28
29
30
31
32
33 Even if the reported concentration spikes in Late Pleistocene sediments are
34 accepted, there are problems in interpreting them as indicators of impact/bolide
35 event(s). Impact/bolide events should result in nearly simultaneous deposition of
36 impact markers with respect to the mean sedimentary rates at a given site. Natural
37 mixing processes (e.g., bioturbation, transport, and redeposition) should thoroughly
38 mix the different mineralogical and geochemical markers within a sediment horizon
39 and widen their distribution vertically in stratigraphic sequences. While some sorting
40 might occur, the peaks in abundance with respect to stratigraphy should
41 approximately overlap for all markers. Multiple abundance peaks for any given
42 marker, and marker peaks that are vertically offset and distinct from one another,
43 would not be expected. At several Carolina Bays (M31 and M33 of Myrtle Beach,
44 South Carolina), two well-separated peaks in magnetic grain abundance are reported,
45 with the peak at the higher stratigraphic level correlated with a peak in charcoal
46 abundance (Firestone *et al.*, 2010a). Firestone *et al.* (2007, 2010a) report at Chobot,
47 Alberta Canada correlated abundance peaks in carbon spherules, glass-like carbon,
48 and charcoal in sediments that lie below sediments with correlated abundance peaks
49
50
51
52
53
54
55
56
57
58
59
60

1
2
3 in magnetic grains and magnetic spherules. At Topper, South Carolina, Firestone *et al.* (2007, 2010a) report that the abundance peaks in glass-like carbon and magnetic
4 grains do not overlap. At the Gainey, Michigan, Firestone *et al.* (2010a) report two
5 peaks in magnetic grain abundance, with the peak at the lower stratigraphic level
6 correlated with a peak in magnetic spherules abundance. At Arlington Canyon, two
7 well separated sets of correlated peaks at ≈ 400 and ≈ 500 cm below surface (cmbs)
8 for charcoal, carbon elongates, carbon spherules, and nanodiamonds are reported that
9 bracket a horizon of gravel to coarse sand (Kennett *et al.*, 2008, 2009b; Kinzie *et al.*,
10 2014). Note that Kennett *et al.* (2008, 2009b) report carbon spherules are absent
11 between 95 to 416 cmbs and their abundance peaks near 500 cmbs, while the
12 abundance of carbon elongates has two resolved peaks near 394 cmbs and 500 cmbs.
13 Kinzie *et al.* (2014), with Kennett as a coauthor, provide no abundance measurements
14 for carbon elongates and instead report two peaks in the abundance of carbon
15 spherules at 394 cmbs and 500.5 cmbs at concentrations that are a sum of carbon
16 spherule and carbon elongate concentrations reported by Kennett *et al.* (2008, 2009b).
17
18
19
20
21
22
23
24
25
26
27
28
29

30 Discussion and Conclusions

31 The YDB nanodiamond data are considered by some as the strongest physical
32 evidence for an YD impact/bolide event. We have analyzed the nanodiamond data
33 used to provide evidence for the YD Impact Hypothesis and have identified critical
34 problems with the collection of those data and/or the data interpretation. In
35 evaluating the evidence we arrived at four main conclusions. In
36
37
38
39

40 1) The presence of lonsdaleite in sedimentary deposits can suggest – but cannot
41 on its own demonstrate – that an impact event occurred. In YDB sediment, however,
42 there is no credible evidence of the presence of lonsdaleite. In previous studies,
43 graphene/graphane aggregates have been misidentified as lonsdaleite, diffraction
44 patterns have been incorrectly indexed to lonsdaleite, and FFT transforms of single
45 high-resolution lattice images used to identify lonsdaleite are known to yield
46 misleading results.
47
48
49
50

51 2) While there is evidence of cubic nanodiamonds in Late Pleistocene sediments,
52 their presence does not provide evidence of an impact because they have not been
53 linked with impact processes. To do so would require correlating the nanodiamonds
54 to an established and recognized impact marker. There are no established reports in
55
56
57
58
59
60

1
2
3 YDB sediments of any of the accepted and recognized shock minerals found at known
4 impact structures (c.f., French and Koeberl, 2010; van Hoesel *et al.*, 2014). Carbon
5 spherules, carbon elongates, and glass-like carbon reported associated with the
6 nanodiamonds are not recognized as impact markers. Furthermore, these associations
7 are reported to occur in sediments that are not limited to the YDB and therefore
8 cannot provide evidence of processes unique to the YD onset.
9

10
11
12
13 3) The use of the controversial “n-diamond” as an impact marker, which
14 constitutes the majority of the nanodiamond evidence for the YD Impact Hypothesis,
15 is problematic due to the presence of native Cu nanocrystals in sediments that can be
16 easily confused for “n-diamond”. Further, “n-diamond” is reported in sediments that
17 do not date to the YD onset, and more importantly, formation of these nanocrystals
18 have not been linked exclusively to shock formation processes.
19
20
21
22

23
24 4) The presence of a single spike in nanodiamond concentration within
25 Pleistocene to Holocene sediments at the YDB layer would strongly suggest that a
26 unique event – but not necessarily an impact – occurred at the YD onset.
27 Nanodiamond abundances from bulk sediments processed by acid dissolution, for
28 crushed carbon spherules, and for ice by Kinzie *et al.* (2014) and those previously
29 published by several of its coauthors in other studies (e.g., Kennett *et al.*, 2009a,b;
30 Kurbatov *et al.*, 2010; Israde-Alcántara *et al.*, 2012a), as well as by a coauthor of
31 Kennett *et al.* (2009a) (Bement *et al.*, 2014) are all based on TEM studies. However,
32 the TEM measurements by Kinzie *et al.* (2014) and others using similar
33 methodologies are not of nanodiamonds, but are of “rounded particles.” More
34 importantly, the many experiment difficulties inherent in using TEM to measure
35 nanodiamond abundances lead to large unconstrained error, rendering this approach
36 infeasible. We find there is no evidence to suggest a unique spike in the
37 nanodiamond concentration at the YDB layer. The distribution of nanodiamonds in
38 Pleistocene to Holocene sediments (and in ice, if present, which has yet to be
39 confirmed by independent groups, see Boslough, 2013b) remains unclear. Therefore,
40 considering conclusions 1-4, the reports of nanodiamonds in Late Pleistocene
41 sediments cannot provide evidence for an YD impact.
42
43
44
45
46
47
48
49
50
51
52
53

54
55 Various criticisms have been raised on both sides of the debate regarding the
56 identification, analysis, and interpretation of proposed YD impact markers. To
57 advance this field, it would be advantageous for working groups to develop and
58
59
60

1
2
3 standardize techniques for collection, splitting/distribution, and analysis of specimens
4 from key YDB sites, in order to try to reconcile conflicting results and prevent the use
5 of inappropriate approaches that lead to erroneous results. To perform the highly
6 challenging measurement of nanodiamond abundance in sediments/ice, methods other
7 than TEM will need to be explored and developed. Any method must be
8 tested/calibrated against control specimens (sediments/ice initially devoid of
9 nanodiamonds, that are spiked with measured ppb amounts of nanodiamonds).
10 Furthermore, unlike previous abundance measurements, future measurements must be
11 conducted as blind studies to preclude unconscious bias.
12
13
14
15
16
17
18
19
20
21
22
23
24
25
26
27
28
29
30
31
32
33
34
35
36
37
38
39
40
41
42
43
44
45
46
47
48
49
50
51
52
53
54
55
56
57
58
59
60

1
2
3 *Acknowledgements.* This research was partially supported by the McDonnell Center
4 for the Space Sciences and Institute for Material Science and Engineering (TLD) as
5 well as grants from the National Geographic Society (8321-07) to NP and from the
6 National Science Foundation (EAR-0746015) to NP and RSA. ACS undertook the
7 completion of this research while in receipt of a Leverhulme Emeritus Fellowship
8 (EM-2012-054), which is gratefully acknowledged. We thank Ph. Claeys (Vrije
9 Universiteit Brussel) for providing YDB sediment specimens from Lommel Belgium.
10 We thank M. Watanabe (Tokyo Metropolitan University, Graduate School of Urban
11 Environmental Sciences) for valuable discussions. We thank the numerous staff at
12 the Channel Islands. ACS thanks Sharon Gibbons and Neil Holloway for technical
13 support. We thank reviewers C. Koeberl and B. Alloway for valuable comments.
14
15
16
17
18
19
20
21
22
23
24
25
26
27

28 *Abbreviations:* DF, dark field; BF, bright field; EDXS, energy dispersive X-ray
29 spectroscopy; EELS, electron energy loss spectroscopy; FFT, fast Fourier
30 transformation; GIF, Gatan imaging filter; NMR, nuclear magnetic resonance; ppb,
31 parts per billion; ppm, parts per million; SDD, silicon drifted detector; HR-TEM,
32 high-resolution transmission electron microscopy; STEM, scanning transmission
33 electron microscopy; TEM, transmission electron microscopy; YD, Younger Dryas;
34 YDB, Younger Dryas Boundary
35
36
37
38
39
40
41
42
43
44
45
46
47
48
49
50
51
52
53
54
55
56
57
58
59
60

References

- Algra RE, Hocevar M, Verheijen MA, Zardo I, Immink GGW, van Enckevort WJP, Abstreiter G, Kouwenhoven LP, Vlieg E, Bakkers EPAM. 2011. Crystal structure transfer in core/shell nanowires. *Nano Letters* **11**: 1690-1694.
- Allan DS, Delair JB. 1994. When the Earth nearly died: Compelling evidence of a catastrophic world change 9500 BC. Gill & Macmillan Ltd, Dublin, Ireland.
- Allan DS, Delair JB. 1997. Cataclysm: Compelling evidence of a cosmic catastrophe in 9500 B.C., Bear & Company, Rochester, VT.
- Amasya A, Narisawa K, Watanabe M. 2015. Analysis of sclerotia-associated fungal communities in cool-temperate forest soils in North Japan. *Microbes Environ* **30**: 113-116.
- Andronikov AV, Subetto DA, Lauretta DS, Andronikova IE, Drosenko DA, Kuznetsov DD, Sapelko TV, Strykh LS. 2014. In search for fingerprints of an extraterrestrial event: Trace element characteristics of sediments from the Lake Medvedevskoye (Karelian Isthmus, Russia). *Doklady Earth Sciences* **457**: 819-823.
- Baker DW, Miranda PJ, Gibbs KE. 2008. Montana evidence for extra-terrestrial impact event that caused ice-age mammal die-off. *EOS Trans. Am. Geophys. Union* **89**: P41A-05.
- Barnosky AD, Koch PL, Feranec RS, Wing SL, Shabel AB. 2004. Assessing the causes of the Late Pleistocene extinctions on the continents. *Science* **306**: 70-75.
- Basu S, Jones AP, Verchovsky AB, Kelley SP, Stuart FM. 2013. An overview of noble gas (He, Ne, Ar, Xe) contents and isotope signals in terrestrial diamond. *Earth-Science Reviews* **126**: 235-249.
- Bement LC, Madden AS, Carter BJ, Simms AR, Swindle AL, Alexander HM, Fine S, Benamara M. 2014. Quantifying the distribution of nanodiamonds in pre-Younger Dryas to recent age deposits along Bull Creek, Oklahoma Panhandle, USA. *Proc. Natl. Acad. Sci. USA* **111**: 1726-1731.
- Benedict JB. 2011. Sclerotia as indicators of mid-Holocene tree-limit altitude, Colorado Front Range, USA. *The Holocene* **21**: 1021-1023.
- Benhamou N, Chet I. 1996. Parasitism of sclerotia of *Sclerotium rolfsii* by *Trichoderma harzianum*: Ultrastructural and cytochemical aspects of the interaction. *Biochemistry and Cell Biology* **86**: 405-416.
- Berger WH. 1990. The Younger Dryas cold spell – a quest for causes. *Palaeogeography, Palaeoclimatology, Palaeoecology* **89**: 219-237.
- Bertnatowicz TJ, Cowsik R, Gibbons PC, Lodders K, Fegley Jr. B, Amari S, Lewis RS. 1996. Constraints on stellar grain formation from presolar graphite in the

- 1
2
3 Murchison meteorite. *The Astrophys. J.* **472**: 760-782.
4
5 Bhargava S, Bist HD, Sahli S, Aslam M, Tripathi HB. 1995. Diamond polytypes in
6 the chemical vapor deposited diamond films. *Appl. Phys. Lett.* **67**: 1706-1708.
7
8 Billinge SJL, Levin I. 2007. The problem with determining atomic structure at the
9 nanoscale. *Science* **316**: 561-565.
10
11 Blaauw M, Holliday VT, Gill JL, Nicoll K. 2012. Age models and the Younger Dryas
12 Impact Hypothesis. *Proc. Natl. Acad. Sci. USA* **109**: E2240.
13
14 Boslough M. 2012. Inconsistent impact hypotheses for the Younger Dryas. *Proc.*
15 *Natl. Acad. Sci. USA* **109**: E2241.
16
17
18 Boslough M, Nicoll K, Holliday V, Daulton TL, Meltzer D, Pinter N, Scott AC,
19 Surovell T, Claeys P, Gill J, Paquay F, Marlon J, Bartlein P, Whitlock C, Grayson
20 D, Jull AJT. 2012. Arguments and evidence against a Younger Dryas impact
21 event. *Climates, Landscapes, and Civilizations. Geophysical Monograph Series*
22 **198**: American Geophysical Union; 13-26.
23
24
25 Boslough M. 2013a. Greenland Pt anomaly may point to noncataclysmic Cape York
26 meteorite entry. *Proc. Natl. Acad. Sci. USA* **110**: E5035.
27
28
29 Boslough M. 2013b. Faulty protocols yield contaminated samples, unconfirmed
30 results. *Proc. Natl. Acad. Sci. USA* **110**: E1651.
31
32
33 Boslough M, Harris AW, Chapman C, Morrison D. 2013. Younger Dryas impact
34 model confuses comet facts, defies airburst physics. *Proc. Natl. Acad. Sci. USA*
35 **110**: E4170.
36
37
38 Boslough M, Nicoll K, Daulton TL, Scott AC, Claeys P, Gill JL, Marlon JR, Bartlein
39 P J. 2015. Incomplete Bayesian model rejects contradictory radiocarbon data for
40 being contradictory. *Proc. Natl. Acad. Sci. USA* **112**: E6722.
41
42
43 Bostick BC, Jones RE, Ernst WG, Chen C, Leech ML, Beane RJ. 2003. Low-
44 temperature microdiamond aggregates in the Maksyutov Metamorphic Complex,
45 South Ural Mountains, Russia. *Am. Mineral.* **88**: 1709-1717.
46
47
48 Brakenridge GR. 1981. Terrestrial paleoenvironmental effects of a Late Quaternary-
49 age supernova. *Icarus* **46**: 81-93.
50
51
52 Brakenridge GR. 2011. Core-collapse supernovae and the Younger Dryas/terminal
53 Rancholabrean extinctions. *Icarus* **215**: 101-106.
54
55
56 Brooks MJ, Taylor BE, Ivester AH. 2010. Carolina Bays: Time capsules of culture
57 and climate change. *Southeastern Archaeology* **29**: 146-163.
58
59
60 Bunch TE, West A, Firestone RB, Kennett JP, Wittke JH, Kinzie CR, Wolbach WS.
2010. Geochemical data reported by Paquay et al. do not refute Younger Dryas
impact event. *Proc. Natl. Acad. Sci. USA* **107**: E58.

- 1
2
3
4 Bunch TE, Hermes RE, Moore AMT, Kennett DJ, Weaver JC, Wittke JH, DeCarli
5 PS, Bischoff JL, Hillman GC, Howard GA, Kimbel DR, Kletetschka G, Lipo CP,
6 Sakai S, Revay Z, West A, Firestone RB, Kennett JP. 2012. Very high-
7 temperature impact melt products as evidence for cosmic airbursts and impacts
8 12,900 years ago. *Proc. Natl. Acad. Sci. USA* **109**: E1903-E1912.
9
- 10
11 Bundy FP, Kasper JS. 1967. Hexagonal diamond—A new form of carbon. *J. Chem.*
12 *Phys.* **46**: 3437-3446.
13
- 14 Burkhard G, Dan K, Tanabe Y, Sawaoka AB, Yamada K. 1994. Formation of cubic
15 carbon by dynamic shock compression of a diamond/amorphous carbon powder
16 mixture. *Jpn. J. Appl. Phys.* **33**: 5875-5885.
17
- 18
19 Carlisle DB, Braman DR. 1991. Nanometre-size diamonds in the Cretaceous/Tertiary
20 boundary clay of Alberta. *Nature* **352**: 708-709.
21
- 22
23 Carlisle DB. 1992. Diamonds at the K/T boundary. *Nature* **357**: 119-120.
24
- 25
26 Carlson AE. 2013. The Younger Dryas Climate Event. Encyclopedia of Quaternary
27 Science, editors S. A. Elias and C. J. Mock (Elsevier, Amsterdam, The
28 Netherlands), vol. 3, pp. 126-134.
29
- 30
31 Cartigny P, Chinn I, Viljoen KS, Robinson D. 2004. Early proterozoic ultrahigh
32 pressure metamorphism: Evidence from microdiamonds. *Science* **304**: 853-855.
33
- 34
35 Cartigny P. 2010. Mantle-related carbonados? Geochemical insights from diamonds
36 from the Dachine komatiite (French Guiana). *Earth and Planetary Science Letters*
37 **296**: 329-339.
38
- 39
40 Cayron C, Hertog MD, Latu-Romain L, Mouchet C, Secouard C, Rouviere J-L,
41 Rouviere E, Simonato J-P. 2008. Odd electron diffraction patterns in silicon
42 nanowires and silicon thin films explained by microtwins and nanotwins. *Journal*
43 *of Applied Crystallography* **42**: 242-252.
44
- 45
46 Cerva H. 1991. High-resolution electron microscopy of diamond hexagonal silicon in
47 low pressure chemical vapor deposited polycrystalline silicon. *J. Mater. Res.* **6**:
48 2324-2336.
49
- 50
51 Chaverri P, Samuels GJ. 2002. *Hypocrea lixii*, the teleomorph of *Trichoderma*
52 *harzianum*. *Mycological Process* **1**: 283-286.
53
- 54
55 Chen CJ, Chang L, Lin TS, Chen FR. 1996. Direct observations of heteroepitaxial
56 diamond on silicon(110) substrate by microwave plasma chemical vapor
57 deposition. *J. Mat. Res.* **11**: 1002-1010.
58
- 59
60 Chopin C, Sobolev NV. 1995. Principal mineralogic indicators of UHP in crustal
rocks. (Chapter 3) in "*Ultrahigh Pressure Metamorphism*" editors R. G. Coleman
and X. Wan (Cambridge University Press, New York, New York, 1995), pp. 96-
131.

- 1
2
3
4 Clarke Jr. RS, Appleman DE, Ross DR. 1981. An Antarctic iron meteorite contains
5 preterrestrial impact-produced diamond and lonsdaleite. *Nature* **291**: 396-398.
6
7
8 Collard M, Buchanan B, Hamilton MJ, O'Brien MJ. 2010. Spatiotemporal dynamics
9 of the Clovis-Folsom transition. *J. Arch. Sci.* **37**: 2513-2519.
10
11 Cooper A, Turney C, Hughen KA, Brook BW, McDonald HG, Bradshaw CJA. 2015.
12 Abrupt warming events drove Late Pleistocene Holarctic megafaunal turnover.
13 *Science* **349**: 602-606.
14
15 Dahmen U, Hetherington CJ, Pirouz P, Westmacott KH. 1989. The formation of
16 hexagonal silicon at twin intersections. *Scripta Metallurgica* **23**: 269-272.
17
18 Dai ZR, Bradley JP, Joswiak DJ, Brownlee DE, Hill HGM, Genge MJ. 2002. Possible
19 in situ formation of meteoritic nanodiamonds in the early Solar System. *Nature*
20 **418**: 157-159.
21
22
23 Daniau A-L, Harrison SP, Bartlein PJ. 2010. Fire regimes during the Last Glacial.
24 *Quaternary Science Reviews* **29**: 2918-2930.
25
26 Darrah TH, Poreda RJ, Kennett JP, Becker L, West A, Kennett DJ, Elrandson JM.
27 2007. Mineralogical and noble gas evidence for an ET impact at the Younger
28 Dryas. *Eos Trans. AGU* **88**: (23) PP41A-04.
29
30
31 Daulton TL, Eisenhour DD, Bernatowicz TJ, Lewis RS, Buseck PR. 1996. Genesis of
32 presolar diamonds: Comparative high-resolution transmission electron
33 microscopy study of meteoritic and terrestrial nano-diamonds. *Geochimica et*
34 *Cosmochimica Acta* **60**: 4853-4872.
35
36 Daulton TL, Bernatowicz TJ, Lewis RS, Messenger S, Stadermann FJ, Amari S.
37 2003. Polytype distribution of circumstellar silicon carbide: Microstructural
38 characterization by transmission electron microscopy. *Geochimica et*
39 *Cosmochimica Acta* **67**: 4743-4767.
40
41
42 Daulton TL. 2006. Extraterrestrial nanodiamonds in the cosmos, (Chapter II) in
43 "*Ultrananocrystalline Diamond: Synthesis, Properties, and Applications*" editors
44 O. Shenderova and D. Gruen, (William Andrew Publishers, Norwich, New York,
45 2006), pp. 23-78.
46
47 Daulton TL, Pinter N, Scott AC. 2010. No evidence of nanodiamonds in Younger-
48 Dryas sediments to support an impact event. *Proc. Natl. Acad. Sci. USA* **107**:
49 16043-16047.
50
51
52 Daulton TL. 2012. Suspect cubic diamond "impact" proxy and a suspect lonsdaleite
53 identification. *Proc. Natl. Acad. Sci. USA* **109**: E2242.
54
55 Deal M. 2005. Palaeoethnobotanical research at Port au Choix. *Newfoundland and*
56 *Labrador Studies* **20**: 131-156.
57
58
59
60

- den Hertog MI, Cayron C, Gentile P, Dhalluin F, Oehler F, Baron T, Rouviere JL. 2012. Hidden defects in silicon nanowires. *Nanotechnology* **23**: 1-10.
- Dennis RL. 1976. *Palaeosclerotium*, a Pennsylvanian age fungus combining features of modern ascomycetes and basidiomycetes. *Science* **192**: 66-68.
- Deutsch A, Koeberl C, Blum JD, French BM, Glass BP, Grieve R, Horn P, Jessberger EK, Kurat G, Reimold WU, Smit J, Stöffler D, Taylor SR. 1994. The impact-flood connection: Does it exist? *Terra Nova* **6**: 644-650.
- de Wit MCJ. 2004. The diamondiferous sediments on the farm Nooitgedacht (66), Kimberley South Africa. *South African Journal of Geology* **107**: 477-488.
- Dobosi G, Kurat G. 2010. On the origin of silicate-bearing diamondites. *Miner. Petrol.* **99**: 29-42.
- Dobrzhinetskaya LF, Eide EA, Larsen RB, Sturt BA, Trønnes RG, Smith DC, Taylor WR, Posukhova TV. 1995. Microdiamond in high-grade metamorphic rocks of the Western Gneiss region, Norway. *Geology* **23**: 597-600.
- Dobrzhinetskaya LF, Wirth R, Green II HW. 2007. A look inside of diamond-forming media in deep subduction zones. *Proc. Natl. Acad. Sci. USA* **104**: 9128-9132.
- Dobrzhinetskaya LF. 2012. Microdiamonds - Frontier of ultrahigh-pressure metamorphism: A review. *Gondwana Research* **21**: 207-223.
- Dobrzhinetskaya LF, Wirth R, Green HW, Schreiber A, Obannon E. 2013. First find of polycrystalline diamond in ultrahigh-pressure metamorphic terrane of Erzgebirge, Germany. *Journal of Metamorphic Geology* **31**: 5-18.
- Dubinchuk VT, Simakov SK, Pechnikov VA. 2010. Lonsdaleite in diamond-bearing metamorphic rocks of the Kokchetav Massif. *Doklady Earth Sciences* **430**: 40-42.
- Elad Y, Barak R, Chet I. 1984. Parasitism of sclerotia of *Sclerotium rolfsii* by *Trichoderma harzianum*. *Soil Biol. Biochem.* **16**: 381-386.
- Elias DC, Nair RR, Mohiuddin TMG, Morozov SV, Blake P, Halsall MP, Ferrari AC, Boukhvalov DW, Katsnelson MI, Geim AK, Novoselov KS. 2009. Control of graphene's properties by reversible hydrogenation: Evidence for graphane. *Science* **323**: 610-613.
- Faith JT, Surovell TA. 2009. Synchronous extinction of North America's Pleistocene mammals. *Proc. Natl. Acad. Sci. USA* **106**: 20641-20645.
- Fallon PJ, Brown LM. 1993. Analysis of chemical-vapour-deposited diamond grain boundaries using transmission electron microscopy and parallel electron energy loss spectroscopy in a scanning transmission electron microscope. *Diamond and Related Materials* **2**: 1004-1011.
- Fayek M, Anovitz LM, Allard LF, Hull S. 2012. Framboidal iron oxide: Chondrite-

- 1
2
3 like material from the black mat, Murray Springs, Arizona. *Earth and Planetary*
4 *Science Letters* **319-320**: 251-258.
5
6 Fedoseev DV, Bukhovets VL, Varshavskaya IG, Lavrent'ev AV, Derjaguin BV.
7 1983. Transition of graphite into diamond in a solid phase under the atmospheric
8 pressure. *Carbon* **21**: 237-241.
9
10 Ferdinandsen C, Winge Ö. 1925. *Cenococcum Fr.*: A monographic study. Den
11 Kongelige Veterinaer-og Landbohøjskole Aarsskrift, 332-382 (in Danish).
12
13 Fiedel SJ. 2011. The mysterious onset of the Younger Dryas. *Quaternary*
14 *International* **242**: 262-266.
15
16 Firestone RB, Topping W. 2001. Terrestrial Evidence of a nuclear catastrophe in
17 Paleoinian times. *Mammoth Trumpet* **16**: 9-16.
18
19 Firestone RB, Topping W. 2002. Response to the comments by J. R. Southon and R.
20 E. Taylor. *Mammoth Trumpet* **17**: 14-17.
21
22 Firestone R, West A, Warwick-Smith S. 2006. The Cycle of Cosmic Catastrophes:
23 Flood, Fire, and Famine in the History of Civilization. Bear & Company,
24 Rochester, VT.
25
26 Firestone RB, West A, Kennett JP, Becker L, Bunch TE, Revay ZS, Schultz PH,
27 Belgya T, Kennett DJ, Erlandson JM, Dickenson OJ, Goodyear AC, Harris RS,
28 Howard GA, Kloosterman JB, Lechler P, Mayewski PA, Montgomery J, Poreda
29 R, Darrah T, Que Hee SS, Smith AR, Stich A, Topping W, Wittke JH, Wolbach
30 WS. 2007. Evidence for an extraterrestrial impact 12,900 years ago that
31 contributed to the megafaunal extinctions and the Younger Dryas cooling. *Proc.*
32 *Natl. Acad. Sci. USA* **104**: 16016-16021.
33
34 Firestone RB. 2009. The case for the Younger Dryas extraterrestrial impact event:
35 Mammoth, megafauna, and Clovis extinction, 12,900 years ago. *Journal of*
36 *Cosmology* **2**: 256-285.
37
38 Firestone RB, West A, Revay Z, Hagstrum JT, Belgya T, Que Hee SS, Smith AR.
39 2010a. Analysis of the Younger Dryas impact layer. *Journal of Siberian Federal*
40 *University Engineering & Technologies* **3**: 30-62.
41
42 Firestone RB, West A, Bunch TE. 2010b. Confirmation of the Younger Dryas
43 boundary (YDB) data at Murray Springs, AZ. *Proc. Natl. Acad. Sci. USA* **107**:
44 E105.
45
46 Fleischer R. 1998. A rift model for the sedimentary diamond deposits of Brazil.
47 *Mineralium Deposita* **33**: 238-254.
48
49 French BM, Koeberl C. 2010. The convincing identification of terrestrial meteorite
50 impact structures: What works, what doesn't, and why. *Earth-Science Reviews* **98**:
51 123-170.
52
53
54
55
56
57
58
59
60

- 1
2
3 Frezzotti M-L, Peccerillo A. 2007. Diamond-bearing COHS fluids in the mantle
4 beneath Hawaii. *Earth and Planetary Science Letters* **262**: 273-283.
5
6 Frezzotti M-L, Huizenga J-M, Compagnoni R, Selverstone J. 2014. Diamond
7 formation by carbon saturation in C-O-H fluids during cold subduction of oceanic
8 lithosphere. *Geochimica et Cosmochimica Acta* **143**: 68-86.
9
10 Frondel C, Marvin UB. 1967. Lonsdaleite, a hexagonal polymorph of diamond.
11 *Nature* **214**: 587-589.
12
13 Geim AK, Novoselov KS. 2007. The rise of graphene. *Nature Materials* **6**: 183-191.
14
15 Gill JL, Williams JW, Jackson ST, Lininger KB, Robinson GS. 2009. Pleistocene
16 megafaunal collapse, novel plant communities, and enhanced fire regimes in
17 North America. *Science* **326**: 1100-1103.
18
19 Gilmour I, Russell SS, Arden JW, Lee MR, Franchi IA, Pillinger CT. 1992.
20 Terrestrial carbon and nitrogen isotopic ratios from cretaceous-tertiary boundary
21 nanodiamonds. *Science* **258**: 1624-1626.
22
23 Gilmour I, French BM, Franchi IA, Abbott JI, Hough RM, Newton J, and Koeberl C.
24 2003. Geochemistry of carbonaceous impactites from the Gardnos impact
25 structure, Norway. *Geochimica et Cosmochimica Acta* **67**: 3889-3903.
26
27 Golovnya SV, Khvostova VP, Makarov ES. 1977. Hexagonal modification of
28 diamond (lonsdaleite) in the eclogites of metamorphic complexes. *Geochem. Int.*
29 **14**: 82-84 (translated from: *Geokhimiya*, 1977(5), 790-793).
30
31 Gorshkov AI, Vinokurov SF, Solodov DI, Bershov LV, Mokhov AV, Solodova YP,
32 Sivtsov AV. 1999. Polycrystalline diamond from the Udachnaya Pipe, Yakutia:
33 Mineralogical, geochemical, and genetic characteristics. *Lithology and Mineral*
34 *Resources* **34**: 397-410.
35
36 Goryainov SV, Likhacheva AY, Rashchenko SV, Shubin AS, Afanas'ev VP,
37 Pokhilenko NP. 2014. Raman identification of lonsdaleite in Popigai impactites. *J.*
38 *Raman Spectros.* **45**: 305-313.
39
40 Grant JA, Brooks MJ, Taylor BE. 1998. New constraints on the evolution of the
41 Carolina Bays from ground-penetrating radar. *Geomorphology* **22**: 325-345.
42
43 Grayson DK. 2007. Deciphering North American Pleistocene extinctions. *J.*
44 *Anthropol. Res.* **63**: 185-213.
45
46 Gurov E, Gurova E, Chernenko Y, Yamnichenko A. 2009. The Obolon impact
47 structure, Ukraine, and its ejecta deposits. *Meteoritics & Planetary Science* **44**:
48 389-404.
49
50 Haggerty SE. 1999. A diamond trilogy: Superplumes, supercontinents, and
51 supernovae. *Science* **285**: 851-860.
52
53
54
55
56
57
58
59
60

- 1
2
3 Haggerty SE. 2014. Carbonado: Physical and chemical properties, a critical
4 evaluation of proposed origins, and a revised genetic model. *Earth Science*
5 *Reviews* **130**: 49-72.
6
7 Hanneman RE, Strong HM, Bundy FP. 1967. Hexagonal diamonds in meteorites:
8 Implications. *Science* **155**: 995-997.
9
10 Hardiman M, Scott AC, Collinson ME, Anderson RS. 2012. Inconsistent redefining
11 of the carbon spherule “impact” proxy. *Proc. Natl. Acad. Sci. USA* **109**: E2244.
12
13 Harris-Parks E. 2014. The micromorphology of Younger Dryas-aged black mats from
14 Nevada, Arizona, Texas and New Mexico. M.S. thesis, The University of
15 Arizona.
16
17 Harris-Parks E. 2016. The micromorphology of Younger Dryas-aged black mats from
18 Nevada, Arizona, Texas and New Mexico. *Quaternary Research*,
19 <http://dx.doi.org/10.1016/j.yqres.2015.11.005>.
20
21
22
23 Hauge HIT, Verheijen MA, Conesa-Boj S, Etzelstorfer T, Watzinger M, Kriegner D,
24 Zardo I, Fasolato C, Capitani F, Postorino P, Kölling S, Li A, Assali S, Stangl J,
25 Bakkers EPAM. 2015. Hexagonal silicon realized. *Nano Lett.* **15**: 5855-5860.
26
27
28 Haynes Jr. C. 2008. Younger Dryas “black mats” and the Rancholabrean termination
29 in North America. *Proc. Natl. Acad. Sci. USA* **105**: 6520-6525.
30
31 Haynes Jr. CV, Boerner J, Domanik K, Lauretta D, Ballenger J, and Goreva J. 2010a.
32 The Murray Springs Clovis site, Pleistocene extinction, and the question of
33 extraterrestrial impact. *Proc. Natl. Acad. Sci. USA* **107**: 9, 4010-4015.
34
35 Haynes Jr. CV, Lauretta DS, Ballenger JAM. 2010b. Reply to Firestone *et al.*: No
36 confirmation of impact at the lower Younger Dryas boundary at Murray Springs,
37 AZ. *Proc. Natl. Acad. Sci. USA* **107**: E106.
38
39 Heaney PJ, Vicenzi EP, De S. 2005. Strange diamonds: The mysterious origins of
40 carbonado and framesite. *Elements* **1**: 85-89.
41
42 Heck PR, Stadermann FJ, Isheim D, Auciello O, Daulton TL, Davis AM, Elam JW,
43 Floss C, Hiller J, Larson DJ, Lewis JB, Mane A, Pellin MJ, Savina MR, Seidman
44 DN, Stephan T. 2014. Atom-probe analysis of nanodiamonds from Allende.
45 *Meteoritics & Planetary Science* **49**: 453-467.
46
47
48 Higgins MD, Lajeunesse P, St-Onge G, Locat J, Duchesne M, Ortiz J, Sanfaçon R.
49 2011. Bathymetric and petrological evidence for a young (Pleistocene?) 4-km
50 diameter impact crater in the Gulf of Saint Lawrence, Canada. *Lunar & Planetary*
51 *Science Conference XLII*: 1504.
52
53
54 Hirai H, Kondo K-I. 1991. Modified phases of diamond formed under shock
55 compression and rapid quenching. *Science* **253**: 772-774.
56
57 Holliday VT, Meltzer DJ. 2010. The 12.9-ka ET impact hypothesis and North
58
59
60

- American Paleoindians. *Current Anthropology* **51**: 575-607.
- Holliday VT, Surovell T, Meltzer DJ, Grayson DK, Boslough M. 2014. The Younger Dryas impact hypothesis: A cosmic catastrophe. *Journal of Quaternary Science* **29**: 515-530.
- Holliday VT. 2015. Problematic dating of claimed Younger Dryas boundary proxies. *Proc. Natl. Acad. Sci. USA* **112**: E6721.
- Hormes A, Karlén W, Possnert G. 2004. Radiocarbon dating of palaeosol components in moraines in Lapland, northern Sweden. *Quaternary Science Reviews* **23**: 2031-2043.
- Hosseini MR, Schaffie M, Pazouki M, Darezereshki E, Ranjbar M. 2012. Biologically synthesized copper sulfide nanoparticles: Production and characterization. *Materials Science in Semiconductor Processing* **15**: 222-225.
- Hough RM, Gilmour I, Pillinger CT, Arden JW, Gilkes KWR, Yuan J, Milledge HJ. 1995. Diamond and silicon carbide in impact melt rock from the Ries impact crater. *Nature* **378**: 41-44.
- Hough RM, Gilmour I, Pillinger CT, Langenhorst F, Montanari A. 1997. Diamonds from the iridium-rich K-T boundary layer at Arroyo el Mimbral, Tamaulipas, Mexico. *Geology* **25**: 1019-1022.
- Huss GR, Lewis RS. 1994. Noble gases in presolar diamonds I: Three distinct components and their implications for diamond origins. *Meteoritics* **29**: 791-810.
- Israde-Alcántara I, Bischoff JL, Domínguez-Vázquez G, Li H-C, DeCarli PS, Bunch TE, Wittke JH, Weaver JC, Firestone RB, West A, Kennett JP, Mercer C, Xie S, Richman EK, Kinzie CR, Wolbach WS. 2012a. Evidence from central Mexico supporting the Younger Dryas extraterrestrial impact hypothesis. *Proc. Natl. Acad. Sci. USA* **109**: E738-E747.
- Israde-Alcántara I, Bischoff JL, DeCarli PS, Domínguez-Vázquez G, Bunch TE, Firestone RB, Kennett JP, West A. 2012b. Reply to Blaauw et al., Boslough, Daulton, Gill et al., and Hardiman et al.: Younger Dryas impact proxies in Lake Cuitzeo, Mexico. *Proc. Natl. Acad. Sci. USA* **109**: E2245-E2247.
- Itoh N, Sakagami N, Torimura M, Watanabe M. 2012. Perylene in Lake Biwa sediments originating from *Cenococcum geophilum* in its catchment area. *Geochim. et Cosmochim. Acta* **95**, 241-251.
- Itoh N, Hashimoto B, Sakagami N, Watanabe M. 2013. The structure of a perylene-containing fossilized sclerotium is maintained by original silica. *Organic Geochemistry* **63**: 37-39.
- Ives JW, Froese D. 2013. The Chobot site (Alberta, Canada) cannot provide evidence of a cosmic impact 12,800 y ago. *Proc. Natl. Acad. Sci. USA* **110**: E3899.

- 1
2
3 Kaminsky FV, Blinova GK, Galimov EM, Gurkina GA, Kliuev YA, Kooptil VI,
4 Krivonos VF, Frolova LN, Khrenov AY. 1985. Polycrystalline aggregates of
5 diamond with lonsdaleite from placers in Yakutiya. *Mineralogical Journal* 7: 27-
6 36 (in Russian).
7
8
9 Kaminsky FV. 1994. Carbonado and yakutite: Properties and possible genesis. in
10 Proceedings of the Fifth International Kimberlite Conference, vol. 2, Diamonds:
11 Characterization, Genesis, and Exploration, edited by H. O. A. Meyer and O. H.
12 Leonardos, pp. 136-143, Companhia de Pesquisa de Recursos Minerais, Rio de
13 Janeiro, Brazil.
14
15 Kennett DJ, Kennett JP, West GJ, Erlandson JM, Johnson JR, Hendy IL, West A,
16 Culleton BJ, Jones TL, Stafford Jr. TW. 2008. Wildfire and abrupt ecosystem
17 disruption on California's Northern Channel Islands at the Ållerød-Younger Dryas
18 boundary (13.0-12.9 ka). *Quaternary Science Reviews* 27: 2530-2545.
19
20 Kennett DJ, Kennett JP, West A, Mercer C, Que Hee SS, Bement L, Bunch TE,
21 Sellers M, Wolbach WS. 2009a. Nanodiamonds in the Younger Dryas boundary
22 sediment layer. *Science* 323: 94.
23
24 Kennett DJ, Kennett JP, West A, West J, Bunch TE, Culleton BJ, Erlandson JM, Que
25 Hee SS, Johnson JR, Mercer C, Shen F, Sellers M, Stafford Jr. TW, Stich A,
26 Weaver JC, Wittke JH, Wolbach WS. 2009b. Shock-synthesized hexagonal
27 diamonds in Younger Dryas boundary sediments. *Proc. Natl. Acad. Sci. USA* 106:
28 12623-12628.
29
30 Kennett JP, Kennett DJ, Culleton BJ, Tortosa JEA, Bischoff JL, Bunch TE, Daniel Jr.,
31 IR, Erlandson JM, Ferraro D, Firestone RB, Goodyear AC, Israde-Alcántara I,
32 Johnson JR, Pardo JFJ, Kimbel DR, LeCompte MA, Lopinot NH, Mahaney WC,
33 Moore AMT, Moore CR, Ray JH, Stafford Jr. TW, Tankersley KB, Wittke JH,
34 Wolbach WS, West A. 2015a. Bayesian chronological analyses consistent with
35 synchronous age of 12,835-12,735 Cal B.P. for Younger Dryas boundary on four
36 continents. *Proc. Natl. Acad. Sci. USA* 112: E4344-E4353.
37
38 Kennett JP, Kennett DJ, Culleton BJ, Tortosa JEA, Bunch TE, Erlandson JM,
39 Johnson JR, Pardo JFJ, LeCompte MA, Mahaney WC, Tankersley KB, Wittke JH,
40 Wolbach WS, West A. 2015a. Reply to Holliday and Boslough et al.:
41 Synchronicity of widespread Bayesian-modeled ages supports Younger Dryas
42 impact hypothesis. *Proc. Natl. Acad. Sci. USA* 112: E6723-E6724.
43
44 Kerr RD. 2008. Experts find no evidence for a mammoth-killer impact. *Science* 319:
45 1331-1332.
46
47 Ketcham RA, Koeberl C. 2013. New textural evidence on the origin of carbonado
48 diamond: An example of 3-D petrography using X-ray computed tomography.
49 *Geosphere* 9: 1-12.
50
51 Kimbel D, West A, Kennett JP. 2008. A new method for producing nanodiamonds
52 based on research into the Younger Dryas extraterrestrial impact. *AGU Fall*
53 *Meeting*, abstract #PP13C-1470.
54
55
56
57
58
59
60

- 1
2
3
4 Kincaid BM, Meixner AE, Platzman PM. 1978. Carbon *K* edge in graphite measured
5 using electron-energy-loss spectroscopy. *Phys. Rev. Lett.* **40**: 1296-1299.
6
7
8 Kinzie CR, Que Hee SS, Stich A, Tague KA, Mercer C, Razink JJ, Kennett DJ,
9 DeCarli PS, Bunch TE, Wittke JH, Israde-Alcántara I, Bischoff JL, Goodyear AC,
10 Tankerseley KB, Kimbel DR, Culleton BJ, Erlandson JM, Stafford TW,
11 Kloosterman JB, Moore AMT, Firestone RB, Aura Tortosa JE, Jordá Pardo JF,
12 West A, Kennett JP, Wolbach WS. 2014. Nanodiamond-rich layer across three
13 continents consistent with major cosmic impact at 12,800 Cal BP. *Journal of*
14 *Geology* **122**: 475-505.
15
16 Koeberl C, Masaitis VL, Shafranovsky GI, Gilmour I, Langenhorst F, Schrauder M.
17 1997. Diamonds from the Popigai impact structure, Russia. *Geology* **25**: 967-970.
18
19
20 Kohno H, Ozaki N, Yoshida H, Tanaka K, Takeda S. 2003. Misleading fringes in
21 TEM images and diffraction patterns of Si nanocrystallites. *Cryst. Res. Technol.*
22 **38**: 1082-1086.
23
24
25 Konyashin I, Zern A, Mayer J, Aldinger F, Babaev V, Khvosov V, Guseva M. 2001.
26 A new carbon modification: “n-diamond” or face-centred cubic carbon? *Diam.*
27 *and Related Mat.* **10**: 99-102.
28
29
30 Kristan-Tollmann E., Tollmann A. 1992. Der Sintflut-Impakt (The flood impact).
31 *Mitteilungen Der Österreichischen Geographischen Gesellschaft* **84**: 1-63 (in
32 German).
33
34
35 Kristan-Tollmann E., Tollmann A. 1994. The youngest big impact on Earth deduced
36 from geological and historical evidence. *Terra Nova* **6**: 209-217.
37
38
39 Ksanda CJ, Henderson EP. 1939. Identification of diamond in the Canyon Diablo
40 Iron. *American Mineralogist* **24**: 677-680.
41
42
43 Kulnitskiy B, Perezhogin I, Dubitsky G, Blank V. 2013. Polytypes and twins in the
44 diamond-lonsdaleite system formed by high-pressure and high-temperature
45 treatment of graphite. *Acta Crystal. Section B* **B69**: 474-479.
46
47
48 Kurat G, Dobosi G. 2000. Garnet and diopside-bearing diamondites (framesites).
49 *Mineralogy and Petrology* **69**: 143-159.
50
51
52 Kurbatov AV, Mayewski PA, Steffensen JP, West A, Kennett DJ, Kennett JP, Bunch
53 TE, Handley M, Introne DS, Que Hee SS, Mercer C, Sellers M, Shen F, Sneed
54 SB, Weaver JC, Wittke JH, Stafford Jr. TW, Donovan JJ, Xie S, Razink JJ, Stich
55 A, Kinzie CR, Wolbach WS. 2010. Discovery of a nanodiamond-rich layer in the
56 Greenland ice sheet. *J. Glaciol.* **56**: 749-759.
57
58
59
60 Kvasnitsa VN, Sobotovich EV, Kovalyukh NN, Litvin AL, Rybalko SI, Sharkin OP,
Egorova LN. 1979. High-pressure carbon polymorphs in the peats of Tunguska
catastrophe region. *Doklady Akademii Nauk USSR* **B12**: 999-1004 (in Russian).

- 1
2
3 Kvasnytsya V, Wirth R, Dobrzhinetskaya L, Matzel J, Jacobsen B, Hutcheon I,
4 Tappero R, Kovalyukh M. 2013. New evidence of meteoritic origin of the
5 Tunguska cosmic body. *Planetary and Space Science* **84**: 131-140.
6
7
8 Lajeunesse P, St-Onge G, Locat J, Duchesne MJ, Higgins MD, Sanfaçon R, Ortiz J.
9 2013. The Corossol structure: A possible impact crater on the seafloor of the
10 northwestern Gulf of St. Lawrence, Eastern Canada. *Meteoritics & Planetary*
11 *Science* **48**: 2542-2558.
12
13 Largent F. 2008. The Clovis Comet Part I: Evidence for a cosmic collision 12,900
14 years ago. *Mammoth Trumpet* **23**: 1-3,19-20.
15
16 LaViolette PA. 1987. Cosmic-ray volleys from the galactic center and their recent
17 impact on the Earth environment. *Earth, Moon, and Planets* **37**: 241-286.
18
19 LaViolette PA. 2005. *Earth Under Fire: Humanity's Survival of the Ice Age*. Bear &
20 Company, Rochester, VT.
21
22 LaViolette PA. 2011. Evidence for a solar flare cause of the Pleistocene mass
23 extinction. *Radiocarbon* **53**: 303-323.
24
25
26 Lewis RS. 1994. Precision noble gas measurements on presolar diamonds from the
27 Murchison meteorite. *Lunar and Planetary Science Conference* **XXV**: 793.
28
29 Lewis RS, Tang M, Wacker JF, Anders E, Steel E. 1987. Interstellar diamonds in
30 meteorites. *Nature* **326**: 160-162.
31
32
33 Lewis RS, Anders E, Draine BT. 1989. Properties, detectability and origin of
34 interstellar diamonds in meteorites. *Nature* **339**: 117-121.
35
36 Lifshitz Y, Duan XF, Shang NG, Li Q, Wan L, Bello I, Lee ST. 2001. Epitaxial
37 diamond polytypes on silicon. *Nature* **412**: 404.
38
39
40 Love SG, Brownlee DE. 1993. A direct measurement of terrestrial mass accretion rate
41 of cosmic dust. *Science* **262**: 550-553.
42
43 Luyten W, van Tendeloo G, Amelinckx S, Collins JL. 1992. Electron microscopy
44 study of defects in synthetic diamond layers. *Philosophical Magazine A* **66**: 899-
45 915.
46
47 Madden A, Swindle A, Bement L, Carter B, Simms A, Benamara M. 2012.
48 Nanodiamonds and carbonaceous grains in Bull Creek Valley, Oklahoma.
49 *Mineral. Mag.* **76**: 2051.
50
51
52 Mahaney WC, Kalm V, Krinsley DH, Tricart P, Schwartz S, Dohm J, Kim KJ,
53 Kapran B, Miner MW, Beukens R, Boccia S, Hancock RGV, Hart KM, Kelleher
54 B. 2010. Evidence from the northwestern Venezuelan Andes for extraterrestrial
55 impact: The black mat enigma. *Geomorphology* **116**: 48-57.
56
57
58 Manceau A, Nagy KL, Marcus MA, Lanson M, Geoffroy N, Jacquet T,
59
60

- 1
2
3 Kirpichtchikova T. 2008. Formation of metallic copper nanoparticles at the soil-
4 root interface. *Environ. Sci. Technol.* **42**: 1766-1772.
5
6 Mandel RD. 2008. Buried paleoindian-age landscapes in stream valleys of the Central
7 Plains, USA. *Geomorphology* **101**: 342-361.
8
9 Marlon JR, Bartlein PJ, Walsh MK, Harrison SP, Brown KJ, Edwards ME, Higuera
10 PE, Power MJ, Anderson RS, Briles C, Brunelle A, Carcaillet C, Daniels M, Hu
11 FS, Lavoie M, Long C, Minckley T, Richard PJH, Scott AC, Shafer DS, Tinner
12 W, Umbanhowar Jr. CE, Whitlock C. 2009. Wildfire responses to abrupt climate
13 change in North America. *Proc. Natl. Acad. Sci. USA* **106**: 8, 2519-2524.
14
15 Masaitis VL, Shafranovsky GI, Grieve RAF, Langenhorst F, Peredery WV, Therriault
16 AM, Balmasov EL, Fedorova IG. 1999. Impact diamonds in the suevitic breccias
17 of the Black member of the Onaping formation, Sudbury structure, Ontario,
18 Canada. in "Large meteorite impacts and planetary evolution II" editors B. O.
19 Dressler and V. L. Sharpton, (Geological Society of America, Boulder, Colorado,
20 2000), pp. 317-321.
21
22 Matyushenko NN, Strel'nitskiĭ VE, Gusev VA. 1979. A dense new version of
23 crystalline carbon C₈. *JETP Lett.* **30**: 199-202.
24
25 McCall GJH. 2009. The carbonado diamond conundrum. *Earth-Science Reviews* **93**:
26 85-91.
27
28 McLaren D, Fedje D, Hay MB, Mackie Q, Walker IJ, Shugar DH, Eamer JBR, Lian
29 OB, Neudorf C. 2014. A post-glacial sea level hinge on the central Pacific coast of
30 Canada. *Quaternary Science Reviews* **97**: 148-169.
31
32 McWeeney L. 1989. What lies lurking below the soil: Beyond the archaeobotanical
33 view of flotation samples. *North Amer. Arch.* **10**: 227-230.
34
35 Melosh HJ. 2009. Airburst in the sky with diamonds? Shock limits to a Younger
36 Dryas impact. *American Geophysical Union, Fall Meeting*, PP33B-03.
37
38 Melton FA, Schriever W. 1933. The Carolina "Bays" – Are they Meteorite Scars? *The*
39 *Journal of Geology* **41**: 52-66.
40
41 Meltzer DJ, Holliday VT. 2010. Would North American Paleoindians have noticed
42 Younger Dryas age climate changes? *J. World Prehist.* **23**: 1-41.
43
44 Meltzer DJ, Holliday VT, Cannon MD, Miller DS. 2014. Chronological evidence fails
45 to support claim of an isochronous widespread layer of cosmic impact indicators
46 dated to 12,800 years ago. *Proc. Natl. Acad. Sci. USA* **111**: E2162-E2171.
47
48 Mützenberger B, Bubner B, Wöllecke J, Sieber TN, Bauer R, Fladung M, Hüttl RF.
49 2009. The ectomycorrhizal morphotype *Pinirhiza sclerotia* is formed by *Acephala*
50 *macrosclerotiorum* sp. nov., a close relative of *Phialocephala fortinii*. *Mycorrhiza*
51 **19**: 481-492.
52
53
54
55
56
57
58
59
60

- 1
2
3 Myasnikov I, Chernysheva M, Badun G, Korobkov V, Kulikova N. 2014. Humic
4 substances alter uptake of nanodiamonds by wheat plants. *Third International*
5 *Conference of CIS IHSS on Humic Innovative Technologies Tenth International*
6 *Conference daRostim Humic Substances and Other Biologically Active*
7 *Compounds in Agriculture HIT-daRostim-2014*, Nov. 19-23, 2014 Lomonosov
8 Moscow State University, Moscow Russia, 59.
9
- 10
11 Nakamuta Y, Aoki Y. 2000. Mineralogical evidence for the origin of diamond in
12 ureilites. *Meteoritics & Planetary Science* **35**: 487-493.
13
- 14 Napier WM, Bunch TE, Kennett JP, Wittke JH, Tankersley KB, Kletetschka G,
15 Howard GA, West A. 2013. Reply to Boslough et al.: Decades of comet research
16 counter their claims. *Proc. Natl. Acad. Sci. USA* **110**: E4171.
17
- 18 Németh P, Garvie LAJ, Aoki T, Dubrovinskaia N, Dubrovinsky L, Buseck PR. 2014.
19 Lonsdaleite is faulted and twinned cubic diamond and does not exist as a discrete
20 material. *Nature Communications* **5**: 5447 doi:10.1038/ncomms6447.
21
22
- 23 Netherlands Patent Release. 1965. No. 6506395, November 22, 1965, E. I. du Pont de
24 Nemours and Company.
25
- 26 Nowicki TE, Moore RO, Gurney JJ, Baumgartner MC. 2007. Chapter 46 Diamonds
27 and associated heavy minerals in kimberlite: A review of key concepts and
28 applications. *Developments in Sedimentology* **58**: 1235-1267.
29
- 30 Ogasawara Y. 2005. Microdiamonds in ultrahigh-pressure metamorphic rocks.
31 *Elements* **1**: 91-96.
32
33
- 34 Ona S, Nakamoto Y, Kagayama T, Shimizu K, Nishikawa Y, Murakami M, Kusakabe
35 K, Watanuki T, Ohishi Y. 2008. Stability of hexagonal diamond under pressure.
36 *Journal of Physics: Conference Series* **121**: 1-3.
37
- 38 Ozima M, Zashu S, Tomura K, Matsuhisa Y. 1991. Constraints from noble-gas
39 contents on the origin of carbonado diamonds. *Nature* **6**: 472-474.
40
41
- 42 Pantidos N, Horsfall LE. 2014. Biological synthesis of metallic nanoparticles by
43 bacteria, fungi and plants. *J. Nanomed. Nanotechnol.* **5**: 233. doi: 10.4172/2157-
44 7439.1000233.
45
- 46 Paquay FS, Goderis S, Ravizza G, Vanhaeck F, Boyd M, Surovell TA, Holliday VT,
47 Haynes Jr. CV, Claeys P. 2009. Absence of geochemical evidence for an impact
48 event at the Bølling-Allerød/Younger Dryas transition. *Proc. Natl. Acad. Sci. USA*
49 **106**: (51), 21505-21510.
50
- 51
52 Paquay FS, Goderis S, Ravizza G, Claeys P. 2010. Reply to Bunch et al.: Younger
53 Dryas impact proponents challenge new platinum group elements and osmium
54 data unresponsive of their hypothesis. *Proc. Natl. Acad. Sci. USA* **107**: E59-E60.
55
- 56 Pechnikov VA, Kaminsky FV. 2008. Diamond potential of metamorphic rocks in the
57 Kokchetav Massif, northern Kazakhstan. *Eur. J. Mineral.* **20**: 395-413.
58
59
60

- 1
2
3
4
5
6
7
8
9
10
11
12
13
14
15
16
17
18
19
20
21
22
23
24
25
26
27
28
29
30
31
32
33
34
35
36
37
38
39
40
41
42
43
44
45
46
47
48
49
50
51
52
53
54
55
56
57
58
59
60
- Perevedentseva E, Hong S-F, Huang K-J, Chiang L-T, Lee C-Y, Tseng Y-T, Cheng C-L. 2013. Nanodiamond internalization in cells and the cell uptake mechanism. *J. Nanopart. Res.* **15**: 1834, 1-12.
- Perraki M, Proyer A, Mposkos E, Kaindl R, Hoinkes G. 2006. Raman microspectroscopy on diamond, graphite, and other carbon polymorphs from the ultrahigh-pressure metamorphic Kimi Complex of the Rhodope Metamorphic Province, NE Greece. *Earth and Planetary Science Letters* **241**: 672-685.
- Petaev MI, Huang S, Jacobsen SB, Zindler A. 2013a. Large Pt anomaly in the Greenland ice core points to a cataclysm at the onset of Younger Dryas. *Proc. Natl. Acad. Sci. USA* **110**: 12917-12920.
- Petaev MI, Huang S, Jacobsen SB, Zindler A. 2013b. Reply to Boslough: Is Greenland Pt anomaly global or local? *Proc. Natl. Acad. Sci. USA* **110**: E5036.
- Petrovsky VA, Filonenko VP, Silaev VI, Zibrov IP, Sukharev AE, Zemnukhov AL, Pomazansky BS. 2013. Yakutit X-ray analysis and evaluation of content of lonsdaleite impurities. *Bulletin of the University of Perm. Geology* **3(20)**: 43-60 (in Russian).
- Pigati JS, Latorre C, Rech JA, Betancourt JL, Martínez KE, Budahn JR. 2012. Accumulation of impact markers in desert wetlands and implications for the Younger Dryas impact hypothesis. *Proc. Natl. Acad. Sci. USA* **109**: (19), 7208-7212.
- Pinter N, Ishman SE. 2008. Impacts, mega-tsunami, and other extraordinary claims. *GSA Today* **18**: 37-38.
- Pinter N, Scott AC, Daulton TL, Podoll A, Koeberl C, Anderson RS, Ishman SE. 2011. The Younger Dryas impact hypothesis: A requiem. *Earth-Science Reviews* **106**: 247-264.
- Quade J, Forester RM, Pratt WL, Carter C. 1998. Black mats, spring-fed streams, and Late-Glacial-age recharge in the Southern Great Basin. *Quaternary Research* **49**: 129-148.
- Rech JA, Pigati JS, Quade J, Betancourt JL. 2003. Re-evaluation of mid-Holocene deposits at Quebrada Puripica, northern Chile. *Paleogeography, Paleoclimatology, Paleoecology* **194**: 207-222.
- Redmond BG, Tankersley KB. 2011. Species response to the theorized Clovis comet impact at Sheriden Cave, Ohio. *Curr. Res. Pleistocene* **28**: 141-143.
- Reichle RE, Alexander JV. 1965. Multiperforate septations, Woronin bodies, and septal plugs in *Fusarium*. *J. Cell Biol.* **24**: 489-496
- Reimold WU, Ferrière L, Deutsch A, Koeberl C. 2014. Impact controversies: Impact recognition criteria and related issues. *Met. & Planet. Sci.* **49**: 723-731.

- 1
2
3
4 Rietmeijer FJM, Mackinnon IDR. 1987. Metastable carbon in two chondritic porous
5 interplanetary dust particles. *Nature* **326**: 162-165.
6
7
8 Rodriguez AB, Waters MN, Piehler MF. 2012. Burning peat and reworking loess
9 contribute to the formation and evolution of a large Carolina-bay basin.
10 *Quaternary Research* **77**: 171-181.
11
12 Rozen OM, Zorin YM, Zayachkovsky AA. 1972. A find of diamonds linked with
13 eclogites of the Precambrian Kokchetav massif. *Akademiya Nauk SSR Doklady*
14 **203**: 674-676 (in Russian).
15
16 Rothwell GW. 1972. *Palaeosclerotium pusillum* gen. et sp. nov., a fossil eumycete
17 from the Pennsylvanian of Illinois. *Can. J. Bot.* **50**: 2353-2356.
18
19 Russell SS, Arden JW, Pillinger CT. 1996. A carbon and nitrogen isotope study of
20 diamond from primitive chondrites. *Meteoritics & Planetary Science* **31**: 343-355.
21
22
23 Salvadori MR, Lepre LF, Ando RA, Oller do Nascimento CA, Corrêa B. 2013.
24 Biosynthesis and uptake of copper nanoparticles by dead biomass of *Hypocrea*
25 *lixii* isolated from the metal mine in the Brazilian Amazon Region. *PLoSone* **8**:
26 eB0519.
27
28 Salvadori MR, Ando RA, Oller do Nascimento CA, Corrêa B. 2014. Bioremediation
29 from wastewater and extracellular synthesis of copper nanoparticles by the fungus
30 *Trichoderma koningiopsis*. *Journal of Environmental Science and Health* **49**:
31 1286-1295.
32
33
34 Sass HR. 1944. When the Comet Struck. *Saturday Evening Post* **217**: 12-13,105-107.
35
36 Schmidt S, Nagel TJ, Froitzheim N. 2010. A new occurrence of microdiamond-
37 bearing metamorphic rocks, SW Rhodopes, Greece. *Eur. J. Mineral.* **22**: 189-198.
38
39 Scott AC, Pinter N, Collinson ME, Hardiman M, Anderson RS, Brain APR, Smith
40 SY, Marone F, Stampanoni M. 2010. Fungus, not comet or catastrophe, accounts
41 for carbonaceous spherules in the Younger Dryas “impact layer”. *Geophys. Res.*
42 *Lett.* **37**: L14302, 1-5.
43
44 Scott AC, Hardiman M, Daulton TL, Pinter N, Anderson RS, Ejarque A, Higham T,
45 Finch P, Carter-Champion A. 2016. Late Quaternary fluvial sequences, Santa
46 Rosa Island, California: Recording, sampling, interpretation, and implications for
47 the Younger Dryas Impact Hypothesis. submitted to *Journal of Quaternary*
48 *Science*.
49
50
51 Shay CT, Kapinga MRM. 1997. *Cenococcum geophilum* sclerotia from an
52 archaeological site in western Canada. *North American Archaeologist* **18**: 363-
53 370.
54
55
56 Shelkov DA, Verchovsky AB, Milledge HJ, Kaminsky FV, Pillinger CT. 1998.
57 Carbon, nitrogen, argon and helium study of impact diamonds from Ebeliakh
58
59
60

- 1
2
3 alluvial deposits and Popigai crater. *Meteoritics & Planetary Science* **33**: 985-992.
4
5 Shirey SB, Cartigny P, Frost DJ, Keshav S, Nestola F, Nimis P, Pearson DG, Sobolev
6 NV, Walter MJ. 2013. Diamonds and the geology of mantle carbon. *Reviews in*
7 *Mineralogy & Geochemistry* **75**: 355-421.
8
9 Shumilova TG, Mayer E, Isaenko SI. 2011. Natural monocrystalline lonsdaleite.
10 *Dokl. Earth Sci.* **441**: 1552-1554.
11
12 Shumilova T, Kis VK, Masaitis V, Isaenko S, Makeev B. 2014. Onion-like carbon in
13 impact diamonds from the Popigai astrobleme. *Eur. J. Mineral.* **26**: 267-277.
14
15 Smith JV, Dawson JB. 1985. Carbonado: Diamond aggregates from early impacts of
16 crustal rocks? *Geology* **13**: 342-343.
17
18 Smith ME, Henkel TW, Rollins JA. 2015. How many fungi make sclerotia? *Fungal*
19 *Ecology* **13**: 211-220.
20
21 Sobolev NV, Shatsky VS. 1990. Diamond inclusions in garnets from metamorphic
22 rocks: A new environment for diamond formation. *Nature* **343**: 742-746.
23
24 Sokhor MI, Polkanov YA, Yeremenko GK. 1973. A find of the hexagonal diamond
25 (lonsdaleite) in placers, USSR. *Doklady Academy of Science USSR* **209**: 118-121
26 (in Russian).
27
28 Southon JR, Taylor RE. 2002. Brief comments on “Terrestrial evidence of a nuclear
29 catastrophe in paleoindian times,” by Richard B. Firestone and William Topping.
30 *Mammoth Trumpet* **17**: 14-17.
31
32 Stöckhert B, Duyster J, Trepmann C, Massonne H-J. 2001. Microdiamond daughter
33 crystals precipitated from supercritical CO₂ + silicate fluids included in garnet,
34 Erzgebirge, Germany. *Geology* **29**: 391-394.
35
36 Stroud RM, Chisholm MF, Heck PR, Alexander CMO'D, Nittler LR. 2011.
37 Supernova shock-wave-induced co-formation of glassy carbon and nanodiamond.
38 *The Astrophysical Journal Letters* **738**: L27.
39
40 Surovell TA, Holliday VT, Gingerich JAM, Ketron C, Haynes Jr. CV, Hilman I,
41 Wagner DP, Johnson E, Claeys P. 2009. An independent evaluation of the
42 Younger Dryas extraterrestrial impact hypothesis. *Proc. Natl. Acad. Sci. USA*
43 **106**: 43, 18155-18158.
44
45 Swart PK, Grady MM, Pillinger CT, Lewis RS, Anders E. 1983. Interstellar carbon in
46 meteorites. *Science* **220**: 406-410.
47
48 Taylor RE, Bar-Yosef O. 2014. Radiocarbon Dating: An Archaeological Perspective.
49 Left Coast Press, Inc: Walnut Creek, CA.
50
51 Taylor TN, Krings M, Taylor EL. 2015. Fossil Fungi. Elsevier Academic Press,
52 London UK.
53
54
55
56
57
58
59
60

- 1
2
3
4 Thy P, Willcox G, Barfod GH, Fuller DQ. 2015. Anthropogenic origin of siliceous
5 scoria droplets from Pleistocene and Holocene archaeological sites in northern
6 Syria. *J. Arch. Sci.* **54**: 193-209.
7
- 8
9 Tian H, Schryvers D, Claeys P. 2011. Nanodiamonds do not provide unique evidence
10 for a Younger Dryas impact. *Proc. Natl. Acad. Sci. USA* **108**: 40-44.
11
- 12 Titkov SV, Gorshkov AI, Vinokurov SF, Bershov LV, Solodov DI, Sivtsov AV.
13 2001. Geochemistry and genesis of carbonado for Yakutian diamond deposits.
14 *Geochemistry International* **39**: 228–236.
15
- 16 Tollmann A. 2001. Kosmische gross-impakte der Jung- und Nacheiszeit (Cosmic
17 mega-impacts during the Late- and Post-Pleistocene). *Sitzungsberichte Abt. I -*
18 *Osterreichische Akademie der Wissenschaften* **208**: 3-13 (in German).
19
- 20
21 Trappe JM. 1931. *Cenococcum graniforme* - Its distribution, ecology, mycorrhiza
22 formation and inherent variation. Ph.D. thesis, University of Washington.
23
- 24 Trappe JM. 1969. Studies on *Cenococcum graniforme*. I. An efficient method for
25 isolation from sclerotia. *Can. J. Bot.* **47**: 1389-1390.
26
- 27 van Hoesel A, Hoek WZ, Braadbaart F, van der Plicht J, Pennock GM, Drury MR.
28 2012. Nanodiamonds and wildfire evidence in the Usselo horizon postdate the
29 Allerød–Younger Dryas boundary. *Proc. Natl. Acad. Sci. USA* **109**: 7648-7653.
30
- 31 van Hoesel A, Hoek WZ, van der Plicht J, Pennock GM, Drury MR. 2013. Cosmic
32 impact or natural fires at the Allerød–Younger Dryas boundary: A matter of dating
33 and calibration. *Proc. Natl. Acad. Sci. USA* **110**: 41, E3896.
34
- 35 van Hoesel A. 2014. The Younger Dryas climate change was it caused by an
36 extraterrestrial impact? Ph.D. thesis, Universiteit Utrecht.
37
- 38 van Hoesel A, Hoek WZ, Pennock GM, Drury MR. 2014. The Younger Dryas impact
39 hypothesis: a critical review. *Quaternary Science Reviews* **83**: 95-114.
40
- 41 van Hoesel A, Hoek WZ, Pennock GM, Kaiser K, Plümper O, Jankowski M, Hamers
42 MF, Schlaak N, Küster M, Andronikov AV, Drury MR. 2015. A search for
43 shocked quartz grains in the Allerød–Younger Dryas boundary layer. *Meteor. &*
44 *Planet. Sci.* **50**: 483-498.
45
- 46 van Peer AF, Müller WH, Boekhout T, Lugones LG, Wösten HAB. 2009.
47 Cytoplasmic continuity revisited: Closure of septa of the filamentous fungus
48 *Schizophyllum commune* in response to environmental conditions. *PLoS One* **4**
49 (e5977): 1-4
50
- 51 Verchovsky AB, Valter AA, Shukolyukov YA. 1991. Noble gases in shock-produced
52 diamond from Popigai meteorite crater. *Europ. Geophys. Soc.* C57.
53
- 54 Verchovsky AB, Ott U, Begemann F. 1993. Implanted radiogenic and other noble
55
56
57
58
59
60

- 1
2
3 gases in crustal diamonds from Northern Kazakhstan. *Earth and Planetary*
4 *Science Letters* **120**: 87-102.
5
6 Vincent L, Patriarche G, Hallais G, Renard C, Gardès C, Troadec D, Bouchier D.
7 2014. Novel heterostructured Ge nanowires based on polytype transformation.
8 *Nano Lett.* **14**: 4828-4836.
9
10 Watanabe M, Fujitake N, Ohta H, Yokoyama T. 2001. Aluminum concentrations in
11 sclerotia from a buried humic horizon of volcanic ash soils in Mt. Myoko, Central
12 Japan. *Soil Sci. Plant Nutr.* **47**: 411-418.
13
14 Watanabe M, Ohishi S, Pott A, Hardenbicker U, Aoki K, Sakagami N, Ohta H,
15 Fujitake N. 2004a. Soil chemical properties and distribution of sclerotium grains
16 in forest soils, Harz Mts., Germany. *Soil Sci. Plant Nutr.* **50**: 863-870.
17
18 Watanabe M, Genseki A, Sakagami N, Inoue Y, Ohta H, Fujitake N. 2004b.
19 Aluminum oxyhydroxide polymorphs and some micromorphological
20 characteristics in sclerotium grains. *Soil Sci. Plant Nutr.* **50**: 1205-1210.
21
22 Wen B, Zhao JJ, Li TJ. 2007. Synthesis and crystal structure of n-diamond.
23 *International Materials Reviews* **3**: 131-151.
24
25 West A, Firestone RB, Kennett JP, Becker L. 2007. Extraterrestrial markers found at
26 Clovis sites across North America. *Eos Trans. AGU* **88**: (23) PP41A-02.
27
28 Wirth R, Rocholl A. 2003. Nanocrystalline diamond from the Earth's mantle
29 underneath Hawaii. *Earth and Planetary Science Letters* **211**: 357-369.
30
31 Wittke JH, Weaver JC, Bunch TE, Kennett JP, Kennett DJ, Moore AMT, Hillman
32 GC, Tankersley KB, Goodyear AC, Moore CR, Daniel IR, Ray JH, Lopinot NH,
33 Ferraro D, Israde-Alcántara I, Bischoff JL, DeCarli PS, Hermes RE, Kloosterman
34 JB, Revay Z, Howard GA, Kimbel DR, Kletetschka G, Nabelek L, Lipo CP, Sakai
35 S, West A, Firestone RB. 2013a. Evidence for deposition of 10 million tonnes of
36 impact spherules across four continents 12,800 y ago. *Proc. Natl. Acad. Sci. USA*
37 **110**: (23), E2088-E2097.
38
39 Wittke JH, Bunch TE, Kennett JP, Kennett DJ, Culleton BJ, Tankersley KB, Daniel
40 Jr. IR, Kloosterman JB, Kletetschka G, West A, Firestone RB. 2013b. Reply to
41 van Hoesel et al.: Impact-related Younger Dryas boundary nanodiamonds from
42 The Netherlands. *Proc. Natl. Acad. Sci. USA* **110**: E3897-3898.
43
44 Wittke JH, Bunch TE, Tankersley KB, Daniel Jr. IR, Kloosterman JB, Kletetschka G,
45 West A, Firestone RB. 2013c. Reply to Ives and Froese: Regarding the impact-
46 related Younger Dryas boundary layer at Chobot site, Alberta, Canada. *Proc.*
47 *Natl. Acad. Sci. USA* **110**: E3900.
48
49 Woodman N, Athfield NB. 2009. Post-Clovis survival of American Mastodon in the
50 southern Great Lakes region of North America. *Quaternary Research* **72**: 359-
51 363.
52
53
54
55
56
57
58
59
60

- 1
2
3 Xiao S-Q, Pirouz P. 1992. On diamond-hexagonal germanium. *J. Mater. Res.* **7**:
4 1406-1412.
5
- 6 Xu S, Okay AI, Ji S, Sengör AMC, Su W, Liu Y, Jiang L. 1992. Diamond from the
7 Dabie Shan metamorphic rocks and its implication for tectonic setting. *Science*
8 **256**: 80-82.
9
- 10 Xu S, Liu Y, Chen G, Ji S, Ni P, Xiao W. 2005. Microdiamonds, their classification
11 and tectonic implications for the host eclogites from the Dabie and Su-Lu regions
12 in central eastern China. *Mineralogical Magazine* **69**: 509-520.
13
- 14 Xu Z, Gleason ML, Mueller DS, Esker PD, Bradley CA, Buck JW, Benson DM,
15 Dixon PM, Monteiro JEBA. 2008. Overwintering of *Sclerotium rolfsii* and *S.*
16 *rolfsii* var. *delphinii* in different latitudes of the United States. *Plant Disease* **92**:
17 719-724.
18
19
- 20 Yada T, Nakamura T, Takaoka N, Noguchi T, Terada K, Yano H, Nakazawa T,
21 Kojima H. 2004. The global accretion rate of extraterrestrial materials in the last
22 glacial period estimated from the abundance of micrometeorites in Antarctic
23 glacier ice. *Earth Planets Space* **56**: 67-79.
24
25
- 26 Yang J, Xu Z, Dobrzhinetskaya LF, Green HW, Pei X, Shi R, Wu C, Wooden JL,
27 Zhang J, Wan Y, Li H. 2003. Discovery of metamorphic diamonds in central
28 China: an indication of a >4000-km-long zone of deep subduction resulting from
29 multiple continental collisions. *Terra Nova* **15**: 370-379.
30
31
- 32 Yang ZQ, Verbeeck J, Schryvers D, Tarcea N, Popp J, Rösler W. 2008. TEM and
33 Raman characterisation of diamond micro- and nanostructures in carbon spherules
34 from upper soils. *Diamond and Related Materials* **17**: 937-943.
35
- 36 Yoshiasa A, Murai Y, Ohtaka O, Katsura T. 2003. Detailed structures of hexagonal
37 diamond (lonsdaleite) and wurtzite-type BN. *Jpn. J. Appl. Phys.* **42**: 1694-1704.
38
39
- 40 Zhang X, Hu W, Li J, Tao L, Wei Y. 2012. A comparative study of cellular uptake
41 and cytotoxicity of multi-walled carbon nanotubes, graphene oxide, and
42 nanodiamond. *Toxicol. Res.* **1**: 62-68.
43
44
45
46
47
48
49
50
51
52
53
54
55
56
57
58
59
60

Figure Captions

Figure 1: (a) A HR-TEM lattice image of a nanocrystal from the Allende meteorite acid-dissolution residue. The nanocrystal exhibits a homoepitaxial interface between two crystal lattices that is consistent with the (b) 3C cubic diamond and 2H lonsdaleite atomic structure (figure adapted from Daulton *et al.*, 1996). The grain displays one domain with close packed tetrahedral planes stacked in the $(A^b)(B^c)(C^a)\dots$ sequence defining the 3C structure and a second domain stacked in the $(A^b)(B^a)\dots$ sequence defining the 2H structure. Through-focus HR-TEM imaging (not shown) is consistent with these atomic structures. Furthermore, since this grain exhibits a homoepitaxial interface of two crystal structures, the possible pairs of candidate phases that comprise the grain are significantly limited. (c) Atomic models of the six unique (fundamental) bilayer planes (A^b , A^c , B^a , B^c , C^a , and C^b) in diamond (top), that comprise stacked tetrahedral planes (depicted normal to stacking direction shown at bottom). The two basic stacking arrangements, $(X^y)(Y^x)$ and $(X^y)(Y^z)$ where X , Y , and Z are all different, form planes of vertex-sharing antiparallel and parallel tetrahedra, respectively.

Figure 2: HR-TEM images of well-ordered (a) $[01\bar{1}]$ zone of cubic diamond and (b) $[010]$ zone of lonsdaleite from products of thermobaric high-pressure, high-temperature treatment of graphite. (c) Calculated HR-TEM image of lonsdaleite for $[010]$ zone axis (figure adapted from Kulnitskiy *et al.*, 2013). (d) HR-TEM image of diamond grown on (100)-oriented Si held at 600 or 700° C by bombardment with 80 or 200 eV ions from a $(\text{CH}_4 \text{ or } \text{C}_2\text{H}_2)/\text{Ar}/\text{H}_2$ -fed Kaufmann source (figure adapted from Lifshitz *et al.*, 2001). (e) Schematic atomic model of lonsdaleite projected along the $[010]$ zone axis.

Figure 3: Shown in top row Fig. 6 part b and part d of Kurbatov *et al.* (2010); its figure caption states, “Lonsdaleite analyses. (b) HR-TEM image showing characteristic lonsdaleite lattice spacings. (d) Fast Fourier transform (FFT) of lonsdaleite ND crystal. All values (Miller indices) are consistent with each other and with the published lattice spacings for lonsdaleite as shown in Table 3. Sample numbers, as referenced in Table 2, are shown in the lower left of

each image.” Shown at bottom is a schematic of the atomic structure of lonsdaleite. In diamond, C atoms covalently bond to four other C atoms in a tetrahedral geometry. The {002} planes in the lonsdaleite structure contain the base of the C tetrahedra that are stacked in the structure. The set of {002} planes are oriented edge-on only in $[hk0]$ zone axes projections, and high-resolution lattice images of $[hk0]$ zone axes display only one set of {002} planes, contrary to the nanocrystal shown by Kurbatov *et al.* (2010).

Figure 4: Shown in top row is Fig. S2 (part B) of Kennett *et al.* (2009b); its figure caption states, “(B) cluster of lonsdaleite crystals and associated diffraction pattern from 4.59-4.64m(AC#348).” We modified the diffraction pattern from the original published by Kennett *et al.* (2009b) by inverting its contrast to aid in visual clarity and by superimposing additional annotations on the pattern. In right of top row, ovals were superimposed to demonstrate the azimuthal asymmetry of the diffraction pattern and the presence of additional partial diffraction rings. Half circles were superimposed to illustrate the predicted reflections for lonsdaleite. The scale of the diffraction pattern was calibrated assuming that the ring labeled (110) by Kennett *et al.* (2009b) corresponds to the (110) reflection of lonsdaleite. Notice, there are many missing lonsdaleite reflections. Left of bottom row is Fig. 15 (part B) of Kinzie *et al.* (2014); its figure caption states, “Younger Dryas Boundary lonsdaleite-like crystal”. This is the same grain shown in Kennett *et al.* (2009b). Shown at right of the bottom row is the diffraction pattern of Kennett *et al.* (2009b) with half circles superimposed to illustrate the predicted reflections for a homogeneous mixture of graphene and graphane where the $\langle 100 \rangle$ d -spacing in graphane is contracted by a factor of 1.054 from that of graphene (Daulton *et al.*, 2010). The scale of the diffraction pattern was calibrated assuming the ring labeled (110) by Kennett *et al.* (2009b) corresponds to the (100) reflection of graphene. Consistent with this diffraction pattern, disordered graphite could be present and predominantly oriented with its [001] crystallographic axis in the electron beam direction. As such, the high-resolution lattice image published for this grain (see Fig. 16, Kinzie *et al.*, 2014) is consistent with a [001] zone axis of graphitic/graphene structure. Similarly, the diffraction pattern identified as lonsdaleite by Redmond and Tankersley (2011) is

1
2
3 consistent with [001] graphite.
4
5

6
7 Figure 5: Typical electron diffraction pattern from aggregates of polycrystalline
8 graphene/graphane recovered from sediments exhibits a) azimuthally
9 asymmetric electron diffraction rings indicative of texturing of two phases
10 (Daulton *et al.*, 2010). Different regions within the *same* aggregate exhibit
11 diffraction rings from b) only graphene (solid triangles), c) both graphene and
12 graphane, or d) only graphane (open triangles). To aid in visual clarity, the
13 diffraction patterns are displayed in reverse contrast.
14
15
16
17
18

19
20 Figure 6: SEM images of carbon spherules from Arlington Canyon YDB sediments
21 (AC-003): a) Fig. 1 (part A), b) Fig. S6 (part E), and c) Fig. S6 (part F) of
22 Kennett *et al.* (2009b). Their figure captions state, “SEM images represent
23 carbon spherules (A)” and “(E) [relabelled B here] Bisected carbon spherule
24 showing typical internal reticulate (honeycomb) structure and thin,
25 nonreticulate crust. (F) [relabelled C here] Close-up of carbon spherule
26 interior shown in E [relabelled B here] with well-organized reticulate
27 (honeycomb) structure and thin, nonreticulate crust.” d) Light microscope
28 image of fungal sclerotia charred at 350°C for 5 mins. e) SEM image of
29 broken fungal sclerotia from charcoal residue of a low-temperature surface
30 fire, Thursley, Common, Surrey, England. f) SEM image of broken fungal
31 sclerotia charred at 350°C for 5 mins showing mesh-like internal structure
32 comprising fused fungal hyphae.
33
34
35
36
37
38
39
40
41
42

43 Figure 7: Left column is Fig. 5 of the supplemental materials of Israde-Alcántara *et*
44 *al.* (2012a). Their figure caption states, “CARBON SPHERULES from the
45 2.8-m layer. A) The upper inset show a whole CSp in reflected light. B) SEM
46 image of a crushed CSp; C) Photomicrograph of the same crushed CSp. D)
47 Closeup of bottom of crushed CSp, illustrating the lack of filamentous texture,
48 as typical of fungal sclerotia, and indicating that these objects are not sclerotia,
49 as speculated by Scott *et al.* (2010).” Right column or panel e) SEM image of
50 the interior of cross-sectioned *C. geophilum* sclerotia displaying a hollow
51 center with smooth interior walls (image courtesy of M. Watanabe).
52
53
54
55
56
57
58
59
60

1
2
3 Figure 8: a) SEM image of the interior of cross-sectioned *C. geophilum* sclerotia
4 displaying micron-sized holes (septal pores), which are morphological features
5 characteristic of sclerotia (image courtesy of M. Watanabe). b) SEM image of
6 the interior of a carbon spherule from Arlington Canyon YDB sediments (AC-
7 003) from Fig. S6 (part F) of Kennett *et al.* (2009b). The originally published
8 image (shown in Fig. 6c of this paper with a modified panel label) has been
9 cropped with circles overlaid to denote several of the submicron-sized holes
10 present in the cell-like walls. Their figure caption states, “(F) Close-up of
11 carbon spherule interior shown in E with well-organized reticulate
12 (honeycomb) structure and thin, nonreticulate crust.” The presence of the
13 holes provides a conclusive identification of the spherule as a sclerotium
14 (private communication M. Watanabe). Both images are reproduced at the
15 same spatial scale.
16
17
18
19
20
21
22
23
24
25

26 Figure 9: High-resolution TEM lattice images (top row) and bright-field (BF) TEM
27 image of nanocrystals embedded within amorphous fragments (middle row)
28 obtained from finely crushed carbon spherules collected from Arlington
29 Canyon YDB sediments (AC-003). Many of the nanocrystals exhibit twinning,
30 particularly $\Sigma=3$ twin boundaries or occasionally $\Sigma=9$ twin boundaries when
31 successive $\Sigma=3$ twin domains impinge on one another (e.g., see Luyten *et al.*,
32 1992; Daulton *et al.*, 2003), characteristic of face centered cubic structures.
33 Shown in the bottom row are Figure 13 (part A) and Figure 6 (part C) from
34 Kinzie *et al.* (2014); their respective figure captions states, “carbon spherules
35 from Gainey, Michigan (Younger Dryas Boundary [YDB]: 3933 ppb at 30 cm
36 below surface [cmbs]” and “nanodiamonds (NDs) in carbon spherules
37 (CS) . . . n-Diamond from Topper, South Carolina (YDB: 108 ppb at 60
38 cmbs).”
39
40
41
42
43
44
45
46
47
48
49

50 Figure 10: Representative diffraction pattern from amorphous grains obtained from
51 finely crushed carbon spherules collected from Arlington Canyon YDB
52 sediments (AC-003) that contain nanocrystals (see, Fig. 6, middle row). The
53 diffraction pattern is displayed in reversed contrast and three different electron
54 exposures are superimposed to cover the large dynamic range of the Bragg
55
56
57
58
59
60

intensities. The diffraction lines of cubic diamond (along with the kinematically forbidden diamond reflections denoted by *) are shown.

Figure 11: Top: Bright-field (BF) and Dark-field (DF) STEM images of nanocrystals embedded within an amorphous grain from finely crushed carbon spherules collected from Arlington Canyon YDB sediments (AC-003). Below are STEM Energy Dispersive X-ray Spectroscopy (EDXS) and Electron Energy Loss Spectroscopy (EELS) maps (in dashed rectangle) of relative elemental composition normalized to the sum of all measured elements. Areas in the maps that exhibit a deficit of C and Fe correlate to areas that show an excess of Cu. For nanocrystals on the surface of the amorphous C-rich and Fe-containing grain, this is a result of the normalization of the compositions. For nanocrystals within the grain, this results from the nanoparticles displacing the amorphous C-rich and Fe-containing matrix. The 256 grey scale look-up table (LUT) is linearly mapped between the minimum and maximum element composition for each map. (The elemental maps are published online in false color with a dynamic range of 1786 colors.) As described in the text, the amorphous matrix had an elemental composition, as determined by EDXS, of 82.49 at.% (70.56 wt.%) C, 13.40 at.% (15.27 wt.%) O, 2.87 at.% (11.41 wt.%) Fe, 0.39 at.% (0.89 wt.%) S, 0.35 at.% (0.70 wt.%) Si, 0.17 at.% (0.47 wt.%) K, 0.12 at.% (0.21 wt.%) Mg, 0.10 at.% (0.29 wt.%) Ca, 0.05 at.% (0.11 wt.%) P, 0.05 at.% (0.10 wt.%) Al.

Figure 12: Top: Bright-field (BF) image of nanocrystals from finely crushed carbon spherules collected from Arlington Canyon YDB sediments (AC-003). Below are STEM Energy Dispersive X-ray Spectroscopy (EDXS) maps of relative elemental composition normalized to the sum of C, O, Cu, and S contributions. Carbon and O is associated with the support film and deficits in those elements occur in the maps where the nanocrystals are located due to the normalization of the elemental compositions to the sum of C, O, Cu, and S contributions. If the nanocrystals contained C, excesses in C would be observed at the locations of the nanocrystals. The 256 grey scale look-up table (LUT) is linearly mapped between the minimum and maximum element composition for each map. (The elemental maps are published online in false

1
2
3
4
5
6
7
8
9
10
11
12
13
14
15
16
17
18
19
20
21
22
23
24
25
26
27
28
29
30
31
32
33
34
35
36
37
38
39
40
41
42
43
44
45
46
47
48
49
50
51
52
53
54
55
56
57
58
59
60

color with a dynamic range of 1786 colors.)

THE NANODIAMOND EVIDENCE

66

Table 1: Lonsdaleite Bragg Reflections

	Predicted†	Bundy and Kasper (1967)	Fronzel and Marvin (1967)	Fedoseev <i>et al.</i> (1983)	Bhargava <i>et al.</i> (1995)	Ona <i>et al.</i> (2008)
(<i>hkl</i>)	d-spacing (Å)					
(100)	2.182	2.19	2.18	2.20-2.18	2.181	2.165
(002)	2.060	2.06	2.061	2.06-2.07	2.045	2.089
(101)	1.928	1.92	1.933	1.92	1.949	1.933
(102)	1.498	1.50	1.50	1.50-1.53		1.504
(110)	1.260	1.26	1.257	1.26-1.27	1.257	1.251
(103)	1.162	1.17	1.17	1.18	1.167	1.172
(200)	1.091					
(112)	1.075	1.075	1.075	1.06-1.07	1.073	1.076
(201)	1.055	1.055			1.067	
(202)	0.964			0.970-0.985		
(203)	0.854			0.870		
(210)	0.825			0.820		
(211)	0.809	0.855				
(105)	0.771	0.820				
(212)	0.766					
(300)	0.727					
(213)	0.707					
(006)	0.687					
(302)	0.686					

† lattice parameters: $a = 2.52 \text{ \AA}$ and $c = 4.12 \text{ \AA}$.

Table 2: Comparison of Cu and Cu₂O Bragg Reflections to those of “n-diamond” and “i-carbon”.

Cu		“n-diamond”	Cu ₂ O		“i-carbon” / “C ₈ ”			
Predicted†		Konyashin <i>et al.</i> (2001)	Predicted‡		Matyushenko <i>et al.</i> (1979)	Hirai and Kono (1991)	Burkhard <i>et al.</i> (1994)	
(<i>hkl</i>)	d-spacing (Å)		(<i>hkl</i>)	Int.	d-spacing (Å)			
(111)	2.087	2.067	(110)	w	3.019	3.02	3.04	3.03
(200)	1.807	1.791	(111)	vs	2.465		2.42	2.49
(220)	1.278	1.261	(200)	m	2.135	2.13	2.08	2.13
(311)	1.090	1.078	(211)	w	1.743	1.74	1.70	1.78
(222)	1.044	1.032	(220)	m	1.510	1.52	1.49	1.59
(400)	0.904	0.892	(221)	vw	1.423			
(331)	0.829	0.817	(310)	w	1.350	1.352		
(420)	0.808	0.796	(311)	w	1.287		1.26	1.29
(422)	0.738	0.727	(222)	w	1.233	1.234	1.19	
(333)	0.696	0.686	(321)	vw	1.141		1.09	1.09
(440)	0.639	0.630	(400)	w	1.067			1.05

† lattice parameter: $a = 3.6149 \text{ \AA}$ ‡ lattice parameter: $a = 4.2696 \text{ \AA}$

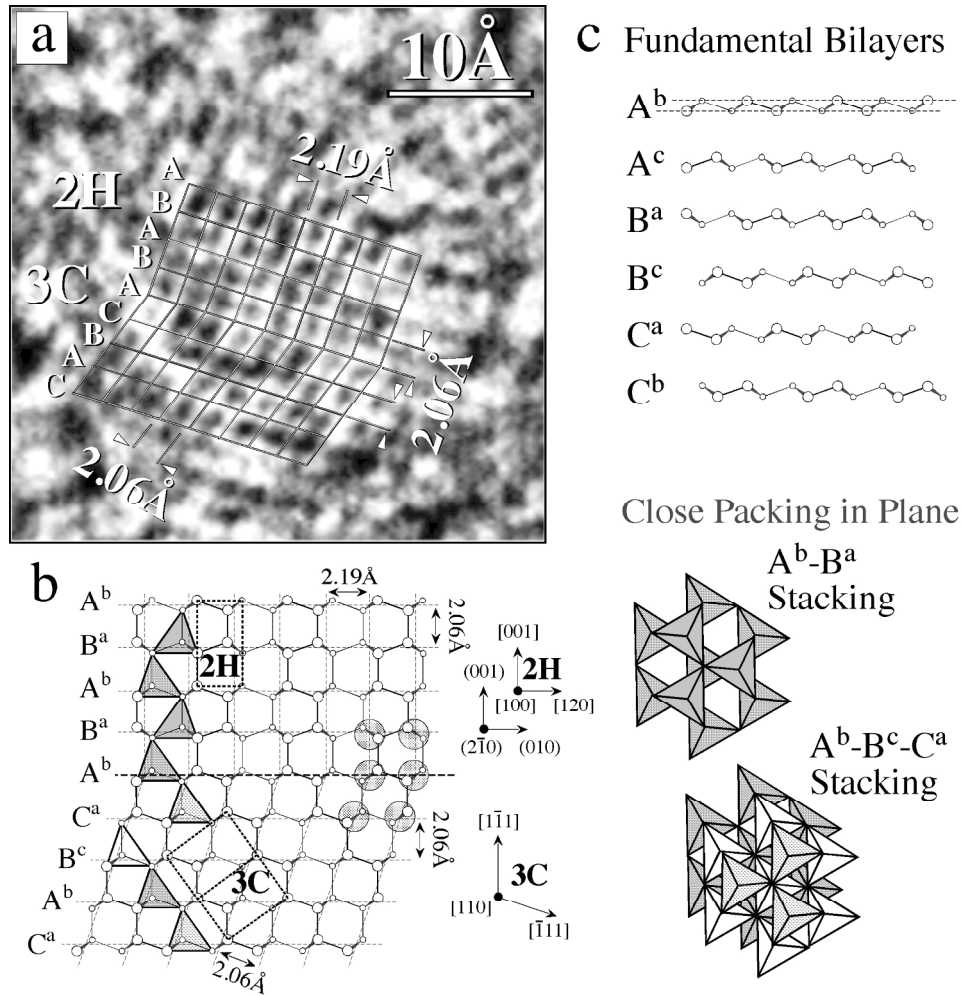


Figure 1 - Print Version

203x202mm (300 x 300 DPI)

1
2
3
4
5
6
7
8
9
10
11
12
13
14
15
16
17
18
19
20
21
22
23
24
25
26
27
28
29
30
31
32
33
34
35
36
37
38
39
40
41
42
43
44
45
46
47
48
49
50
51
52
53
54
55
56
57
58
59
60

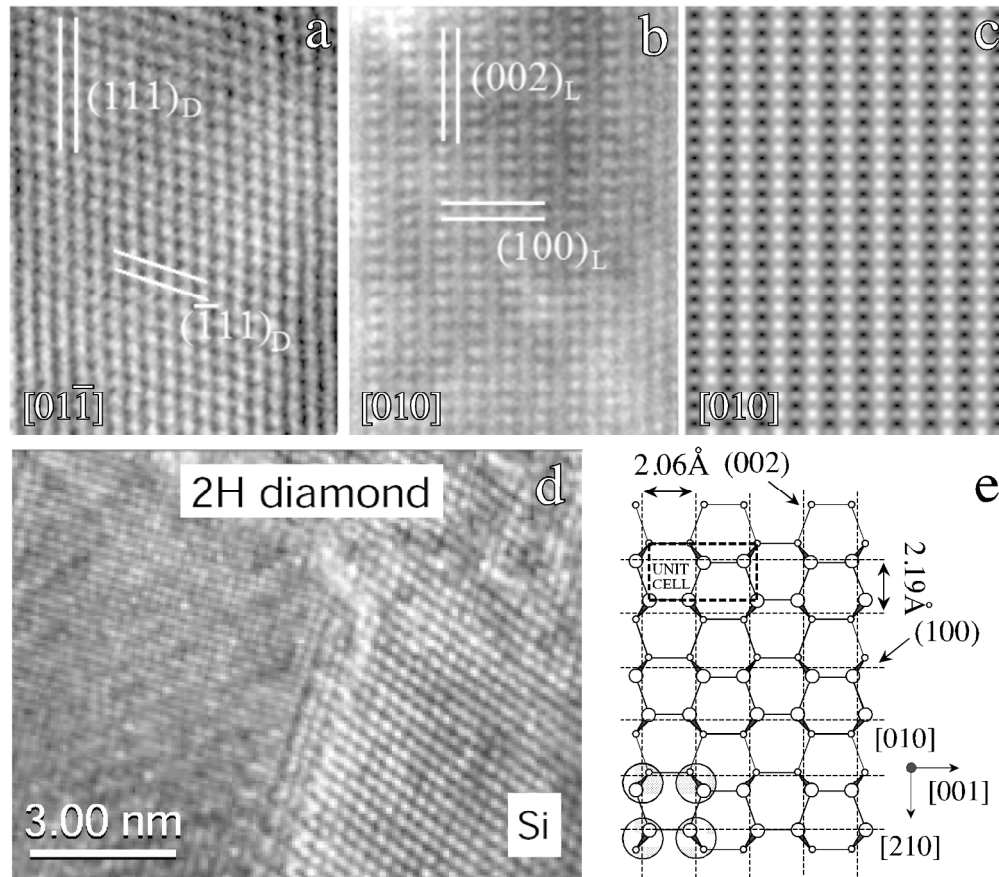


Figure 2 - Print Version

203x177mm (300 x 300 DPI)

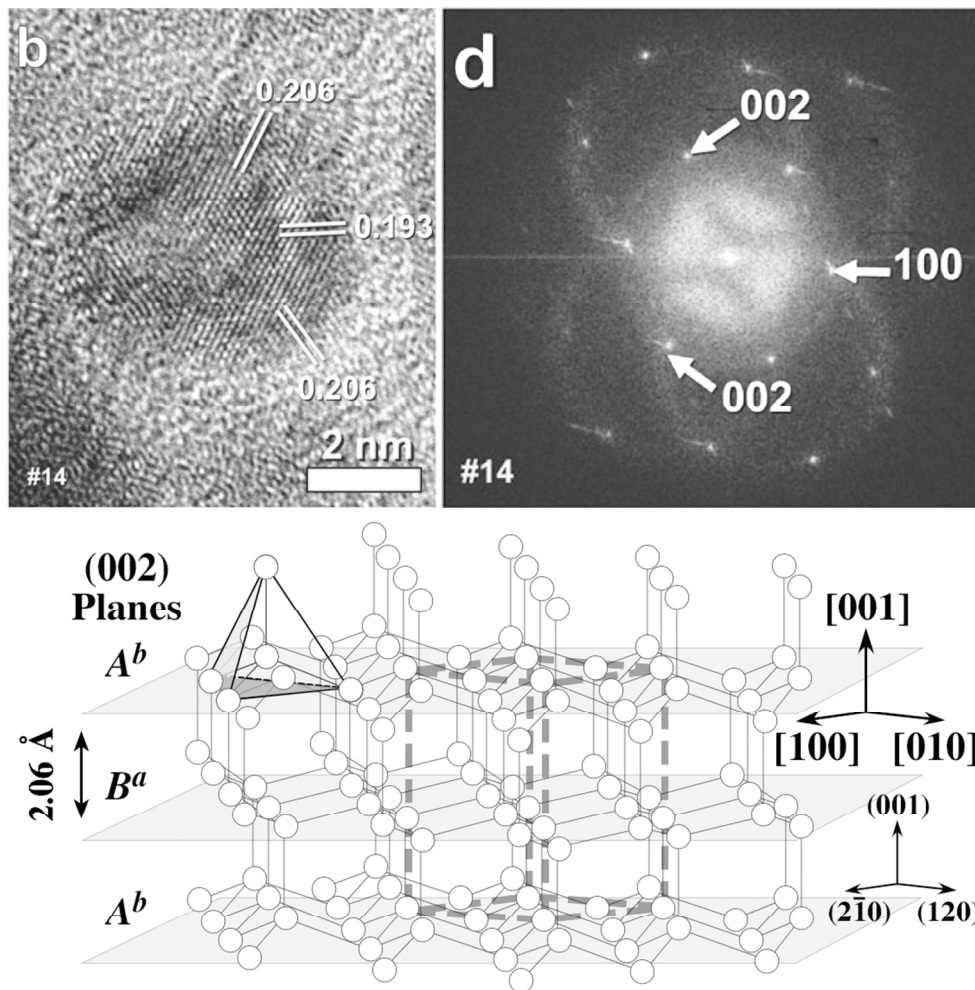


Figure 3 - Print Version

202x206mm (145 x 145 DPI)

1
2
3
4
5
6
7
8
9
10
11
12
13
14
15
16
17
18
19
20
21
22
23
24
25
26
27
28
29
30
31
32
33
34
35
36
37
38
39
40
41
42
43
44
45
46
47
48
49
50
51
52
53
54
55
56
57
58
59
60

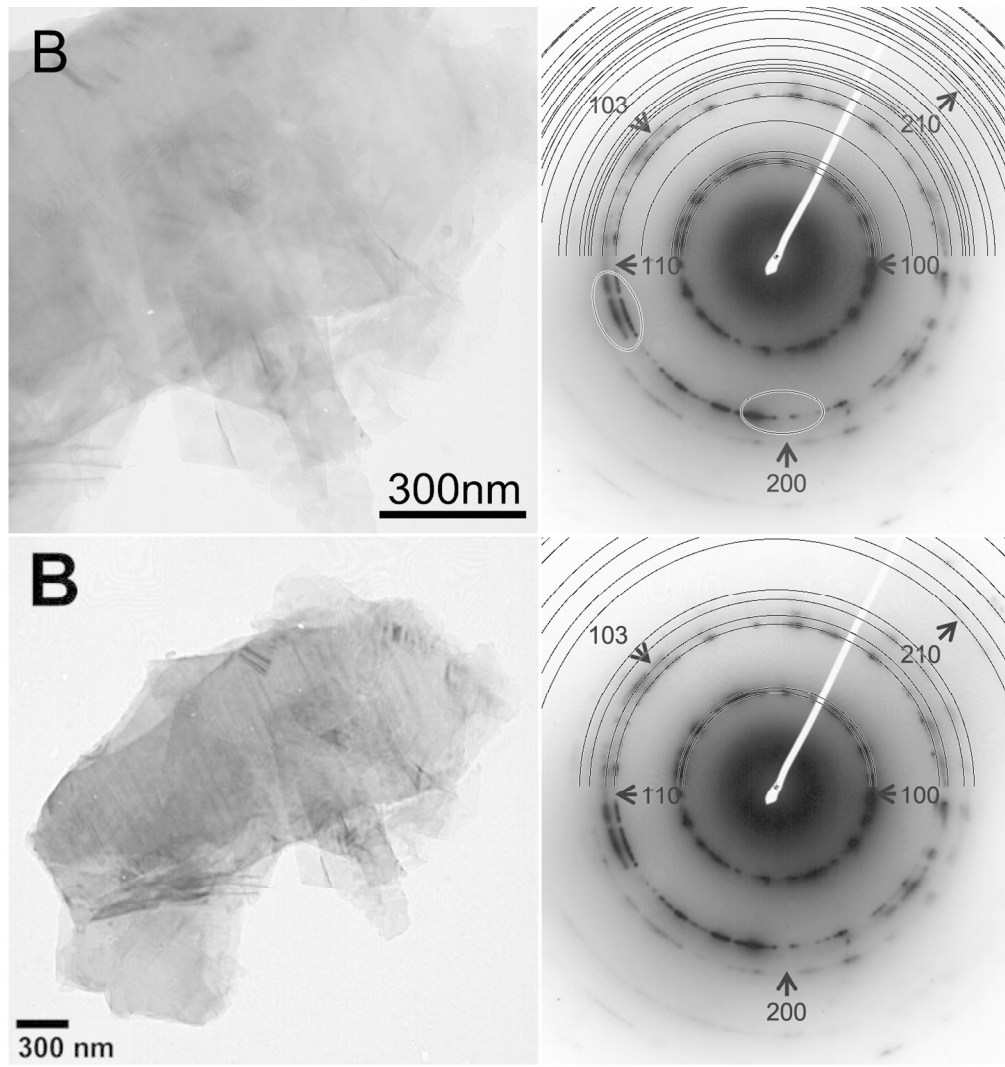


Figure 4 - Print Version
203x218mm (186 x 186 DPI)

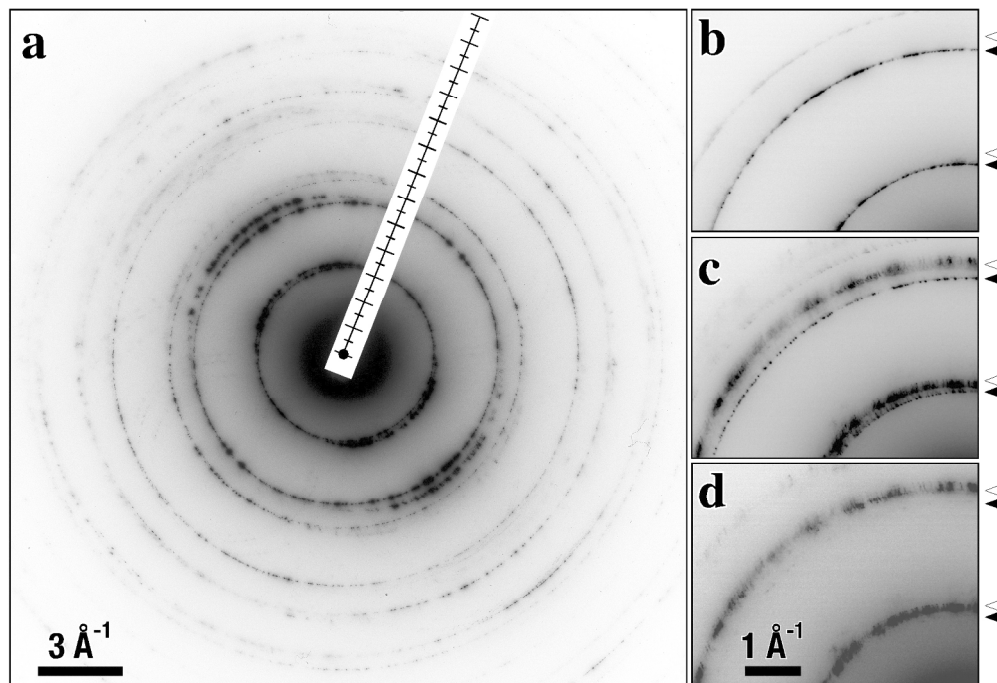


Figure 5 - Print Version

203x142mm (300 x 300 DPI)

1
2
3
4
5
6
7
8
9
10
11
12
13
14
15
16
17
18
19
20
21
22
23
24
25
26
27
28
29
30
31
32
33
34
35
36
37
38
39
40
41
42
43
44
45
46
47
48
49
50
51
52
53
54
55
56
57
58
59
60

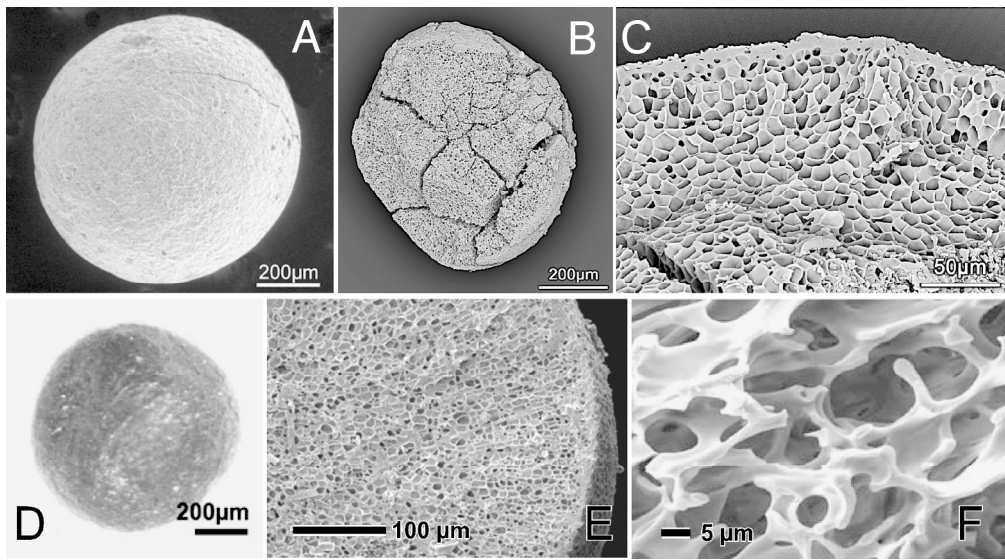


Figure 6 - Print Version
203x112mm (300 x 300 DPI)

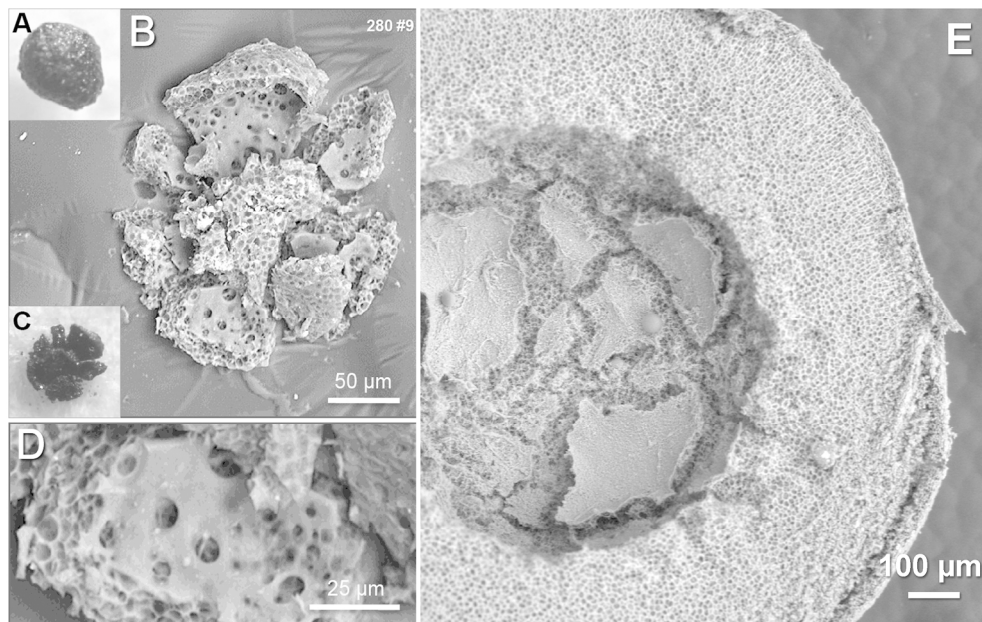


Figure 7 - Print Version

203x128mm (300 x 300 DPI)

1
2
3
4
5
6
7
8
9
10
11
12
13
14
15
16
17
18
19
20
21
22
23
24
25
26
27
28
29
30
31
32
33
34
35
36
37
38
39
40
41
42
43
44
45
46
47
48
49
50
51
52
53
54
55
56
57
58
59
60

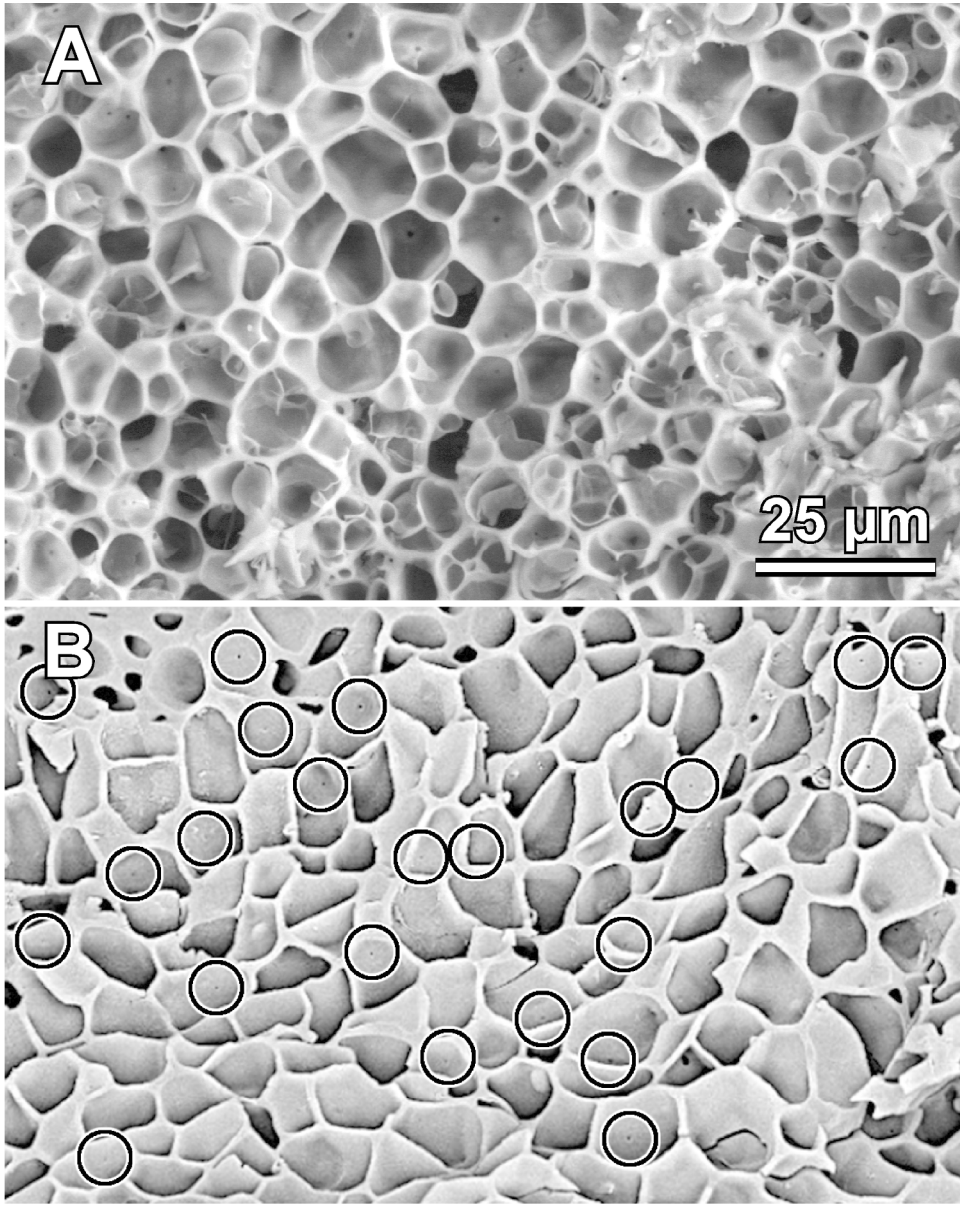


Figure 8 - Print Version

203x254mm (300 x 300 DPI)

1
2
3
4
5
6
7
8
9
10
11
12
13
14
15
16
17
18
19
20
21
22
23
24
25
26
27
28
29
30
31
32
33
34
35
36
37
38
39
40
41
42
43
44
45
46
47
48
49
50
51
52
53
54
55
56
57
58
59
60

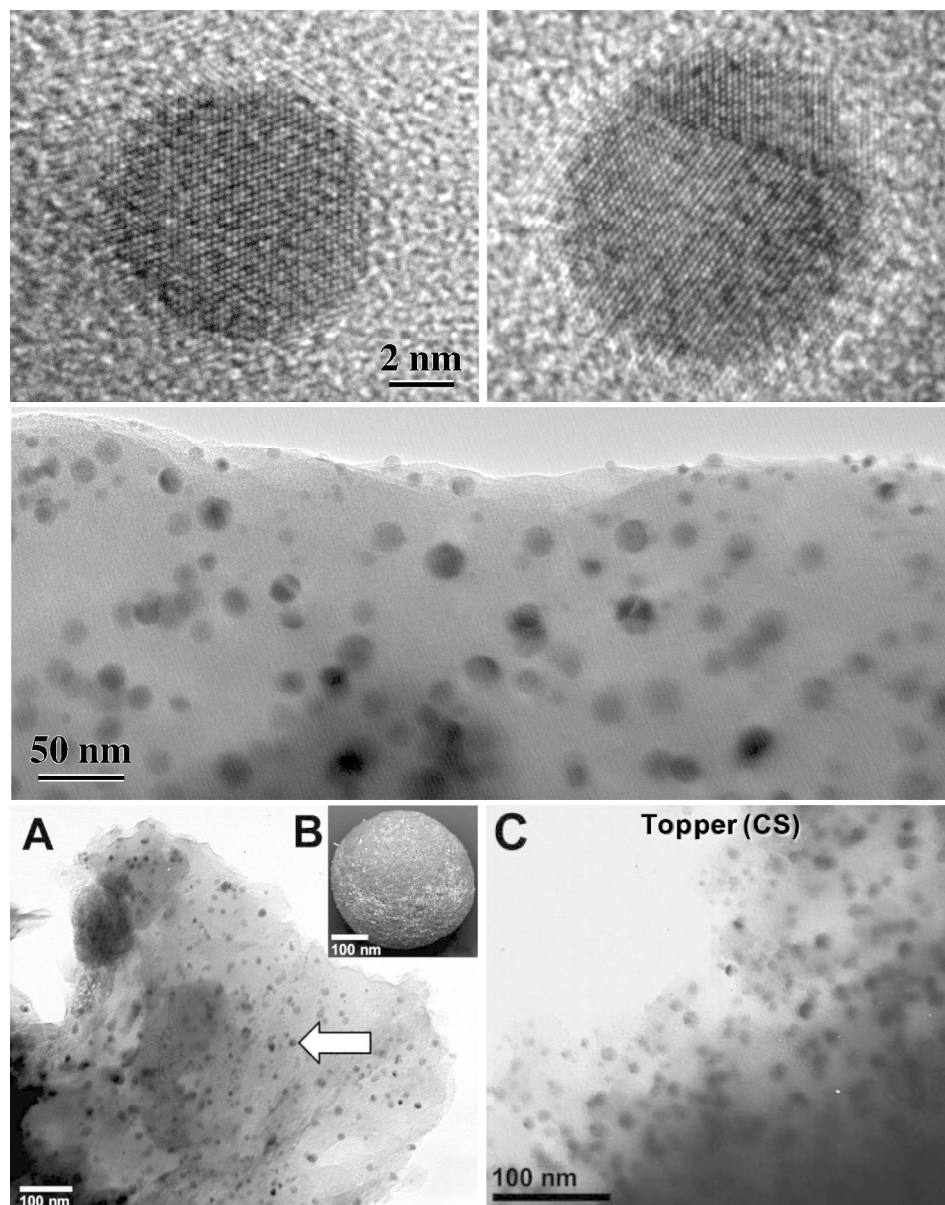


Figure 9 - Print Version

499x634mm (122 x 122 DPI)

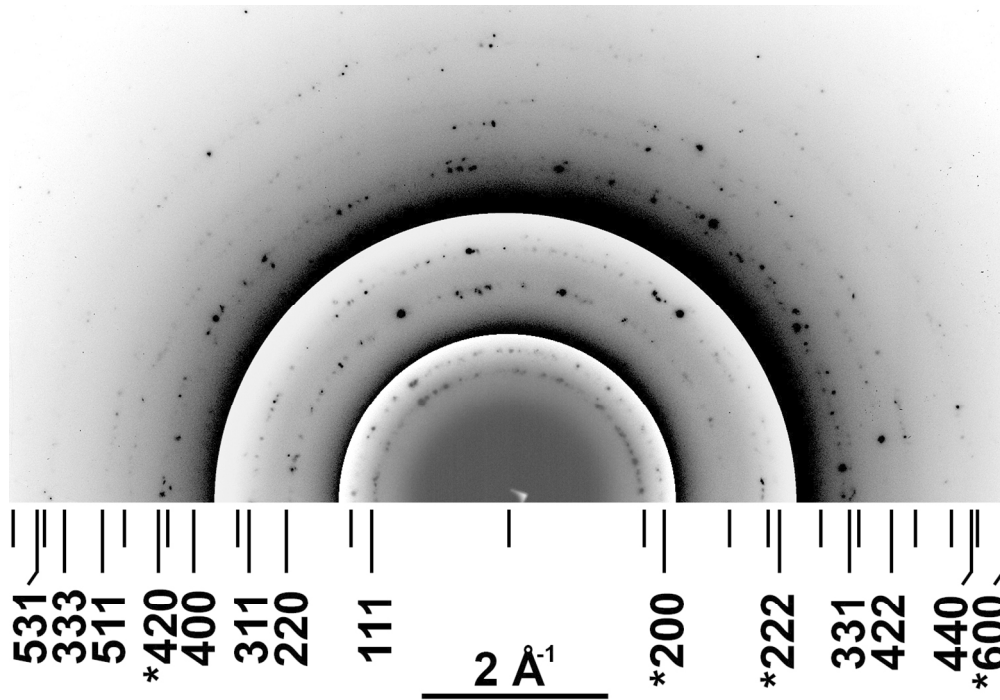


Figure 10 - Print Version

202x141mm (188 x 188 DPI)

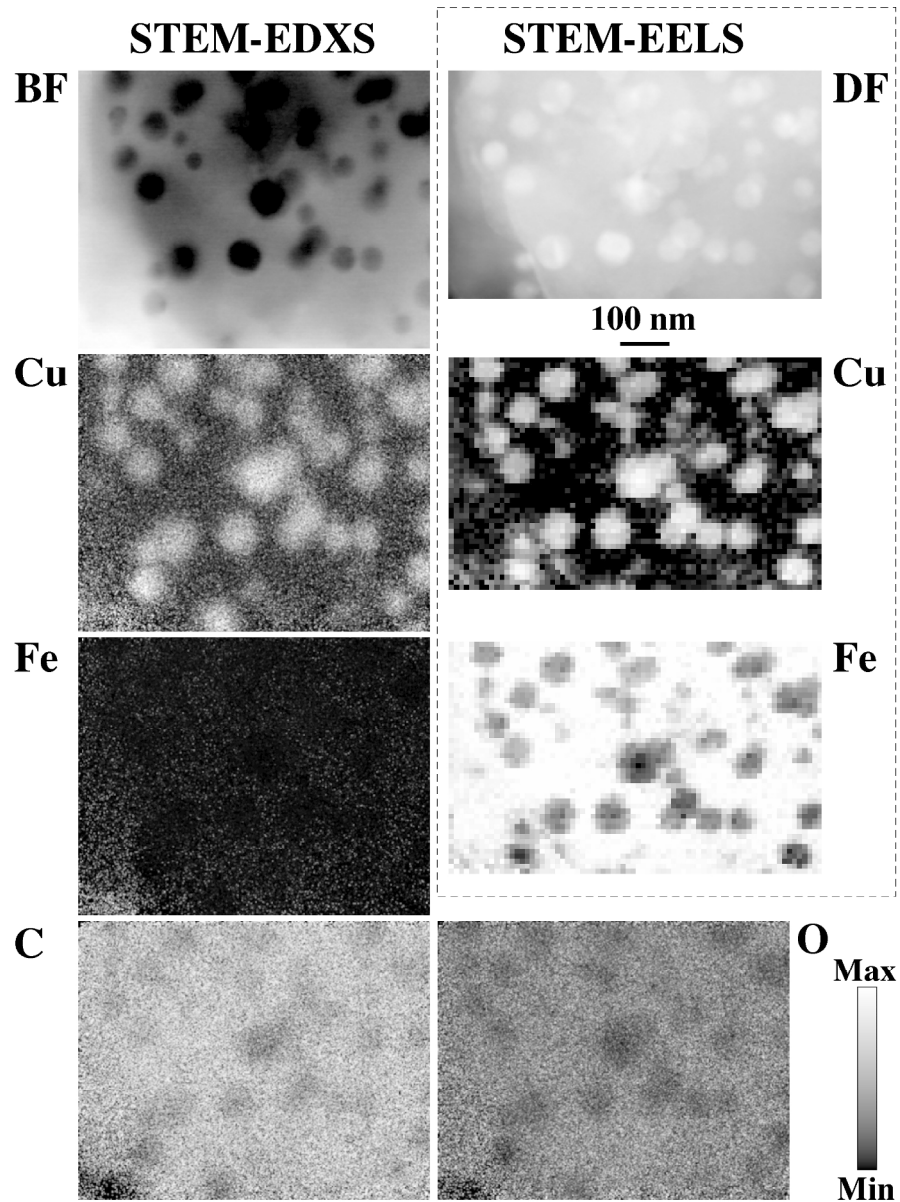


Figure 11 - Print Version
203x275mm (300 x 300 DPI)

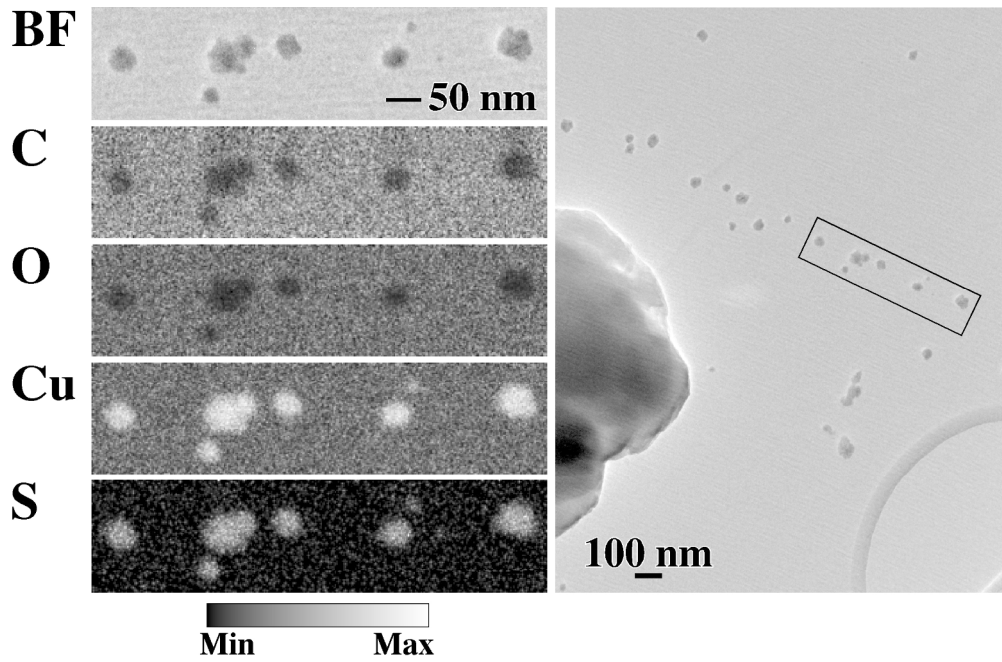


Figure 12 - Print Version

203x132mm (300 x 300 DPI)